PREDICTING THE EFFECTS OF STRETCH-ACTIVATED REACTIVE OXYGEN SPECIES SIGNALING ON CARDIAC EXCITATION-CONTRACTION COUPLING

by

Sarita Limbu

A Dissertation
Submitted to the
Graduate Faculty
of
George Mason University
in Partial Fulfillment of
The Requirements for the Degree
of
Doctor of Philosophy
Bioinformatics and Computational Biology

Committee:

_____ Dr. M. Saleet Jafri, Dissertation Director

_____ Dr. Dmitri Klimov, Committee Member

_____ Dr. Patrick Gillevet, Committee Member

_____ Dr. Iosif Vaisman, Acting Director, School of Systems Biology

_____ Dr. Donna M. Fox, Associate Dean, Office of Student Affairs & Special Programs, College of Science

_____ Dr. Peggy Agouris, Dean, College of Science

Date: _____ Summer Semester 2016
George Mason University
Fairfax, VA

Predicting the Effects of Stretch-Activated Reactive Oxygen Species Signaling on Cardiac Excitation-Contraction Coupling

A dissertation submitted in partial fulfillment of the requirements for the degree of Doctor of Philosophy at George Mason University

By

Sarita Limbu
Master of Science
University of Akron, 2009

Director: M. Saleet Jafri, Professor
School of Systems Biology, College of Science

Summer Semester 2016
George Mason University
Fairfax, VA

DEDICATION

This dissertation is dedicated to my mother Narmaya Limbu for dedicating herself to raise and educate me, to my husband Desh Raj Sonyok for his love and support and to my son Namjung.

ACKNOWLEDGEMENTS

I am greatly indebted to many people for their help, support and inspiration during my journey of six years as a graduate student and a researcher. Firstly, I am grateful to my advisor Dr. M. Saleet Jafri. This dissertation would not be possible without his continuous guidance and support throughout my research work. I am also thankful to our collaborators Dr. W. Jonathan Lederer and Dr. Benjamin L. Prosser for their invaluable help in achieving our research objectives.

I do like to extend my thanks to my dissertation committee members Dr. Dmitri Klimov and Dr. Patrick Gillevet for their guidance and valuable time. I am thankful to Diane St. Germain for providing me with necessary help and information whenever I needed. I also like to thank my friends from the lab Tuan M. Hoang-Trong, Aman Ullah, Sangeeta Shukla, Nasrin Afzal, Roshan Paudel and Lamya Alomair who made my journey as a graduate student memorable. My special thanks to Tuan for his continuous help.

My utmost thanks to my father late Dilli Bahadur Limbu for his contributions in my life although he could not be here to share this moment, to my mother Narmaya Limbu for her eternal support and encouragement and to my sister Kahani Limbu. My hearty thanks to my husband Desh R. Sonyok for his love and support and to my new love Namjung Sonyok, our son.

TABLE OF CONTENTS

LIST OF TABLES

LIST OF FIGURES

ABSTRACT

PREDICTING THE EFFECTS OF STRETCH-ACTIVATED REACTIVE OXYGEN SPECIES SIGNALING ON CARDIAC EXCITATION-CONTRACTION COUPLING

Sarita Limbu, Ph.D.

George Mason University, 2016

Dissertation Director: Dr. M. Saleet Jafri

Calcium (Ca^{2+}) is an important second messenger in cardiac myocytes and regulates the excitation-contraction (EC) coupling, the process which converts electrical signal into the mechanical contraction of the myocytes. Regulation of the Ca^{2+} released from sarcoplasmic reticulum (SR), the Ca^{2+} store in cardiac myocytes, via ryanodine receptor 2 (RyR2), the Ca^{2+} release channel in the SR, is crucial for physiological functioning of the myocyte. Reactive oxygen species (ROS) regulate cardiac Ca^{2+} signaling by oxidizing and increasing the open probability of RyR2s. Stretching of a cardiac myocyte has been shown to induce Nox2 mediated ROS production in a process termed X-ROS signaling that abruptly increases the Ca^{2+} released from the SR. A computational model of the rat cardiac ventricular myocyte with X-ROS signaling was developed. The model was used to investigate the underlying mechanisms of regulation of EC coupling by X-ROS. The X-ROS dependent effects of oxidative stress on EC coupling during pathology, such as heart failure, were studied. Stretching a

cardiomyocyte elevates the intracellular Ca^{2+} concentration via X-ROS but on the other hand, the increase in affinity of troponin for Ca^{2+} increases the Ca^{2+} buffering and decreases the free cytosolic Ca^{2+} concentration. The X-ROS mediated effects of length dependent change in Ca^{2+} binding affinity of troponin and its subsequent effects on Ca^{2+} dynamics were also studied. The model was integrated into the spatial model and the spatial model of a ventricular myocyte model with X-ROS signaling was developed to understand various spatial components which would contribute towards abnormalities such as arrhythmia during pathologies.

CHAPTER 1: INTRODUCTION

ABSTRACT

Reactive oxygen species have been shown to play an important role in cell signaling. Recently, experimental studies have observed that the stretch induced production of reactive oxygen species regulate the release of calcium from the sarcoplasmic reticulum in the heart. This mechanism has been called X-ROS signaling and involves the activation of NADPH oxidase by increasing stress on the microtubule network. This could have significant implications for the regulation of heart function, because calcium is the crucial intermediate step between the electrical excitation of the heart and contraction. This X-ROS signaling mechanism has also been shown to be enhanced in diseases such as Duchenne muscular dystrophy. Experimental studies have explored the X-ROS mechanism in isolated resting cardiac myocytes. To extend to role of X-ROS signaling to more physiological situations, this dissertation has developed a computational modeling of X-ROS signaling in the rat ventricular myocyte and has performed a series of simulations to explore the mechanisms that govern X-ROS signaling and predict its physiological role.

BACKGROUND

The heart is a muscular organ that pumps blood to the entire body through the cardiovascular system comprising of heart, arteries, veins and capillaries. Cardiac muscle cells are striated muscle cells, comprising of repeating functional unit called sarcomeres. A heart beats with the rhythmic contraction and relaxation of the cardiomyocyte which is known as systole and diastole phase of the heart. Action potential, the electrical stimulus, is generated by the sinoatrial (SA) node in the heart and initiates contraction. Membrane bound voltage gated Ca^{2+} channels (L-type Ca^{2+} channel, LCC) in the cardiomyocytes opens in response to the stimulus to allow Ca^{2+} influx into the myocyte which allows more Ca^{2+} release from sarcoplasmic reticulum (SR), the Ca^{2+} store in the myocyte, into the subspace via ryanodine receptors (RyRs, the Ca^{2+} release channels). This elevates the myoplasmic Ca^{2+} concentration and initiates muscle contraction.

Reactive oxygen species (ROS) are highly reactive oxygen derived molecules such as superoxide anion and hydrogen peroxide. ROS oxidizes sulfhydryl (SH) group of cysteine residues in the RyRs and increases the channel open probability. Oxidative stress occurs either by the increase in the ROS production or by the decrease in the reducing capacity of the cell so that the ratio of reducing to oxidizing agents decreases. The result is oxidation of cellular components such as proteins that can cause various pathological conditions. For example, sustained oxidation of the RyRs causes excessive diastolic Ca^{2+} release from SR, depleting the SR Ca^{2+} concentration and thus resulting in a weak systolic force of contraction. Various experiments have shown that physiologic stretch of cardiac myocytes increases Ca^{2+} release from SR by transiently inducing NADPH

oxidase (Nox2) dependent ROS production mediated by the microtubule network (1). , Pathological conditions such as cardiac hypertrophy have been associated with microtubule proliferation (2, 3). Increase in microtubule network density increases stiffness and viscosity of the cytoplasm and induces contractile dysfunction (4). Either microtubule or Nox2 inhibition returns the process of the disease progression back to normal in the diseased cardiac myocytes.

EXCITATION-CONTRACTION COUPLING (ECC)

The heart is a muscular organ that pumps blood through the blood vessels which include arteries, veins and capillaries. Cardiac muscle cells also known as cardiomyocytes are striated muscle cells, composed of bundles of myofibrils with repeating contractile unit called sarcomeres, similar to skeletal muscle cells. The sarcomere is myofilament region between two z-lines and is composed of the thick filament known as myosin and the think filament known as actin. The cardiac cycle of a heart starts with an action potential (AP, the electrical stimulus) and continues till the next AP is generated and comprises of the rhythmic contraction and relaxation of cardiac myocyte separated by isovolumetric contraction and relaxation. The contraction is initiated by an AP generated from the sinoatrial (SA) node. The excitation-contraction coupling (ECC) is the process that transduces the electrical stimulus into the mechanical contraction of the muscle cells.

Ryanodine Receptors (RyRs) are the Ca^{2+} channels located in the membrane of sarcoplasmic reticulum (SR), the Ca^{2+} store in the myocytes. RyRs exist in 3 isoforms

(RyR1, RyR2 & RyR3) and the isoform RyR2 is primarily expressed in the cardiac myocytes. Release of calcium from the calcium store via the calcium channels (RyR2s) and the controlled changes in the free cytosolic calcium concentration controls the process of muscle contraction (5).

In cardiac myocytes, during systole, the AP triggers the influx of Ca^{2+} from extracellular space through the voltage-gated L-type Ca^{2+} channels (LCCs) which results in a small elevation of Ca^{2+} in the dyadic subspace (a small region) in between the L-type Ca^{2+} channel located in t-tubule and cluster of RyR2s located in the membrane of SR (6). This subspace Ca^{2+} triggers the Ca^{2+}-gated RyR2 channels to open causing elementary Ca^{2+} release events termed Ca^{2+} sparks (7), releasing more calcium from sarcoplasmic reticulum (SR) to the subspace and the mechanism is termed Calcium-Induced-Calcium-Release (CICR). CICR produces Ca^{2+} spark as there will be high flow of Ca^{2+} through this cluster of RyR2s termed as Ca^{2+} release unit (CRU). The intracellular Ca^{2+} concentration is significantly increased due to overall contribution from Ca^{2+} sparks produced locally in each CRU. The free cytoplasmic Ca^{2+} binds to troponin C in the actin and causes conformational changes in the tropomyosin, forcing it to reveal the myosin cross-bridge binding site in the actin and thus muscle contraction is initiated. The intracellular Ca^{2+} in the myoplasm is pumped back to the SR by the Sarcoplasmic/Endoplasmic Reticulum Ca^{2+} ATPase (SERCA) pump as well as extruded to the extracellular space via Na^{+}/Ca^{2+} exchanger (NCX) and plasma membrane Ca^{2+} ATPase (PMCA). The resulting depletion of free intracellular Ca^{2+} initiates muscle relaxation during diastole.

It is vital for the RyR2s to function properly to maintain normal physiological condition by maintaining Ca^{2+} homeostasis, which means that RyR2s are to be modulated in such a way that they release large calcium during the muscle contraction and no or very little calcium during muscle relaxation. During diastole, there is a small amount of spontaneous Ca^{2+} release due to Ca^{2+} sparks produced by random opening of the RyR2 channels. Aberrantly high Ca^{2+} release from SR during the diastole due to abnormal modulation of RyR2 channels could result in arrhythmogenic Ca^{2+} waves and this inefficiency in Ca^{2+} handling could give rise to many pathological conditions.

The cardiac muscle isoform of the ryanodine receptor (RyR2) is regulated by various ions (such as calcium (Ca^{2+}), magnesium (Mg^{2+})) and proteins such as calsequestrin (CSQ), calmodulin (CaM), triadin and kinases (8). Various phosphorylation sites and free cysteines, that could undergo redox modification, have been identified in the RyR channels. Both, phosphorylation by kinases (PKA and CaMKII) and oxidation by thiols oxidizing reagents, have been identified as the mechanism that increases [Ca^{2+}] sensitivity of a channel and increases its open probability (9). Hence, phosphorylation/dephosphorylation and reduction/oxidation (redox) modification are the key mechanisms for modulating the RyR channels activities. Ca^{2+} is a very important second messenger of the signaling cascade that controls the muscle contraction and relaxation.

REACTIVE OXYGEN SPECIES (ROS)

Reactive oxygen species (ROS) are oxygen derived molecules and is believed to play a significant role in the physiological processes. When oxygen (O_2) undergo incomplete reduction, reactive oxygen species (ROS) such as superoxide anion ($\cdot O_2^-$), hydrogen peroxide (H_2O_2), and hydroxyl ion ($\cdot OH$) are produced. ROS are highly reactive molecules.

$$O_2 + e^- \rightarrow \cdot O_2^- + e^- \rightarrow H_2O_2 + e^- \rightarrow \cdot OH + e^- \rightarrow H_2O + O_2$$

ROS are produced, either as the byproducts of reactions involving oxygen (for example, by mitochondria during oxidative phosphorylation due to e^- leakage from complex I and complex III of electron transport chain that reduces O_2 molecules), or by nicotinamide adenine dinucleotide phosphate (NADPH) oxidase (NOX) family. NOX is a membrane-bound protein that produces superoxide anion (O_2^-) by transferring electrons from NADPH to oxygen molecules (O_2) across the membrane (10) and is the major ROS producer in the cardiac muscles. Superoxide anions are short-lived as they are immediately dismutated to H_2O_2 either spontaneously or by the enzyme superoxide dismutase (SOD).

$$\cdot O_2^- \xrightarrow{\text{SOD}} H_2O_2 \xrightarrow{\text{Catalase/GSPx}} H_2O$$

The intermediate product H_2O_2 is further reduced to H_2O molecules by ROS scavengers which include catalase and glutathione peroxidase (GSPx). But instead of being reduced to H_2O by scavengers, H_2O_2 may undergo Fenton reaction in the presence of free metals (Fe, Cu) to form highly reactive $\cdot OH$.

$$Fe^{2+} + H_2O_2 + H^+ \rightarrow Fe^{3+} + \cdot OH + H_2O$$

Oxidative stress arises when the ratio of oxidizing agent to its reducing agents/scavengers increases above physiological limit which can lead to various pathological conditions such as inflammation, hypertrophy, apoptosis and fibrosis. SOD, catalase and GSPx are the main enzymes actively involved in cellular defense against oxidative stress and its negative consequences, either by directly scavenging ROS or by reducing mechanism. A physiological balance should be maintained between the total ROS production and its removal for normal functioning of the cell. The normal physiological level of H_2O_2 is as low as 20 nM and the concentration above 1 μM is estimated to be toxic to the cell (11). The phagocytic respiratory ROS burst increases the level of H_2O_2 concentration to 5-15 μM during inflammation (12).

Under normal condition, ROS is believed to play a significant role in the physiological processes including cellular signaling, cell growth, apoptosis, aging process, apoptosis, gene expression and defense against microbial pathogens(10, 13). $\cdot O_2^-$ and $\cdot OH$ are extremely unstable as they are highly reactive. H_2O_2 is comparatively more stable and is believed to be the one involved in cellular signaling. H_2O_2 is highly reactive towards cysteine residues than towards free cysteine or loosely bound metals (11). ROS can mediate the posttranslational modifications of various proteins and regulate their activity or also can activate enzymes such as protein kinase A (PKA), calcium/calmodulin-dependent protein kinase II (CaMKII) which can modulate the activities of these proteins.

NADPH Oxidase (NOX), the source of ROS

NOX is the only source of ROS whose sole known function is to produce ROS, all other sources produce ROS as byproduct. The transmembrane proteins of NOX family produce ROS by transferring electrons from NADPH across the membrane to reduce oxygen molecule to produce superoxide anion (ROS) (10). Five known isoforms of NOX exist, NOX1, NOX2, NOX3, NOX4 and NOX5. The first NOX identified responsible for the phagocytic respiratory burst and ROS production was gp91phox, now known as Nox2 (the NOX2 isoform of NOX). Nox2 is located in the membrane along with $p22^{phox}$ (gp91phox and $p22^{phox}$ together is known as cytochrome b_{558}), which stabilizes Nox2. Activation of Nox2 for ROS production requires translocation of other cytosolic subunits $p47^{phox}$, $p67^{phox}$, $p40^{phox}$ and Rac1 to the Nox2/$p22^{phox}$ complex. $p47^{phox}$ is a regulatory protein which undergoes conformational change when phosphorylated and translocates to the membrane bound complex along with other proteins $p67^{phox}$ and $p40^{phox}$. $p67^{phox}$ is the activator subunit of this complex that activates Nox2.

RyR and ROS

ROS is involved in cellular signaling by mediating the posttranslational modifications of various proteins. Some of the targets of ROS in the cardiac myocytes include RyR2s, Na^+/Ca^{2+} exchanger (NCX), SERCA pump and L-type Ca^{2+} channels (14). The RyR2 has a total of 364 cysteine residues and approximately 84 are free i.e. in a reduced state (15). ROS can oxidize sulfhydryl (SH) groups of these free cysteine residues in the RyR2 channels (14, 16). This activates these Ca^{2+} channels to increase

their cytosolic $[Ca^{2+}]_i$ sensitivity, increases their open probability (9, 17) and hence increases the Ca^{2+} sparks frequency. In the 80's, oxidation of sulfhydryl group (in the Ca^{2+} channels) to disulfide group by metals (18, 19) and oxidizing compounds (20) were shown to increase the release of calcium from the SR and the addition of reducing agents such as glutathione (GSH) or dithiothreitol (DTT) reversed this increase in calcium release (19, 20). Abramson and Salama (21) in 1989 presented a conceptual model which suggested that reversible oxidation and reduction of SH groups in RyRs resulted in the opening and closing of the Ca^{2+} channels.

Modulation of RyR2 activity by redox active compounds depends on the type and concentration of these compounds. The overall concentration of oxidizing and reducing agents in a cell determines the intracellular redox potential of the cell (14). At smaller concentrations, the redox active compounds are capable of reversibly oxidizing the RyR2s (or any other targets) and make them function optimally. But at larger concentrations and prolonged exposure in diseased state, these compounds can activate RyR2s irreversibly (16, 22). Increased RyR2 open probability resulting in an increased SR Ca^{2+} leak and decreased SR Ca^{2+}causing reduced SR Ca^{2+} concentration has been identified as the cause of the reduction in cytoplasmic Ca^{2+} concentration and impaired muscle contractility in diseased condition such as heart failure (23). ROS/reactive nitrogen species (RNS) are the major redox active compounds that can activate RyR2 by oxidation/nitrosylation.

In the event of pathological conditions, the level of ROS increases and the redox modification of RyR2 channels by ROS causes the SR Ca^{2+} leak (24).This type of

aberrant Ca^{2+} dynamics leads to conditions including arrhythmias and myocardial dysfunction.

STRETCHING MYOCYTES

A regular heart-beat comprises of rhythmic contraction and relaxation of myocytes. The myocytes stretching depends on the diastolic load imposed by the blood volume during relaxation (diastole) and affects the force of contraction. Larger the volume of blood filling the ventricles (end diastolic volume, EDV) greater will be the force of contraction of the heart. This is known as the Frank-Starling law. Stretch-activated channels (SACs) have been implicated in the stretch-induced changes in the cytosolic Ca^{2+} concentration in various cells.

Mechanotransduction is the conversion of a mechanical stimulus into a cellular response. Various stretch-activated mechanotransduction signaling pathways have been identified in cardiac myocytes (25). Prosser et al have demonstrated that physiologically stretching the cardiac myocyte activates a mechano-chemo transduction pathway where mechanical stress is transduced to change in myoplasmic Ca^{2+} concentration by a Nox2 mediated increase in ROS production in a process termed X-ROS signaling (1). Diastolic stretching of rat ventricular myocytes has been shown experimentally to cause a burst of Ca^{2+} sparks resulting from the rapid release of Ca^{2+} from the sarcoplasmic reticulum (SR). N-acetylcysteine (NAC), an antioxidant which scavenges ROS and RNS, blocked the stretch-induced burst of Ca^{2+} sparks which implies that the oxidation of RyRs by ROS is the main reason for this abnormally high amount of Ca^{2+} sparks. Diphenyleneiodonium

(DPI), a NOX inhibitor, also blocked the stretch-induced burst of Ca^{2+} sparks which suggests that NOX is the source of ROS that oxidizes RyR2 to increase their open probability and hence, produce the stretch-induced burst of Ca^{2+} sparks. Depolymerizing microtubule with colchicine also blocked the stretch-induced burst of Ca^{2+} sparks as well as the stretch-induced increase in ROS production suggesting that stretch-activated ROS production (and hence, burst of Ca^{2+} sparks) requires activation of NOX2 via microtubule network involving a mechano-chemo signal transduction pathway. Inhibition of Rac1, a microtubule associated protein (26) and a required subunit for Nox2 activation (10), blocked the stretch-induced ROS production. The physiologic stretch of dystrophic skeletal muscle of mdx mouse, a model of Duchenne muscular dystrophy (DMD), activated NADPH Oxidase dependent ROS production via microtubule dependent pathway (27). Stretch increased microtubule network density in adult mdx mice or in young mdx mice treated with Taxol (chemical that polymerizes microtubules) and increased the ROS production. Treatment with microtubule network destabilizer or Nox2 inhibitor, both inhibited the stretch-activated X-ROS production suggesting that the microtubule-dependent ROS production by Nox2 underlie dysfunction in DMD.

Mechanical Stretch Increases SR Ca^{2+} Release

Axial stretching of guinea pig ventricular myocytes enhanced the SR Ca^{2+} leak reducing the SR Ca^{2+} concentration than compared at shorter length (28). Stretching cardiac myocytes have been shown to cause an abrupt increase in Ca^{2+} spark rate (1, 29, 30) and this increase in spark rate was reversed when the stretching was removed (1, 29).

Axial stretching of rat ventricular myocytes caused an abrupt increase in Ca^{2+} spark rate reducing the SR Ca^{2+} concentration, sustained stretching of the myocyte for 1 min almost returned the Ca^{2+} spark rate to the control level, blocking the stretch-activated channels and nitric oxide synthesis did not affect the stretch-induced increase in the Ca^{2+} spark rate, and applying colchicine eliminated the stretch-induced increase in the Ca^{2+} spark rate suggesting microtubule mediated modulation of ryanodine receptor function could be the cause of the increase in Ca^{2+} spark rate (30).

Mechanical Stress Activates/Proliferates Microtubules

Mechanical stress such as stretching or pressure overload has been associated with microtubule proliferation in the cardiac myocytes. Pressure overloading causes proliferation of the microtubules in the cardiac myocytes cytoskeleton and deteriorates contractile function of the muscle and application of colchicine, which depolymerizes microtubule, normalized the contractility in the myocytes (31, 32). Microtubule polymerization by taxol increases the stiffness and viscosity of the cytoplasm and thus, results in contractile dysfunction in the muscles due to pressure overload (4). Both the contractile activity and the stretching of neonatal rat cardiac myocytes was shown to increase β-tubulin (which polymerizes to microtubules) by increasing β-tubulin mRNA (33). Tachycardia-induced cardiomyopathy, associated with left ventricular dilation and increased wall stress also increased tubulin content in pigs cardiac myocytes (34). Stretch-induced arrhythmia increases in cardiac myocytes treated with taxol which polymerizes microtubules, whereas there was no increase in cardiac myocytes treated

with colchicine indicating that the stretch-induced arrhythmias are mediated by the microtubule proliferation (35). Treatment with colchicine inhibited microtubule polymerization in stretch-induced hypertrophy of rat ventricular myocytes (36). Microtubule proliferation was also observed in the right ventricle of rat myocytes with pulmonary hypertension but this did not have an effect on the muscle contraction (37).

Nox2 as the source of ROS production

Cytochrome b_{558} consists of gp91phox (now known as Nox2) and p22phox (38). Cytochrome b_{558} was first associated with ROS production in phagocytes in 1978 (39). Cytochrome b_{558} was identified as a missing component in the neutrophils of all four chronic granulomatous disease (CGD) patients. CGD is a disease associated with difficulty in ROS production needed to kill pathogens ingested inside phagocytes. ROS produced by NADPH oxidase activity stimulates Ca^{2+} release in skeletal muscles by activating the RyR1 channels (40). Expression of NADPH oxidase subunits gp91phox, p67phox and rac1 were increased in the skeletal muscle of mdx mice along with the superoxide production leading to oxidative stress (41). Inhibition of NADPH oxidase activity reduced the resulting intracellular rise in Ca^{2+}. Mechanical stretch has been shown to induce increased ROS production by increasing NOX activity in endothelial cells (42, 43), pulmonary epithelial cells (44) and retinal pericytes (45).

ROS IN CARDIAC DISEASES

Cardiac hypertrophy is the situation of enlargement of heart due to an increase in the myocyte size due to chronic hypertension or myocardial infarction (MI) and is associated with contractile dysfunction eventually leading to heart failure. Various cardiac and endothelial pathological conditions including MI, cardiac hypertrophy, cardiomyopathy, heart valve disease, coronary artery disease (CAD) and hypertension can lead to heart failure (HF). Various phenotypes which could end up in HF include hypertrophy, contractile dysfunction, arrhythmia, ventricular remodeling and cell death. HF is a diseased condition when the heart is not able to pump enough amount of blood as required by the body. Shortness of breath, swollen feet and fatigue/exercise intolerance are the common symptoms of HF.

Pathological stresses including pressure/volume overload and hypoxia accelerate protein synthesis and increases number of sarcomeres in terminally differentiated myocytes resulting in compensatory hypertrophy of myocytes (46) with compensated structure and function. AngiotensinII, catecholamines, or aldosterone could be one of various factors that could activate myocyte hypertrophic signaling pathways mediated by ROS. Hypertrophic condition of heart is a form of adaptation against the oxidative stress and has been associated with increased antioxidant enzyme activity (47). Oxidative stress is responsible for these phenotypes such as myocardial dysfunction, ventricular remodeling and apoptosis which are implicated in the progression of HF (48).

Myocyte apoptosis is the cause for ventricular remodeling and HF progression (49, 50). Also, the apoptosis could contribute to myocardial restoration after injury by

replacement via mitosis but an imbalance between myocyte loss and replacement could lead to the progression of HF (51). Oxidative stress is responsible for the cardiomyocyte apoptosis by activating various death pathways such as the sustained activation of calcium-calmodulin kinase II (CaMKII) (52) or the activation of mitochondrial permeability transition pore (MPTP) mitochondrial death pathway (53). A smaller increase of ROS causes myocytes hypertrophy whereas a larger increase causes apoptosis (54). Whereas, apoptosis is found to be inhibited by antioxidants or substances with antioxidant activities (55).

Microtubule proliferation was observed in pressure overload induced left ventricular hypertrophy in human (2) as well as in animals (3). Microtubule depolymerization has been found to normalize the pressure overload induced left ventricular hypertrophy (3). A persistent and progressive increase in the microtubule network density observed in the myocytes during transition from hypertrophy to heart failure was normalized by microtubule depolymerization (56). β-adrenoceptor activation-induced cardiac myopathy and heart failure in mice showed increased Nox2-induced ROS production and Nox2 inhibitor preserved contractile function (57). Doxorubicin chemotherapy induces contractile dysfunction and cardiac remodeling by Nox2-induced ROS production and these cardiac dysfunctions were attenuated in Nox2-deficient mice (58). Cardiomyocyte of Rac1 null mice induced no pressure overload hypertrophy (59). These findings suggest that either microtubule network or Nox2 or Rac1 can be targeted for therapeutic intervention in order to eliminate the excessive ROS production leading to the progression of cardiac diseases.

MYOCYTE MODELS

A cardiac computational model comprises of mathematical equations representing every transmembrane ionic mechanisms as electrical events such as current and voltage. Due to the similarities between cardiac and nerve cells, most of the cardiac computational models are based on the Hodgkin-Huxley model (60) that describes action potential in squid nerve axon. These models of the heart are developed based on the data obtained experimentally. Computational models of the heart using differential equations to represent kinetics of ion channels carry a long history beginning as early as 1960 for Purkinje cell by Noble (61) that included sodium and potassium currents. Since then, various cardiac computational models have been developed for different types of cardiac myocytes such as Purknje cells (62, 63), ventricular cells (64-66), atrial cells (67-69) and sinoatrial node cells (70). The cardiac ventricular myocytes model was first published in 1977 by Beeler and Reuter (64) that included excitatory inward sodium current, slow inward calcium current and various outward potassium currents and was the basis for many models in the later years. DiFrancesco and Noble in 1985 developed a Purkinje fibre model (63) which was the extension of the MNT model (62) developed in 1975 and Beeler and Reuter model (64) and was the first model to incorporate intracellular and extracellular ion concentration changes, sodium-calcium exchange pump, sodium-potassium exchange pump and the calcium-induced calcium release hypothesis by Fabiato and Fabiato (71). Hilgemann and Noble model developed in 1987 (67) was the earliest atrial cell model and was a rabbit model that incorporated Ca^{2+} dynamics

associated with sodium-calcium exchange, calcium channels and SR to generate action potential, and intracellular and extracellular Ca^{2+} transients.

The mammalian ventricular myocyte model by Beeler and Reuter was later modified for guinea pig by Luo and Rudy in 1991 which is known as LR1 or Luo-Rudy phase I model (65) and again in 1994 which is known as LR2 or Luo-Rudy phase II model (66). Fast inward sodium current and outward potassium currents were formulated in LR1 model while retaining the Beeler and Reuter's formulation of slow inward current. The LR2 or phase II model included more detailed Ca^{2+} regulatory processes where SR is subcompartmentalized to junctional SR (JSR) and network SR (NSR). The model incorporated pumps and exchangers, Ca^{2+} translocation from NSR to JSR, Ca^{2+} leak from NSR and Ca^{2+} release from JSR. The model also included Ca^{2+} buffers troponin and calmodulin in the myoplasm, and calsequestrin in the SR. All of these components contributed in the more precise simulation of dynamic change in intracellular Ca^{2+} ion concentration. Priebe-Beuckelmann model is the human heart model developed based on the LR2 model in 1998 (72) for heart failure condition.

The Ca^{2+} released from SR is a continuous function of the amount of trigger Ca^{2+} entering via L-type Ca^{2+} channel, a phenomenon termed as graded Ca^{2+} release, first observed by Fabiato et al and the ratio of Ca^{2+} released to the trigger Ca^{2+} is termed as ECC gain. But these earlier models were deterministic common pool models that failed to capture the graded release phenomenon as shown by Stern. The common pool model assumes that the trigger calcium and the released calcium efflux into a common pool and due to calcium-induced calcium release the Ca^{2+} concentration in this pool results in all-

or-none instead of graded Ca^2 release from the deterministic model of the SR ion channels. In order to capture the graded Ca^{2+} release, Stern formulated two main concepts: 1) "local control" and 2) stochastic opening of Ca^{2+} channels. In the "local control" model, one L-type calcium channel triggers only a set of directly opposed SR channels. Stern demonstrated that the stochastic opening of both the L-type calcium channels and SR channels along with "local control" model could capture the graded Ca^{2+} release.

Jafri, Rice and Winslow developed a cardiac ventricular myocyte model in 1998 (73) that first introduced restricted subspace, which is the total of all the dyadic subspaces, located between T-tubule and JSR where the Ca^{2+} from both the L-type Ca^{2+} channel and the RyR empty into. The model was based on LR2 model for the membrane currents and Ca^{2+} buffers, on Imredy and Yue's mode switching concept (74) for L-type Ca^{2+} channel model and on Keizer and Levine's RyR model with adaptation (75) for the RyR model which made the model simulate the calcium dynamics more realistically. This model was also the first model to develop Markov model for the L-type calcium channels for stochasticity to produce mechanistic ECC. Many later models incorporated Markov model of ion channels.

RESEARCH OBJECTIVES

The mechanisms behind the increase in sparks rate during diastolic stretch of a cardiomyocyte were investigated. The rat ventricular myocyte model by Wagner et al. (76) is used to incorporate the X-ROS signaling and a 4-state RyR2 model that

demonstrates the sudden burst of Ca^{2+} sparks after the stretching of the myocytes has been developed (77). When the myocyte is stretched, the stretch-induced ROS may oxidize the RyR2, increase their sensitivity to cytosolic Ca^{2+} and increase their probability of opening. The model is a compartmental model where the subspace, SR and myoplasm are considered as a single compartment with equal Ca^{2+} concentration everywhere. This newly developed model was used in investigating impacts such stretch-induced ROS could have upon the Ca^{2+} transients and other physiological parameters of EC coupling during physiological as well as pathological conditions in order to get an in-depth understanding of the mechanisms behind X-ROS signaling and its physiological implications. For example, the following topics have been investigated in this dissertation:

- Oxidative stress has been implicated in many cardiac diseases which progress to heart failure conditions. Hence, the impact of oxidative stress in the X-ROS signaling was investigated.
- Troponin C (TnC) is the Ca^{2+} buffer in the myofilament that undergoes conformational change when Ca^{2+} binds to it and thus, exposes the myosin binding sites on actin to initiate muscle contraction. Stretching the myocyte also increases the Ca^{2+} binding affinity of TnC and thus, slightly reduces the $[Ca^{2+}]_i$ elevated due to X-ROS signaling. This stretch-induced characteristic of cardiomyocyte was also studied to understand the impact of stretch on Ca^{2+} transient and on Ca^{2+} buffering by integrating the length dependent change in the calcium binding affinity of troponin.

- The spatial extent of X-ROS signaling was studied using a new spatial model of a rat ventricular myocyte developed. This model is used in studying the effect of stretch-induced ROS in diseased condition such as Duchenne's muscular dystrophy and how it might contribute to cardiac arrhythmia.

REFERENCES

1. Prosser, B. L., C. W. Ward, and W. J. Lederer. 2011. X-ROS signaling: rapid mechano-chemo transduction in heart. Science 333:1440-1445.

2. Zile, M. R., G. R. Green, G. T. Schuyler, G. P. Aurigemma, D. C. Miller, and G. t. Cooper. 2001. Cardiocyte cytoskeleton in patients with left ventricular pressure overload hypertrophy. Journal of the American College of Cardiology 37:1080-1084.

3. Koide, M., M. Hamawaki, T. Narishige, H. Sato, S. Nemoto, G. DeFreyte, M. R. Zile, G. I. Cooper, and B. A. Carabello. 2000. Microtubule depolymerization normalizes in vivo myocardial contractile function in dogs with pressure-overload left ventricular hypertrophy. Circulation 102:1045-1052.

4. Tagawa, H., N. Wang, T. Narishige, D. E. Ingber, M. R. Zile, and G. t. Cooper. 1997. Cytoskeletal mechanics in pressure-overload cardiac hypertrophy. Circulation research 80:281-289.

5. Bers, D. M. 2002. Cardiac excitation-contraction coupling. Nature 415:198-205.

6. Capes, E. M., R. Loaiza, and H. H. Valdivia. 2011. Ryanodine receptors. Skeletal muscle 1:18.

7. Cheng, H., W. J. Lederer, and M. B. Cannell. 1993. Calcium sparks: elementary events underlying excitation-contraction coupling in heart muscle. Science 262:740-744.

8. Franzini-Armstrong, C., and F. Protasi. 1997. Ryanodine receptors of striated muscles: a complex channel capable of multiple interactions. Physiological reviews 77:699-729.

9. Niggli, E., N. D. Ullrich, D. Gutierrez, S. Kyrychenko, E. Polakova, and N. Shirokova. 2013. Posttranslational modifications of cardiac ryanodine receptors: Ca(2+) signaling and EC-coupling. Biochimica et biophysica acta 1833:866-875.

10. Bedard, K., and K. H. Krause. 2007. The NOX family of ROS-generating NADPH oxidases: physiology and pathophysiology. Physiological reviews 87:245-313.

11. D'Autreaux, B., and M. B. Toledano. 2007. ROS as signalling molecules: mechanisms that generate specificity in ROS homeostasis. Nature reviews. Molecular cell biology 8:813-824.

12. Chen, K., and J. F. Keaney, Jr. 2012. Evolving concepts of oxidative stress and reactive oxygen species in cardiovascular disease. Current atherosclerosis reports 14:476-483.

13. Hancock, J. T., R. Desikan, and S. J. Neill. 2001. Role of reactive oxygen species in cell signalling pathways. Biochemical Society transactions 29:345-350.

14. Zima, A. V., and L. A. Blatter. 2006. Redox regulation of cardiac calcium channels and transporters. Cardiovascular research 71:310-321.

15. Xu, L., J. P. Eu, G. Meissner, and J. S. Stamler. 1998. Activation of the cardiac calcium release channel (ryanodine receptor) by poly-S-nitrosylation. Science 279:234-237.

16. Marengo, J. J., C. Hidalgo, and R. Bull. 1998. Sulfhydryl oxidation modifies the calcium dependence of ryanodine-sensitive calcium channels of excitable cells. Biophys J 74:1263-1277.

17. Anzai, K., K. Ogawa, A. Kuniyasu, T. Ozawa, H. Yamamoto, and H. Nakayama. 1998. Effects of hydroxyl radical and sulfhydryl reagents on the open probability of the purified cardiac ryanodine receptor channel incorporated into planar lipid bilayers. Biochemical and biophysical research communications 249:938-942.

18. Abramson, J. J., J. L. Trimm, L. Weden, and G. Salama. 1983. Heavy metals induce rapid calcium release from sarcoplasmic reticulum vesicles isolated from skeletal muscle. Proceedings of the National Academy of Sciences of the United States of America 80:1526-1530.

19. Trimm, J. L., G. Salama, and J. J. Abramson. 1986. Sulfhydryl oxidation induces rapid calcium release from sarcoplasmic reticulum vesicles. The Journal of biological chemistry 261:16092-16098.

20. Zaidi, N. F., C. F. Lagenaur, J. J. Abramson, I. Pessah, and G. Salama. 1989. Reactive disulfides trigger Ca2+ release from sarcoplasmic reticulum via an oxidation reaction. The Journal of biological chemistry 264:21725-21736.

21. Abramson, J. J., and G. Salama. 1989. Critical sulfhydryls regulate calcium release from sarcoplasmic reticulum. Journal of bioenergetics and biomembranes 21:283-294.

22. Santos, C. X., N. Anilkumar, M. Zhang, A. C. Brewer, and A. M. Shah. 2011. Redox signaling in cardiac myocytes. Free radical biology & medicine 50:777-793.

23. Kubalova, Z., D. Terentyev, S. Viatchenko-Karpinski, Y. Nishijima, I. Gyorke, R. Terentyeva, D. N. da Cunha, A. Sridhar, D. S. Feldman, R. L. Hamlin, C. A. Carnes, and S. Gyorke. 2005. Abnormal intrastore calcium signaling in chronic heart failure. Proceedings of the National Academy of Sciences of the United States of America 102:14104-14109.

24. Terentyev, D., I. Gyorke, A. E. Belevych, R. Terentyeva, A. Sridhar, Y. Nishijima, E. C. de Blanco, S. Khanna, C. K. Sen, A. J. Cardounel, C. A. Carnes, and S. Gyorke. 2008. Redox modification of ryanodine receptors contributes to sarcoplasmic reticulum Ca2+ leak in chronic heart failure. Circulation research 103:1466-1472.

25. Lammerding, J., R. D. Kamm, and R. T. Lee. 2004. Mechanotransduction in cardiac myocytes. Annals of the New York Academy of Sciences 1015:53-70.

26. Best, A., S. Ahmed, R. Kozma, and L. Lim. 1996. The Ras-related GTPase Rac1 binds tubulin. The Journal of biological chemistry 271:3756-3762.

27. Khairallah, R. J., G. Shi, F. Sbrana, B. L. Prosser, C. Borroto, M. J. Mazaitis, E. P. Hoffman, A. Mahurkar, F. Sachs, Y. Sun, Y. W. Chen, R. Raiteri, W. J. Lederer, S. G. Dorsey, and C. W. Ward. 2012. Microtubules underlie dysfunction in duchenne muscular dystrophy. Science signaling 5:ra56.

28. Iribe, G., and P. Kohl. 2008. Axial stretch enhances sarcoplasmic reticulum Ca2+ leak and cellular Ca2+ reuptake in guinea pig ventricular myocytes: experiments and models. Progress in biophysics and molecular biology 97:298-311.

29. Petroff, M. G., S. H. Kim, S. Pepe, C. Dessy, E. Marban, J. L. Balligand, and S. J. Sollott. 2001. Endogenous nitric oxide mechanisms mediate the stretch dependence of Ca2+ release in cardiomyocytes. Nature cell biology 3:867-873.

30. Iribe, G., C. W. Ward, P. Camelliti, C. Bollensdorff, F. Mason, R. A. Burton, A. Garny, M. K. Morphew, A. Hoenger, W. J. Lederer, and P. Kohl. 2009. Axial stretch of rat single ventricular cardiomyocytes causes an acute and transient increase in Ca2+ spark rate. Circulation research 104:787-795.

31. Tsutsui, H., K. Ishihara, and G. t. Cooper. 1993. Cytoskeletal role in the contractile dysfunction of hypertrophied myocardium. Science 260:682-687.

32. Zile, M. R., M. Koide, H. Sato, Y. Ishiguro, C. H. Conrad, J. M. Buckley, J. P. Morgan, and G. t. Cooper. 1999. Role of microtubules in the contractile dysfunction of hypertrophied myocardium. Journal of the American College of Cardiology 33:250-260.

33. Watson, P. A., R. Hannan, L. L. Carl, and K. E. Giger. 1996. Contractile activity and passive stretch regulate tubulin mRNA and protein content in cardiac myocytes. The American journal of physiology 271:C684-689.

34. Eble, D. M., and F. G. Spinale. 1995. Contractile and cytoskeletal content, structure, and mRNA levels with tachycardia-induced cardiomyopathy. The American journal of physiology 268:H2426-2439.

35. Parker, K. K., L. K. Taylor, J. B. Atkinson, D. E. Hansen, and J. P. Wikswo. 2001. The effects of tubulin-binding agents on stretch-induced ventricular arrhythmias. European journal of pharmacology 417:131-140.

36. Yutao, X., W. Geru, B. Xiaojun, G. Tao, and M. Aiqun. 2006. Mechanical stretch-induced hypertrophy of neonatal rat ventricular myocytes is mediated by beta(1)-integrin-microtubule signaling pathways. European journal of heart failure 8:16-22.

37. Stones, R., D. Benoist, M. Peckham, and E. White. 2013. Microtubule proliferation in right ventricular myocytes of rats with monocrotaline-induced pulmonary hypertension. Journal of molecular and cellular cardiology 56:91-96.

38. Vignais, P. V. 2002. The superoxide-generating NADPH oxidase: structural aspects and activation mechanism. Cellular and molecular life sciences : CMLS 59:1428-1459.

39. Segal, A. W., O. T. Jones, D. Webster, and A. C. Allison. 1978. Absence of a newly described cytochrome b from neutrophils of patients with chronic granulomatous disease. Lancet 2:446-449.

40. Hidalgo, C., G. Sanchez, G. Barrientos, and P. Aracena-Parks. 2006. A transverse tubule NADPH oxidase activity stimulates calcium release from isolated triads via

ryanodine receptor type 1 S -glutathionylation. The Journal of biological chemistry 281:26473-26482.

41. Whitehead, N. P., E. W. Yeung, S. C. Froehner, and D. G. Allen. 2010. Skeletal muscle NADPH oxidase is increased and triggers stretch-induced damage in the mdx mouse. PloS one 5:e15354.
42. Hishikawa, K., and T. F. Luscher. 1997. Pulsatile stretch stimulates superoxide production in human aortic endothelial cells. Circulation 96:3610-3616.

43. Howard, A. B., R. W. Alexander, R. M. Nerem, K. K. Griendling, and W. R. Taylor. 1997. Cyclic strain induces an oxidative stress in endothelial cells. The American journal of physiology 272:C421-427.

44. Chapman, K. E., S. E. Sinclair, D. Zhuang, A. Hassid, L. P. Desai, and C. M. Waters. 2005. Cyclic mechanical strain increases reactive oxygen species production in pulmonary epithelial cells. American journal of physiology. Lung cellular and molecular physiology 289:L834-841.

45. Suzuma, I., T. Murakami, K. Suzuma, H. Kaneto, D. Watanabe, T. Ojima, Y. Honda, H. Takagi, and N. Yoshimura. 2007. Cyclic stretch-induced reactive oxygen species generation enhances apoptosis in retinal pericytes through c-jun NH2-terminal kinase activation. Hypertension 49:347-354.

46. Katz, A. M. 1994. The cardiomyopathy of overload: an unnatural growth response in the hypertrophied heart. Annals of internal medicine 121:363-371.

47. Gupta, M., and P. K. Singal. 1989. Higher antioxidative capacity during a chronic stable heart hypertrophy. Circulation research 64:398-406.

48. Korantzopoulos, P., D. Galaris, D. Papaioannides, and K. Siogas. 2003. The possible role of oxidative stress in heart failure and the potential of antioxidant intervention. Medical science monitor : international medical journal of experimental and clinical research 9:RA120-125.

49. Wencker, D., M. Chandra, K. Nguyen, W. Miao, S. Garantziotis, S. M. Factor, J. Shirani, R. C. Armstrong, and R. N. Kitsis. 2003. A mechanistic role for cardiac myocyte apoptosis in heart failure. The Journal of clinical investigation 111:1497-1504.

50. van Empel, V. P., A. T. Bertrand, L. Hofstra, H. J. Crijns, P. A. Doevendans, and L. J. De Windt. 2005. Myocyte apoptosis in heart failure. Cardiovascular research 67:21-29.

51. Hare, J. M. 2001. Oxidative stress and apoptosis in heart failure progression. Circulation research 89:198-200.

52. Palomeque, J., O. V. Rueda, L. Sapia, C. A. Valverde, M. Salas, M. V. Petroff, and A. Mattiazzi. 2009. Angiotensin II-induced oxidative stress resets the Ca2+ dependence of Ca2+-calmodulin protein kinase II and promotes a death pathway conserved across different species. Circulation research 105:1204-1212.

53. Remondino, A., S. H. Kwon, C. Communal, D. R. Pimentel, D. B. Sawyer, K. Singh, and W. S. Colucci. 2003. Beta-adrenergic receptor-stimulated apoptosis in cardiac myocytes is mediated by reactive oxygen species/c-Jun NH2-terminal kinase-dependent activation of the mitochondrial pathway. Circulation research 92:136-138.

54. Siwik, D. A., J. D. Tzortzis, D. R. Pimental, D. L. Chang, P. J. Pagano, K. Singh, D. B. Sawyer, and W. S. Colucci. 1999. Inhibition of copper-zinc superoxide dismutase induces cell growth, hypertrophic phenotype, and apoptosis in neonatal rat cardiac myocytes in vitro. Circulation research 85:147-153.

55. Buttke, T. M., and P. A. Sandstrom. 1994. Oxidative stress as a mediator of apoptosis. Immunology today 15:7-10.

56. Tagawa, H., M. Koide, H. Sato, and G. t. Cooper. 1996. Cytoskeletal role in the contractile dysfunction of cardiocytes from hypertrophied and failing right ventricular myocardium. Proceedings of the Association of American Physicians 108:218-229.

57. Xu, Q., A. Dalic, L. Fang, H. Kiriazis, R. H. Ritchie, K. Sim, X. M. Gao, G. Drummond, M. Sarwar, Y. Y. Zhang, A. M. Dart, and X. J. Du. 2011. Myocardial oxidative stress contributes to transgenic beta(2)-adrenoceptor activation-induced cardiomyopathy and heart failure. British journal of pharmacology 162:1012-1028.

58. Zhao, Y., D. McLaughlin, E. Robinson, A. P. Harvey, M. B. Hookham, A. M. Shah, B. J. McDermott, and D. J. Grieve. 2010. Nox2 NADPH oxidase promotes pathologic cardiac remodeling associated with Doxorubicin chemotherapy. Cancer research 70:9287-9297.

59. Satoh, M., H. Ogita, K. Takeshita, Y. Mukai, D. J. Kwiatkowski, and J. K. Liao. 2006. Requirement of Rac1 in the development of cardiac hypertrophy. Proceedings of the National Academy of Sciences of the United States of America 103:7432-7437.

60. Hodgkin, A. L., and A. F. Huxley. 1952. A quantitative description of membrane current and its application to conduction and excitation in nerve. The Journal of physiology 117:500-544.

61. Noble, D. 1960. Cardiac action and pacemaker potentials based on the Hodgkin-Huxley equations. Nature 188:495-497.

62. McAllister, R. E., D. Noble, and R. W. Tsien. 1975. Reconstruction of the electrical activity of cardiac Purkinje fibres. The Journal of physiology 251:1-59.

63. DiFrancesco, D., and D. Noble. 1985. A model of cardiac electrical activity incorporating ionic pumps and concentration changes. Philosophical transactions of the Royal Society of London. Series B, Biological sciences 307:353-398.

64. Beeler, G. W., and H. Reuter. 1977. Reconstruction of the action potential of ventricular myocardial fibres. The Journal of physiology 268:177-210.

65. Luo, C. H., and Y. Rudy. 1991. A model of the ventricular cardiac action potential. Depolarization, repolarization, and their interaction. Circulation research 68:1501-1526.

66. Luo, C. H., and Y. Rudy. 1994. A dynamic model of the cardiac ventricular action potential. I. Simulations of ionic currents and concentration changes. Circulation research 74:1071-1096.

67. Hilgemann, D. W., and D. Noble. 1987. Excitation-contraction coupling and extracellular calcium transients in rabbit atrium: reconstruction of basic cellular mechanisms. Proceedings of the Royal Society of London. Series B, Biological sciences 230:163-205.

68. Rasmusson, R. L., J. W. Clark, W. R. Giles, K. Robinson, R. B. Clark, E. F. Shibata, and D. L. Campbell. 1990. A mathematical model of electrophysiological activity in a bullfrog atrial cell. The American journal of physiology 259:H370-389.

69. Nygren, A., C. Fiset, L. Firek, J. W. Clark, D. S. Lindblad, R. B. Clark, and W. R. Giles. 1998. Mathematical model of an adult human atrial cell: the role of K+ currents in repolarization. Circulation research 82:63-81.

70. Yanagihara, K., A. Noma, and H. Irisawa. 1980. Reconstruction of sino-atrial node pacemaker potential based on the voltage clamp experiments. The Japanese journal of physiology 30:841-857.

71. Fabiato, A., and F. Fabiato. 1975. Contractions induced by a calcium-triggered release of calcium from the sarcoplasmic reticulum of single skinned cardiac cells. The Journal of physiology 249:469-495.

72. Priebe, L., and D. J. Beuckelmann. 1998. Simulation study of cellular electric properties in heart failure. Circulation research 82:1206-1223.

73. Jafri, M. S., J. J. Rice, and R. L. Winslow. 1998. Cardiac Ca2+ dynamics: the roles of ryanodine receptor adaptation and sarcoplasmic reticulum load. Biophys J 74:1149-1168.

74. Imredy, J. P., and D. T. Yue. 1994. Mechanism of Ca(2+)-sensitive inactivation of L-type Ca2+ channels. Neuron 12:1301-1318.

75. Keizer, J., and L. Levine. 1996. Ryanodine receptor adaptation and Ca2+(-)induced Ca2+ release-dependent Ca2+ oscillations. Biophysical journal 71:3477-3487.

76. Wagner, E., M. A. Lauterbach, T. Kohl, V. Westphal, G. S. Williams, J. H. Steinbrecher, J. H. Streich, B. Korff, H. T. Tuan, B. Hagen, S. Luther, G. Hasenfuss, U. Parlitz, M. S. Jafri, S. W. Hell, W. J. Lederer, and S. E. Lehnart. 2012. Stimulated emission depletion live-cell super-resolution imaging shows proliferative remodeling of T-tubule membrane structures after myocardial infarction. Circulation research 111:402-414.

77. Limbu, S., T. M. Hoang-Trong, B. L. Prosser, W. J. Lederer, and M. S. Jafri. 2015. Modeling Local X-ROS and Calcium Signaling in the Heart. Biophysical journal 109:2037-2050.

CHAPTER 2: MODELING LOCAL X-ROS AND CALCIUM SIGNALING IN HEART

ABSTRACT

Stretching single ventricular cardiac myocytes experimentally has been shown to activate transmembrane nicotinamide adenine dinucleotide phosphate oxidase type 2 to produce reactive oxygen species (ROS) and increase the Ca^{2+} spark rate in a process called "X-ROS" signaling. The increase in Ca^{2+} spark rate is thought to be due to an increase in ryanodine receptor type 2 (RyR2) open probability by direct oxidation of the RyR2 protein complex. In this manuscript, a computational model examines the regulation of ROS and calcium homeostasis by local, subcellular X-ROS signaling and its role in cardiac excitation-contraction coupling. To this end, a 4-state RyR2 model was developed that includes an X-ROS dependent RyR2 mode-switch. When activated, $[Ca^{2+}]_i$ -sensitive RyR2 open probability increases, and the Ca^{2+} spark rate changes in a manner consistent with experimental observations. This, to our knowledge, new model is used to study the transient effects of diastolic stretching and subsequent ROS production on RyR2 open probability, Ca^{2+} sparks and the myoplasmic calcium concentration ($[Ca^{2+}]_i$) transient during excitation-contraction coupling. The model yields several predictions: 1) [ROS] is produced locally near the RyR2 complex during X-ROS signaling and increases by an order of magnitude more than the global ROS signal during myocyte stretching; 2) X-ROS activation just before the action potential, corresponding

to ventricular filling during diastole, increases the magnitude of the Ca^{2+} transient; 3) during prolonged stretching, the X-ROS induced increase in Ca^{2+} spark rate is transient so that long-sustained stretching does not significantly increase sarcoplasmic reticulum Ca^{2+} leak. 4) when the chemical reducing capacity of the cell is decreased, activation of X-ROS signaling increases sarcoplasmic reticulum Ca^{2+} leak and contributes to global oxidative stress, thereby increases the possibility of arrhythmia. The model provides quantitative information not currently obtainable through experimental means and thus provides a framework for future X-ROS signaling experiments.

INTRODUCTION

Reactive oxygen species (ROS) are oxygen-derived molecules that play a significant role in physiological processes. ROS are involved in cellular signaling by mediating the posttranslational modifications of various proteins, commonly through oxidation of sulfhydryl (SH) groups in cysteine residues (1, 2). Lipid bilayer studies incorporating SR vesicles have suggested sulfhydryl oxidation of the ryanodine receptor 2 (RyR2) channel complex (3, 4). This ROS-induced sensitization of RyR2 increases $[Ca^{2+}]_i$ sensitivity, increasing RyR2 open probability (P_o) and hence the frequency of Ca^{2+} sparks (5).

Modulation of RyR2 activity by redox active compounds depends on the type and concentration of these compounds. The overall concentration of oxidizing and reducing agents in a cell determines the intracellular redox potential of the cell (4, 6). At low concentrations, the redox active compounds are capable of reversibly oxidizing the

RyR2s (or any other targets) in order to tune their function. But at larger concentrations these compounds can activate RyR2s irreversibly (3, 7), resulting in increased Ca^{2+} sensitivity and hyper-activity of RyR2 channels. This increases Ca^{2+} leak and decreases SR Ca^{2+} content resulting in diminished SR Ca^{2+} release and weakened muscle contraction during systole. Under some conditions, these same events may increase the risk of arrhythmia. Oxidative Stress (OS) can thus lead to pathological conditions such as systolic dysfunction, arrhythmia and heart failure (HF) (8). In the event of pathological conditions such as HF, a decrease in the ratio of reduced to oxidized glutathione elevates cytosolic ROS levels, thus increasing the redox modification of RyR2 channels resulting in enhanced SR Ca^{2+} leak (9).

In the working heart, diastolic stretching of ventricular cardiac myocytes occurs with every heartbeat as the ventricles fill with blood. This cellular extension activates membrane-bound nicotinamide adenine dinucleotide phosphate (NADPH) oxidase type 2 (Nox2)-dependent ROS production in a process that depends on the microtubule cytoskeleton. These elements lead to a burst of elevated ROS in the dyadic subspace in a process termed 'X-ROS signaling'. The dyadic subspace is the microdomain created at the Z-line bounded by the junctional SR and transverse tubule (T-tubule) membranes. The locally elevated ROS increases the sensitivity of RyR2s to $[Ca^{2+}]_i$, thus triggering a burst of diastolic Ca^{2+} sparks, rapid Ca^{2+} release events from the SR (10, 11). N-acetylcysteine (NAC), an antioxidant that scavenges ROS and reactive nitrogen species (RNS), as well as diphenyleneiodonium (DPI) and gp91ds-tat, both Nox2 inhibitors, all block the stretch-induced burst of Ca^{2+} sparks, identifying Nox2 as the source of ROS

(11, 12). Stretching the cardiomyocytes of a mouse model of Duchenne muscular dystrophy (DMD, the *mdx* mouse) reveals that such stretch-induced ROS production can result in arrhythmogenic Ca^{2+} waves. Of note, a similar X-ROS mechanism has been identified in skeletal muscle with important and distinctive differences (13).

To examine our understanding of X-ROS signaling and explore how it might play a role in cellular physiology and pathophysiology, a computational model of excitation-contraction (EC) coupling and Ca^{2+} signaling in the heart was created that included stretch-induced X-ROS signaling. In this model, RyR2 SR Ca^{2+} release channels could be reversibly activated by local ROS and depended on the cytosolic redox state. This model simulates the experimentally observed stretch-induced ROS production and the sudden burst of Ca^{2+} sparks upon stretching. The kinetics of the process is consistent with the hypothesized local reversible ROS signaling. Furthermore, the model demonstrates how X-ROS signaling may lead to altered local Ca^{2+} signaling and oxidative stress during changes in cellular redox status. This model accounts for Ca^{2+} signaling changes that are attributed to X-ROS signaling in heart.

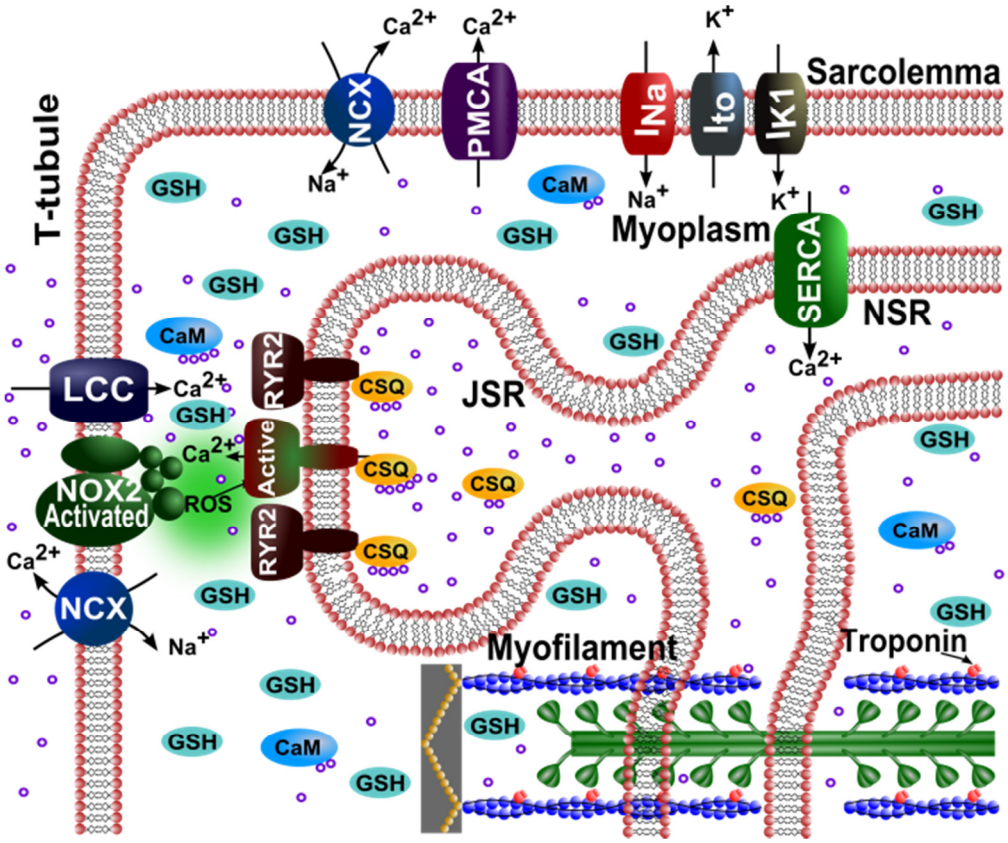

FIGURE 1: Schematic of the calcium handling model. ROS are produced by Nox2 at the Ca^{2+} release site as a result of stretching. Only one of the 20,000 Ca^{2+} release units is shown. Purple circles indicate calcium ions (Ca^{2+}). NCX, Na^{+}-Ca^{2+} exchanger; PMCA, plasmalemmal Ca^{2+}-ATPase; $I_{Na,}$ sodium current; $I_{to,}$ transient outward potassium current; $I_{K1,}$ potassium current; LCC, L-type Ca^{2+} current; RYR2, ryanodine receptor channel; ROS, reactive oxygen species; Nox2, NADPH oxidase type 2; CSQ, calsequestrin; JSR, junctional SR; NSR, network SR; CaM, calmodulin; GSH, reduced glutathione.

METHODS

The model

A new Ca^{2+} spark based model of EC coupling in cardiac ventricular myocytes has been developed to include X-ROS signaling. To this end, the rat ventricular myocyte model for EC coupling used in Wagner et al. (14) is extended to include a description for X-ROS signaling. The model (Fig. 1) includes 20,000 calcium release units (CRUs), each containing 49 stochastically gating RyR2s and seven stochastically gating L-type Ca^{2+} channels (LCCs) interacting via dyadic subspace $[Ca^{2+}]$ ($[Ca^{2+}]_{ds}$). The dyadic subspaces equilibrate by diffusion with a myoplasmic $[Ca^{2+}]$ ($[Ca^{2+}]_i$) compartment. The opening rate of the Ca^{2+}-gated RyR2 homotetramer is sensitive to both the $[Ca^{2+}]_{ds}$ and the junctional SR (JSR) luminal $[Ca^{2+}]$ ($[Ca^{2+}]_{JSR}$). During diastole, the LCCs are normally closed and Ca^{2+} release from the JSR RyR2s is initialized by the probabilistic openings of RyR2s themselves. During systole, Ca^{2+} release via openings of the RyR2 channels is initiated by the rise in the subspace Ca^{2+} entering due to opening of one or more voltage-gated LCCs. Once Ca^{2+} release in a CRU is initiated, then the nature of a Ca^{2+} spark is similar whether the release was initiated in diastole or systole. Inclusion of X-ROS signaling requires the development of an RyR2 model that describes the action of ROS on RyR2 open probability. Therefore, we developed, to our knowledge, a novel four-state model consisting of the closed state (C1) and the open state (O1) in mode 1, and a new closed state (C2) and the open state (O2) in mode 2. The conducting levels at state O1 and O2 are the same. At basal ROS levels, the RyR2s mostly function in mode 1 and are similar to the two-state Markov-chain developed by Williams et al (15) (Fig. 2 – Mode

1). On the other hand, in the presence of stretch-induced ROS production, the RyR2s have a higher possibility of being oxidized by ROS and switching to mode 2 (Fig. 2). In mode 2, the transition probability from closed state C2 to open state O2 is higher than the mode 1 transition probability from closed state C1 to the open state O1. In the presence of ROS, the overall lifetime of channels in the open state increases and that in the closed state decreases, as observed by Boraso et al. (5). Hence, for mode 2, the association rate constant ($k1^+$) is increased and dissociation rate constant ($k1^-$) is decreased compared to mode 1. The function φ ($= \varphi_m[Ca^{2+}]_{JSR} + \varphi_b$) describing the effect of luminal Ca^{2+} on opening, and the dependence term η, describing the positive feedback of $[Ca^{2+}]_{ds}$ remain unchanged for the two modes. The probability of transition of an RyR2 from mode 1 to mode 2 (from C1 to C2) depends upon the rate constant for oxidation by $[ROS]_{ds}$ ($k2^+$) (16) and the dependence on $[ROS]_{ds}$, β. The transition probability from mode 2 to mode 1 is dependent on the reduction rate constant ($k2^-$). This rate falls in the experimental range for the oxidation of thiols (16) and is further constrained to give appropriate activation and deactivation dynamics to match experimental results by Prosser et al.(11).

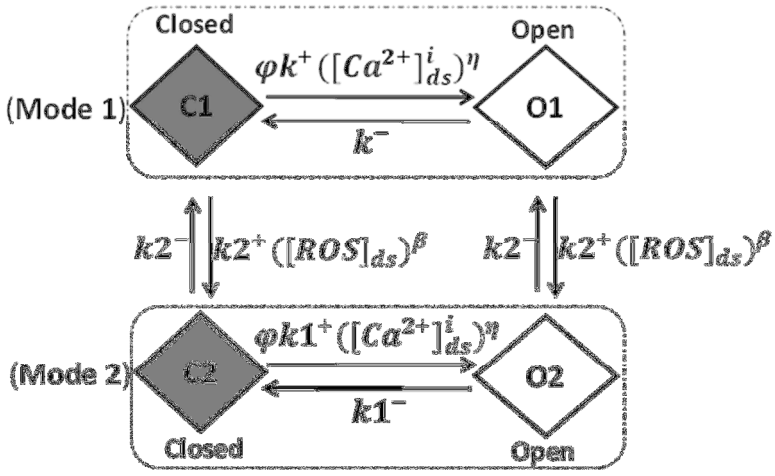

FIGURE 2: The four-state mode-switching model of a single RyR2. The RyR2 channels assume mode 1 in the absence of ROS. Elevation of ROS causes a fraction of the channels to switch from mode 1 to mode 2, which displays a higher open probability due to an increased opening rate and decreased closing rate. C1, closed-state mode 1; O1, open-state mode 1; C2, closed-state mode 2; O2, open-state mode 2; φ, SR luminal dependence function; $k1^+$, association rate constant; $k1^-$, dissociation rate constant; $k2^+$, oxidizing rate constant; $k2^-$, reduction rate constant; η, cooperativity of activating Ca^{2+} binding to RyR2.

Modeling methods

The ordinary differential equations (ODEs) for Ca^{2+} dynamics calculations are the same N = 20,000 equations representing the Markov chain Monte Carlo model described by Williams et al. (15). During diastolic stretching, it is assumed that ROS is produced at the membranes of each release site equally. The ODEs for calculating the ROS concentration in the k^{th} dyadic subspace and the myoplasm are given by Eqs. 1 and 2.

ROS in subspace is described by the differential equation

$$\frac{d[ROS]^k_{ds}}{dt} = \frac{1}{\lambda_{ds}}\left(J^k_{ROSProduction} - J^k_{ROSEfflux} - J^k_{ROSReduction_{ds}}\right), \quad (1)$$

ROS in myoplasm is described by the differential equation

$$\frac{d[ROS]_i}{dt} = J^T_{ROSEfflux} - J_{ROSReduction_i}, \quad (2)$$

where $\lambda_{ds} = \frac{V_{ds}}{V_{myo}}$ is the fraction of myoplasmic volume for the dyadic subspace, V_{ds}^T is the total dyadic subspace volume, and $V_{ds} = \frac{V_{ds}^T}{N}$. The index k is any one of the subspace ($1 \leq k \leq N$). The flux of ROS from the k^{th} subspace to the bulk myoplasm is given by

$$J_{ROSEfflux}^k = \frac{v_{ROSEfflux}^T}{N}([ROS]_{ds}^k - [ROS]_i). \quad (3)$$

The total flux of ROS from N dyadic subspace to the myoplasm is given by

$$J_{ROSEfflux}^T = \sum_{k=1}^N J_{ROSEfflux}^k = \sum_{k=1}^N \frac{v_{ROSEfflux}^T}{N}([ROS]_{ds}^k - [ROS]_i), \quad (4)$$

where $v_{RosEfflux}^T$ is the rate of total ROS efflux out of the subspace.

Because, it is assumed that each subspace releases the same amount of ROS, the above equation becomes

$$J_{ROSEfflux}^T = v_{ROSEfflux}^T([ROS]_{ds}^k - [ROS]_i) . \quad (5)$$

The amount of ROS removed from each subspace is given by

$$J_{ROSReduction_{ds}}^k = v_{ROSReduction}(\lambda_{ds})(GSH)([ROS]_{ds}^k) \quad . \quad (6)$$

The amount of ROS removed from the bulk myoplasm is given by

$$J_{ROSReduction_i} = v_{ROSReduction}((GSH)[ROS]_i - [ROS]_{ibase}), \quad (7)$$

where $v_{ROSReduction}$ is the rate of ROS removal and$[ROS]_{ibase}$ is the base (steady state) ROS in the myoplasm. The relative concentration of the reduced form of glutathione is $(GSH) = 1$ under normal physiological condition, i.e. without OS.

When stretched, the actual amount of ROS produced ($J_{ROSProduction}^k$) by Nox2 in each subspace (see Fig. 4 *C*) is given by a set of four time-dependent equations:

(8)

i) $J^k_{ROSProduction} = ROS_{preStr} + \frac{(.0002 - ROS_{preStr})}{.12} t$ for $t < t_{Str}$

ii) $J^k_{ROSProduction}$= .000036(t^2) - .000122(t) +.000214 $t_{Str} \leq t < 1.5s$

iii) $J^k_{ROSProduction}$= .000001(t^2) - .0000152(t)+.0001326716 $1.5s \leq t <$ 4s

iv) $J^k_{ROSProduction}$= .0001259488($exp^{-.09t}$) $t \geq$ 4s

where ROS_{preStr} is the rate of stretch-induced ROS production just before the stretching is done (= $J^k_{ROSProduction}$ at the time of stretching) and is equal to 0 s^{-1} in the resting condition, and t_{Str} is the time taken for reaching the peak stretching. The coefficients and order of the equations were selected such that the outcome would resemble the trend of the ROS production rate obtained experimentally by Prosser et al. (11). The case when myocyte length is returned to normal is referred to here as "release of stretch". If *time_after_release* $\leq time_{ROSEnd}$ (the time taken for stretch-induced ROS production to cease after the release of stretch), then

v) $J^k_{ROSProduction}$= $ROS_{prerelease}(1 - \frac{time\_after\_release}{time_{ROSEnd}})$

where $ROS_{prerelease}$ is the rate of ROS production just before the release of stretch is done (= $J^k_{ROSProduction}$ at the time of release of stretch).

The rate of ROS production is observed experimentally using the 2',7'-dichlorofluorescein (DCF) fluorescence which is activated by ROS. The model describes the activation of DCF in the subspace and myoplasm by the fluxes into the activated state as

$$J_{ROSDCFed_{ds}} = v_{ROSDCF}([DCF])([ROS]^k_{ds}) \quad (9)$$

$$J_{ROSDCFed_i} = v_{ROSDCF}([DCF])([ROS]_i) \quad (10)$$

where v_{ROSDCF} is the rate of DCF activation by ROS.

The total concentration of ROS-activated DCF is thus given by

$$\frac{d[ROSDCFed]_{Total}}{dt} = \frac{((V_{ds})(J_{ROSDCFed_{ds}})+(V_{myo})(J_{ROSDCFed_i}))}{V_{ds}+V_{myo}} \quad (11)$$

Numerical methods

The program for the model was developed using FORTRAN 95 programming language with CUDA parallel computing platform. The simulations were run in the cluster containing Fermi based GPU C2050 graphics card with CUDA driver version 4.1. The simulation program makes use of Euler's method of numerical integration to calculate the Ca^{2+} and ROS dynamics in the myocytes. The algorithm implements ultrafast Monte Carlo method for stochastic modeling of the Ca^{2+} dynamics (17). Matlab and Inkscape were used for visualization.

Constraining the model: Ca^{2+} dynamics

The newly developed EC coupling model for rat ventricular cardiac myocyte is able to produce Ca^{2+} spark frequency results similar to the experimental results reported by Prosser et al.(11). When a cell is stretched for a continuous 10 seconds period from a resting slack length of about 1.8 micron sarcomere spacing to a longer length, the number of Ca^{2+} sparks increases rapidly by about two-fold and then drops gradually during the 10 seconds of sustained stretching (Fig. 3 *A*). The Ca^{2+} spark frequency drops by

approximately 25% by the end of the 10 second period of stretching and then rapidly drops to its pre-stretched level within a second of its return to its control length.

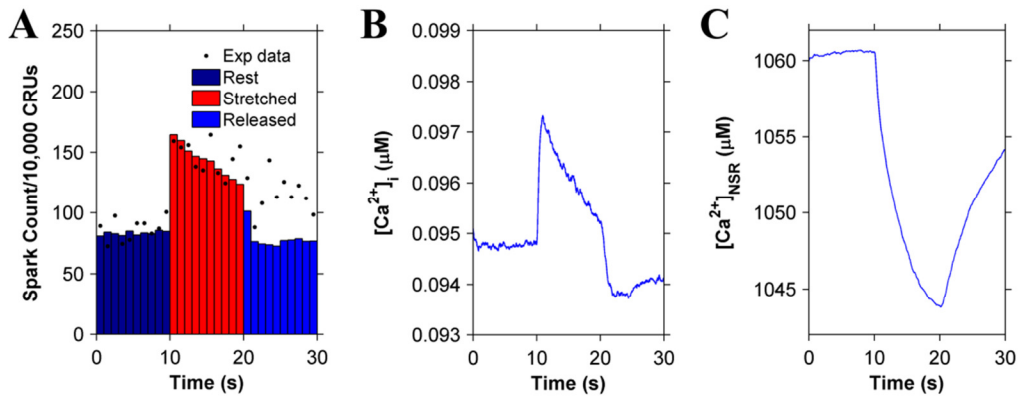

FIGURE 3: Simulation results using the four-state ventricular cardiac myocyte model (n = 50 simulations) (*A*) Ca^{2+} spark histograms for 1 s bins, Black solid circles show experimental data from Prosser et al. (11). (*B*) Myoplasmic Ca^{2+} concentration ($[Ca^{2+}]_i$) and (*C*) Network SR Ca^{2+} concentration ($[Ca^{2+}]_{NSR}$). The myocyte is stretched continuously from 10-20 s displaying a transient increase in Ca^{2+} spark rate.

With the increase in the Ca^{2+} spark rate during stretching, the model exhibits a small transient rise in $[Ca^{2+}]_i$ and a correspondingly small decrease in the network SR (NSR) $[Ca^{2+}]$ ($[Ca^{2+}]_{NSR}$), as seen in Fig. 3, *B* and *C*, respectively. These findings, although clearly demanded by mass action, are seen quantitatively here. . The spark rate drops gradually during the 10 s of sustained stretching, mainly due to the gradual dropping of ROS concentration. The NSR Ca^{2+} concentration does play a small role, as demonstrated in Fig. 3, *A* and *C*, by comparing the values both pre- and poststretching. There is a small decline in spark rate poststretch (Fig. 3 *A*) due to the slightly lower NSR Ca^{2+} concentration (Fig. 3 *C*).

Constraining the model: ROS dynamics

The basal steady-state [ROS] used in the model is assumed to be 10 nM, which is similar to the physiological level of H_2O_2 estimated from experiments (≤ 20 nM) (16, 18). In the simulations, only 50% of the myocyte was considered during stretching and release of stretch protocols to be consistent with experiments that only stretch a portion of the myocyte. The volumes and model components have been scaled to reflect this. The bulk myoplasmic [ROS] ($[ROS]_i$) is estimated to peak at 0.6 μM during the sustained stretching (Fig. 4 *A*). This estimation is consistent with Barbieri et al. (19), where it is stated that ROS generation increases from 50- to 100- fold during skeletal muscle contraction. The dyadic subspace transients ($[ROS]_{ds}$) are predicted to be 10-fold higher than the myoplasmic values ($[ROS]_i$) with faster rising and falling kinetics (Fig. 4 *B*). The shape of the time-dependent $[ROS]_{ds}$ closely follows the ROS production flux due to the small size of the subspace (Fig. 4 *C*).

Experimental estimation of myoplasmic ROS concentration measured using DCF fluorescence is simulated using Eqs. 10 and 11 and shown in Fig. 4, *D* and *E*, respectively, as the concentration of ROS-activated DCF. The calculated value of the total ROS-activated DCF is similar in appearance to the actual experimentally measured DCF fluorescence (11). This can be thought of as simulated fluorescence. The rate of rise of ROS-activated DCF is adaptive rather than constant, as seen by the slightly better r^2 value. This is supported further by the experiments with sustained stretch, which show that the ROS production returns to normal levels if the stretch is sufficiently prolonged (12). For this reason, the model assumes that the ROS production rate decreases with

prolonged stretch (Fig. 4 *F*, *blue*). Fig. 4 *F* (*red*) shows the consequence of a constant rate of ROS production. The fit to the data for the adaptive production is slightly better than that of a constant rate of ROS production. The assumption that ROS production occurs primarily in release sites allows the generation of a significant increase in local ROS concentration that can sensitize the RyR2s, resulting in increased open probability(see Fig. 6, below). This assumption allows ROS to rise locally near the RyR2s while keeping cellular ROS concentrations below the presumably toxicologically significant levels of >10 μM (20).

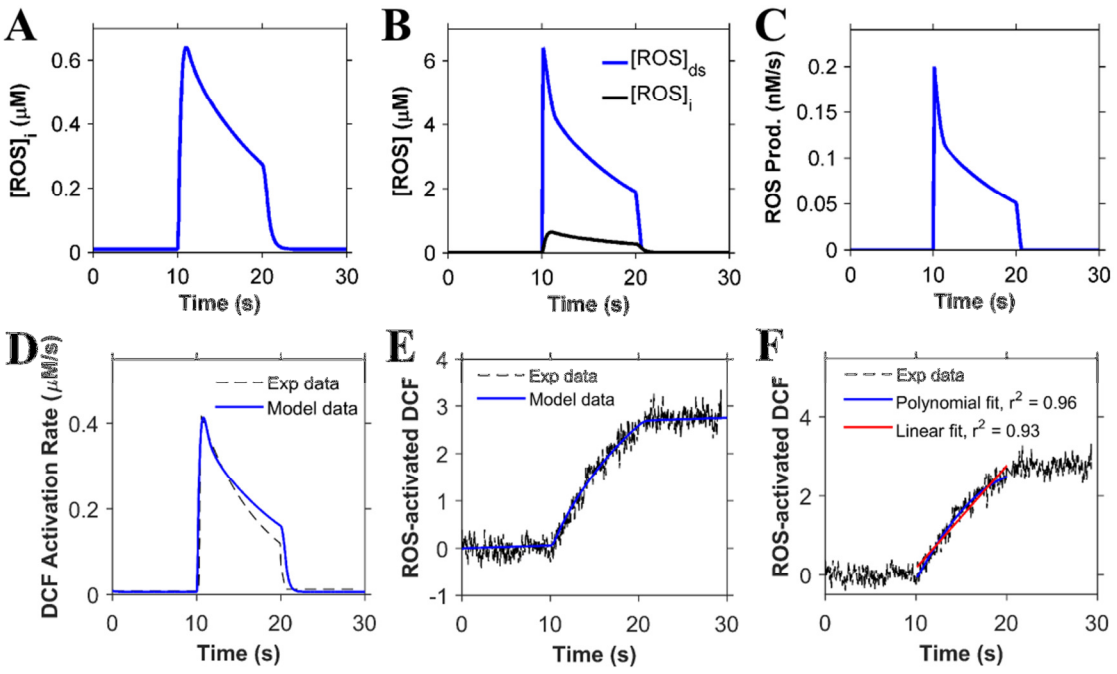

FIGURE 4: ROS dynamics during the stretching protocol used in Fig. 3. (*A*) Concentration of ROS in the myoplasm ($[ROS]_i$). (*B*) Concentration of ROS in the dyadic subspace($[ROS]_{ds}$) compared to $[ROS]_i$. (*C*) ROS production flux. (*D*) Rate of ROS-activation of DCF. (*E*) Total concentration of activated DCF. The myocyte is stretched continuously from 10 to 20 s. (*F*) The rate of ROS production is adaptive (*blue*) rather than constant (*red*). Black dashed lines in (*E*) and (*F*) show experimental data from Prosser et al. (11).

Selection of parameters

The values of the parameters are specified in Table 1 along with reference to their source. Model parameters were selected within the following constraints: 1) the model output should match published experimental results; 2) parameters should fall within the range of experimentally determined values; or 3) parameters should be derived from experimental observation. The parameter adjustments were made by hand to obtain result simulation experimental data. The parameters for the opening rate (k^+), closing rates (k^-), subspace volume (V_{ds}^T) and myocyte volume (V_{myo}) come from our previously published spark model which was constrained by experimental observation (14, 15). This constrains the parameters for mode 1. Parameters for ROS regulation of the RyR2, i.e. mode 2, were constrained from bilayer experiments that indicated that the channel open dwell time increased two-fold in the presence of H_2O_2, whereas the closed dwell time decreased (5) This indicates that the closing rate in the ROS oxidized state ($k1^-$) should be half that of the non-oxidized rate (k^-), whereas the opening rate ($k1^+$) should be increased over k^+.

The rate of transition from mode 1 to the ROS-oxidized mode 2 is not well constrained by experimental measurements of thiol oxidation, which have been reported to be in the range of 10-10^6 $M^{-1}s^{-1}$ (16). Therefore, this transition rate ($k2^+$) is selected in this range and constrained further, along with $k2^-$ and β, so that the response to stretching and recovery from stretch response of the spark rate matches the experimental observations (11).

TABLE 1: Parameters

Parameter	Definition	Value	Reference
$k1^+$	association rate constant for RyR2 and Ca^{2+} in mode2	24 $\mu M^{-\eta}s^{-1}$	(5)
$k1^-$	dissociation rate constant for RyR2 and Ca^{2+} in mode2	250 s^{-1}	(5)
$k2^+$	oxidizing rate constant of RyR2 by ROS	1$\mu M^{-\beta}s^{-1}$	(16)
$k2^-$	reducing rate constant of RyR2	14 s^{-1}	(11)
β	dependence of RyR2 oxidation by ROS	0.4	(11)
V_{ds}^T	total subspace volume	0.027 pL	(14, 15)
V_{myo}	myoplasmic volume	18 pL	(15)
$v_{ROSEfflux}^T$	total rate of ROS efflux out of subspace	0.3125 s^{-1}	(11)
$v_{ROSReduction}$	rate of ROS removal	2 s^{-1}	(11)
$time_{ROSEnd}$	time taken for stretch-induced ROS production to cease after release of stretch	0.6 s	(11)
v_{ROSDCF}	rate of DCF activation by ROS	0.85 s^{-1}	(11)

The parameters governing ROS dynamics are $v_{ROSEfflux}^T$, $v_{ROSReduction}$, $time_{ROSEnd}$ and v_{ROSDCF}, These parameters were adjusted such that the DCF activation rate in Fig. 4 *D* would closely match the derivative of the experimental DCF fit in Prosser et al. (11), as shown in Fig. 4 *E*.

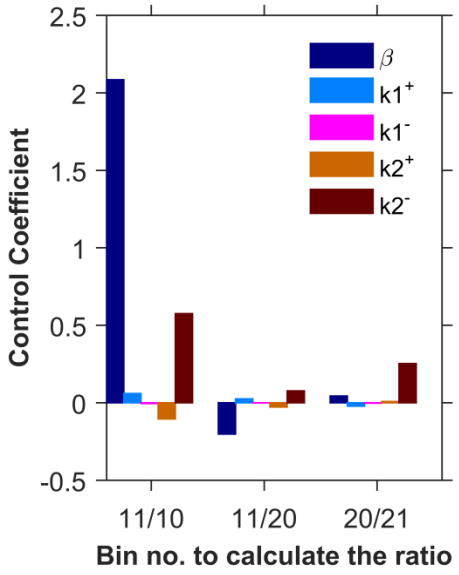

FIGURE 5: Control coefficients for uncertainty analysis of parameters β, $k1^+$, $k1^-$, $k2^+$ and $k2^-$ (n = 20 simulations). The parameters were varied by 10%. Control Coefficient = d(output)/d(parameter) = (output ratio$_i$ - output ratio$_c$)/(increased parameter$_i$ – control parameter$_c$); output ratio$_i$ = spark-count ratio of x^{th} to y^{th} bins for the increased parameter, output ratio$_c$ = spark-count ratio of x^{th} to y^{th} bins for control parameter, where x/y = 11/10 (activation by stretch), 11/20 (decline during stretch) and 20/21 (recovery after end of stretch). (n= 20 simulations)

When constraining model parameters to match X-ROS experiments simulated in Fig. 3 *A*, certain features were emphasized, such as the increase in spark rate with the onset of stretching, the decline of the spark rate during stretch, and the recovery of the spark rate after the relaxation of stretch. In Fig. 3 *A* the data is separated into bins. The last bin before stretching is bin 10 and the first bin during the period of stretching is bin 11. Thus, the amount of spark rate increase by stretching can be quantified as the ratio of value of bin 11 to bin 10, which serves as the first output quantity calculated in the control coefficients. The ratio of bin 11 to bin 20, which demonstrates the decline of spark rate during stretching, is the second output quantity. The third output quantity is

the ratio of bin 20 to bin 21, which shows the ratio of the last bin during stretching compared to the first bin after stretching ends. This demonstrates the recovery of spark rate from stretching. Fig. 5 demonstrates the sensitivity of the model by showing the changes in these three model-output responses when the parameters β (*dark blue*), $k1^+$ (*light blue*), $k1^-$ (*fuchsia*), $k2^+$ (*tan*) and $k2^-$ (*brown*) were each increased by 10% individually. The ratio of the change in output response to the change in the parameter (control coefficient = $\Delta J/\Delta p$ = [{change in output}/{change in parameter}]) yields the control coefficients, which are shown graphically. The numerical values of the control coefficients are also shown in Table 2. The calculations of the control coefficients show that the increase in spark rate due to stretching is most sensitive to changes in β, but also very sensitive to $k2^-$, the transition rate from mode 2 to mode 1 (Fig 5, *11/10*). The decline in spark rate during stretching is most sensitive to β (Fig 5, *11/20*). The recovery from stretching is most sensitive to $k2^-$, the transition rate from mode 2 to mode 1 (Fig.5, *20/21*).

TABLE 2: Control Coefficients

Bin/Bin Spark-Count Ratio	Control Coefficients for 10% Increase in the Parameters				
	β	$k1^+$	$k1^-$	$k2^+$	$k2^-$
11/10	2.085	0.059	-0.005	-0.105	0.575
11/20	-0.203	0.025	-0.001	-0.027	0.077
20/21	0.043	-0.022	-0.003	0.007	0.252

RESULTS

The model of X-ROS signaling described above was developed and shown to simulate experimentally observed X-ROS signaling in the context of normal cellular and subcellular Ca^{2+} signaling. In addition, this, to our knowledge, new X-ROS model was designed to provide insight by carrying out model-dependent experiments that could not yet be done with single cells. Thus, simulations were performed to suggest the physiological significance of X-ROS signaling beyond that which is directly measurable experimentally, and to gain insight into how X-ROS signaling may be altered in disease states and may contribute to pathology.

Mechanisms of X-ROS signaling

The simulation results shown in Figs. 3 and 4 assume that ROS is produced locally in the membranes of subspace. To test this assumption, the next set of simulations explores the consequences of global ROS production during stretch, i.e., at sarcolemmal and T-tubular membranes everywhere in the cell. In the case of localized ROS release, when a cardiomyocyte is stretched, the concentration of subspace ROS ($[ROS]_{ds}$) (Fig. 3 *A*) sharply increases due to rapid ROS production during the process of stretching (first few milliseconds), but the decrease is also sharp initially due to the decrease in the ROS production rate (after the stretching is done and the myocyte is held at a constant length), as well as due to the ROS efflux from subspace towards the bulk myoplasm contributing to the myoplasmic ROS ($[ROS]_i$) (Fig. 3 *B*). This sharp increase and decline of ($[ROS]_{ds}$ makes the sudden twofold increase of spark rate within 0-1 s of

the stretch possible while making sure that, similar to the experimental results, the spark frequency does not increase even more during the 1-2 or 2-3 s after stretching (Fig. 3 *A*, *solid circles*). In the case of global ROS release, the stretching results in the same ROS production pattern in both the subspace and in the myoplasm (Fig. 6, *A* and *B*). Hence, there is no significant net efflux of ROS to or from the subspace, which is why the ($[ROS]_{ds}$) and ($[ROS]_i$) are consistent over time. This reduces the rate of decline in the ($[ROS]_{ds}$) and results in higher spark frequency during the 1-2 s compared to 0-1 s after stretching. Hence, simulations with local ROS production better captured this aspect of the experimental results than did the simulations with global ROS production. Therefore, the model favors the hypothesis that ROS signaling during stretching likely occurs locally in or near the dyad.

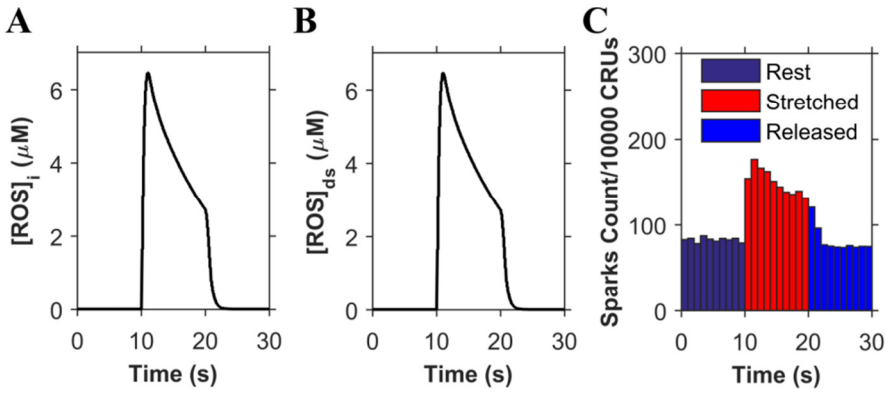

FIGURE 6: Simulations demonstrating consequences of global ROS release. (*A*) Concentration of ROS in the myoplasm ($[ROS]_i$). (*B*) Concentration of ROS in the subspace ($[ROS]_{ds}$). (*C*) The resulting spark frequency for n=20 simulations.

The model assumes that ROS oxidation of the RyR2s is a reversible process. To test this assumption, simulations were performed that assumed that the oxidation of RyR2s by ROS was irreversible, i.e., the switch from mode 1 to mode 2 in the model was irreversible. With X-ROS signaling irreversibly oxidizing the RyR2s, the spark frequency increases abruptly (Fig. 7 *A*) as the number of channels in mode 2 goes from 1.1% to 85% within 1 s of stretching and to 97% within 2 s of stretching (data not shown here). The number of channels in mode 2 continues to increase until all the channels are oxidized, but due to the depletion of SR Ca^{2+} ($[Ca^{2+}]_{NSR}$), the spark frequency gradually goes to a steady-state value and does not change even when the myocyte is released from stretch (Fig. 7 *B*). Had the oxidation always been irreversible, even at the nanomolar concentration of ROS (resting condition), then the average spark frequency would have been much higher with all the RyR2s in mode 2 (Fig. 7 *C*). The stretch-induced X-ROS signaling would have no effect on the spark frequency. These results suggest that X-ROS signaling does not cause an irreversible oxidation, because irreversible oxidation should result in no change in spark frequency when the myocyte is released from stretch after 10 s of continuous stretching.

As an additional test of the model, simulation data were compared to experiments other than those used to constrain model parameters. The first set of experiments test how the model responds to prolonged stretch. The experimental Ca^{2+} spark counts in Fig. 5 *B* of Prosser et al. were normalized to the minimum and maximum Ca^{2+} spark count of the simulation results so that the comparisons would be more illustrative (12). As seen in

Fig. 8 *A*, the simulation results in the return of spark rate to its prestretch value, as does the experimental spark rate, and the average spark rate remains the same poststretching.

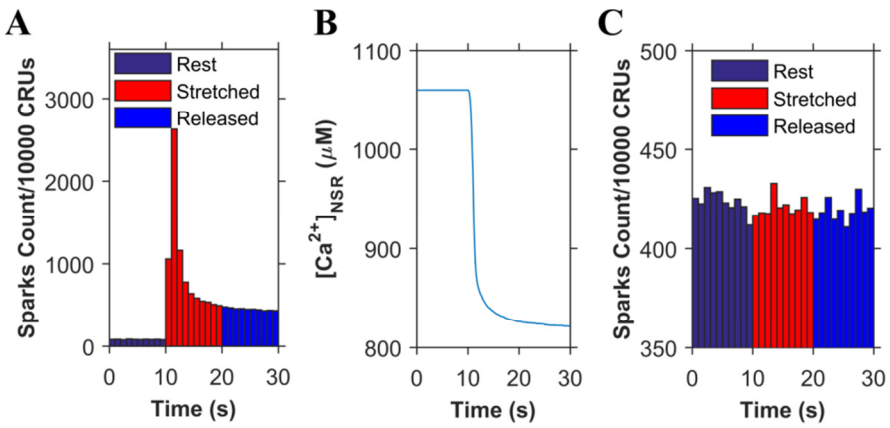

FIGURE 7: Simulations demonstrating consequences of irreversible oxidation of RyR2s. (*A*) Ca^{2+} spark frequency when stretch-induced ROS results in irreversible oxidization of RyR2s. (*B*) The sudden increase in Ca^{2+} spark frequency after stretching depletes the $[Ca^{2+}]_{NSR,}$ which stabilizes at a new steady-state value. (*C*) The Ca^{2+} spark frequency when ROS is at resting level results in irreversible oxidization of RyR2s so that almost all RyR2s switch to mode 2 with time so that stretching has no effect on spark rate. n=20 simulations.

The second set of simulations explores how ROS levels increase with cyclic stretch. The normalized experimental DCF values in Fig. 2 *C* of Prosser et al. (12) compare well with experimental values over 90 s simulation time at 1 Hz and 4 Hz (Fig. 8 *B*). This demonstrates that X-ROS signaling is enhanced and graded by the frequency of stretch, as the DCF concentration is elevated at 4 Hz in comparison to 1 Hz. Furthermore, it suggests that the ROS dynamics are in agreement with experimental

results. These two results indicate that the model can simulate experiments not used to constrain the model.

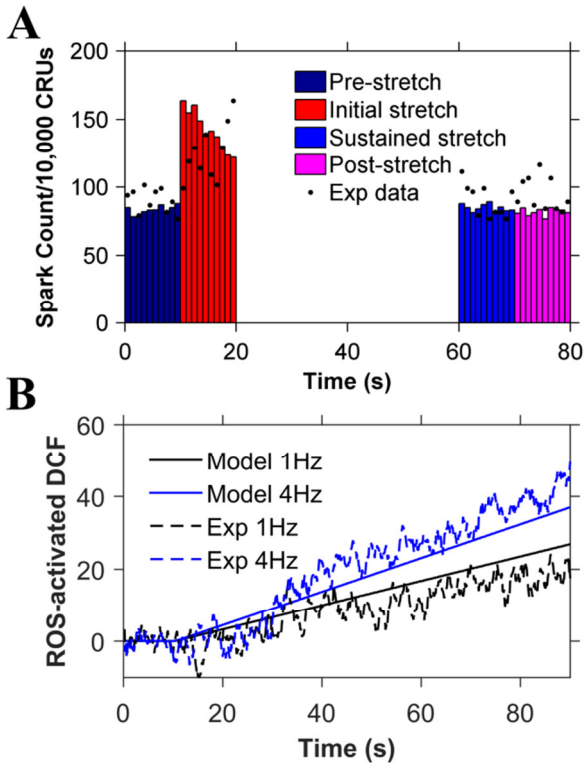

FIGURE 8: Comparison of simulation results modeled for 8% stretch (11) to experimental results for 10% stretch (12). Experimental data were normalized to the model data to compensate for the difference in the amount of stretch. (*A*) Ca^{2+} spark histograms for 1s bins when the model is simulated for 80 s and the myocyte is stretched from 10 to 70 s (n = 11 simulations). The spark frequency returns to its prestretch value during the last 10 s of stretching, as seen in the experimental data, represented by black dots. (*B*) Comparison of simulated values (*solid lines*) to the experimental values (*dashed lines*) of the total concentration of activated DCF at 1 Hz (*black*) and 4 Hz (*blue*) of cyclic stretching from 10 to 90 s.

Physiological implication of X-ROS signaling

In the beating heart, ventricular cardiac myocytes undergo regular (rhythmic) contractions and relaxations. Accompanying each contraction cycle is a period of

stretching (diastolic filling) and shortening (pumping) separated by isometric force increase and isometric relaxation. Given that stretching affects Ca^{2+} spark dynamics in ventricular myocytes, the next three series of numerical experiments seek to understand what impact the contraction cycle may have on X-ROS signaling. To understand how the stretching of ventricular myocytes can have an impact on ROS dynamics and subsequent Ca^{2+} dynamics, alternating equal periods of stretching and release of stretch were applied at 1 Hz, 2 Hz, and 4 Hz starting from the resting unstretched condition (Fig. 5). During this process, $[ROS]_{ds}$ and $[ROS]_i$ were calculated as a function of time. No periods of isometric force or relaxation were applied.

Oscillation of $[ROS]_{ds}$ or $[ROS]_i$ were observed. At 1 Hz frequency, the subspace ROS oscillates between 1.43 μM and 6.84 μM and the myoplasmic ROS oscillates between 515 nM and 734 nM (Fig. 9 *A*). At 2 Hz frequency, the subspace ROS oscillates between 4.25 μM and 7.08 μM and the myoplasmic ROS between 770 nM and 831 nM (Fig. 9 *B*). At 4 Hz frequency, the subspace ROS oscillates between 5.92 μM and 7.2 μM and the myoplasmic ROS oscillates between 889 nM to 903 nM (Fig. 9 *C*). Although the sustained elevation of $[ROS]_i$ during cyclic stretching and release of stretch has been demonstrated experimentally (12), neither calibration of the concentration nor oscillations of the signal could be measured.

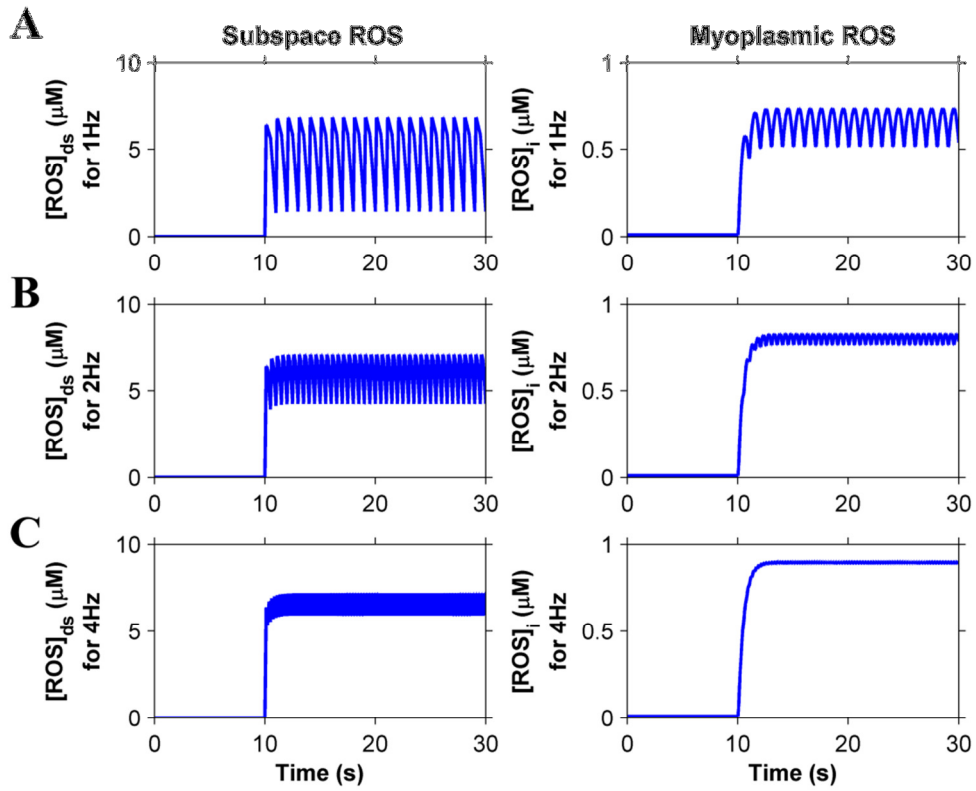

FIGURE 9: Subspace and myoplasmic ROS concentration are elevated when the ventricular cardiac myocyte is cyclically stretched with equal periods of stretching and release of stretch from 10 to 30 s at (*A*) 1 Hz, (*B*) 2 Hz, and (*C*) 4 Hz.

The higher ROS concentration in the subspace is thought to oxidize protein targets. In this model, we focused on changes in RyR2 $[Ca^{2+}]_i$ sensitivity only as described in the presentation of the model. This increased sensitivity of RyR2 led to the increase in Ca^{2+} spark frequency (Fig. 10 *A*) and the resting $[Ca^{2+}]_i$ (Fig. 10 *B*). The Ca^{2+} spark frequency and $[Ca^{2+}]_i$ increase further as the frequency increases from 1 to 2 Hz, with little additional change as frequency increases even more to 4 Hz. This is due to the

increase in fraction of channels (FoC) in mode 2 (M2) with the increase in stretching-release of stretch frequency (Fig. 10 *D*).

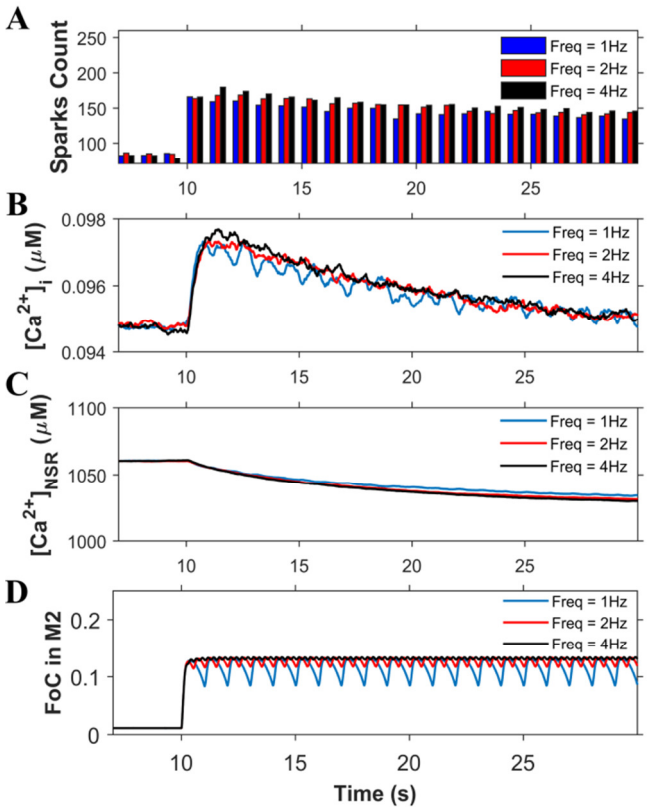

FIGURE 10: Analysis of Ca^{2+} dynamics for the protocol from Fig. 9 reveal that the small variations in spark rate lead to fluctuations in myoplasmic calcium that are governed by the fraction of channels in mode 2. (*A*) Ca^{2+}-spark count. (*B*) $[Ca^{2+}]_i$. (*C*) $[Ca^{2+}]_{NSR}$. (*D*) Fraction of channels (FoC) in mode 2 (M2) when stretched (from 10 to 30 s) at 1 Hz, 2 Hz, and 4 Hz (n = 20 simulations). The myocyte is stretched and released from stretch continuously from 10 to 30 s. The beats before 10 s show the response without stretching. If the ROS-induced activation of RyRs were not present, this level of sparks would persist regardless of stretching.

We also used the model to study the details of a more physiological sequence of numerical experiments. In this case, the myocyte is stretched before an electrical

depolarization produces an action potential (AP) that initiates EC coupling and the $[Ca^{2+}]_i$ transient. The heart rate was set to 1 Hz. Before each AP, the ventricular cardiac myocyte was stretched for 200 ms to mimic diastolic filling starting at one of the following times: 1) 0 ms (i.e., from 0 to 200 ms), 2) 200 ms (i.e., from -200 to 0 ms), 3) 400 ms (i.e. from -400 to -200 ms), 4) 600 ms (i.e. from -600 to -400 ms), and 5) 800 ms (i.e. from -800 to -600 ms), where 0 is the time of application of the stimulus for the AP. The results of these five different simulation cases, along with the result for control myocytes (that have not been stretched), were compared. We observed that the peak value of $[Ca^{2+}]_i$ (Fig. 11 *A*) and the peak value of RyR2 P_O (not shown) were maximum when the myocyte was stretched 200 ms before the application of stimulus. In this situation, the stimulus occurs when the ROS concentration is highest. As a result, the $[Ca^{2+}]_{NSR}$ is depleted most as well (Fig. 7 *B*). There is also a decline of the peak $[Ca^{2+}]_i$ and $[Ca^{2+}]_{NSR}$ with each successive beat (Fig. 11).

The peak $[Ca^{2+}]_i$ decreases with the heartbeat number in each of the five cases of simulations (for example Fig 11A). To ascertain whether depletion of $[Ca^{2+}]_{NSR}$ is the underlying cause for this decrease of peak $[Ca^{2+}]_i$ as the heartbeat continues, similar simulations with constant $[Ca^{2+}]_{NSR}$ were performed (Fig. 11 *C*) for stretching of the myocyte 200 ms before the application of stimulus. The result clearly shows that with constant $[Ca^{2+}]_{NSR}$, the resulting peak $[Ca^{2+}]_i$ does not decrease with the heartbeat number.

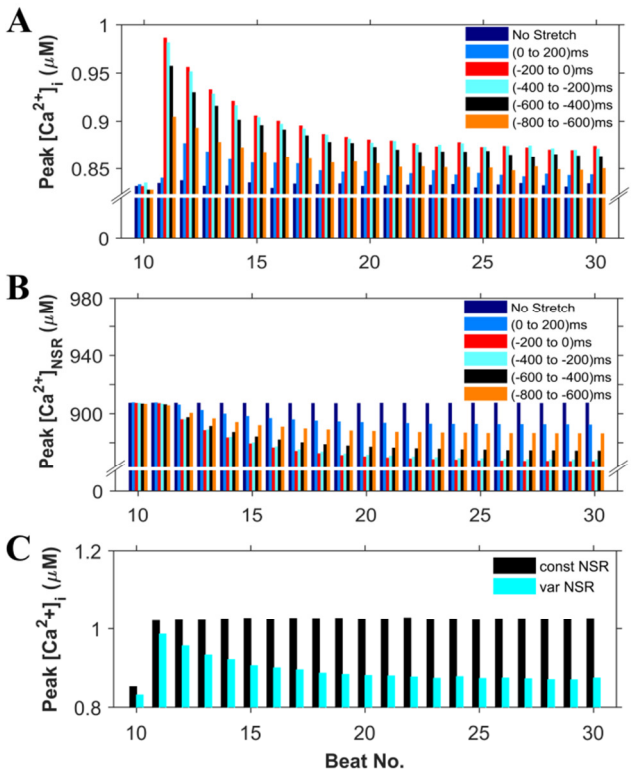

FIGURE 11: Simulations of a 200 ms period of stretching at different points during the cardiac cycle at 1 Hz pacing during beats 11-30. Electrical stimulation occurs at 0 ms. (*A* and *B*) Comparison of maximum value reached by (*A*) $[Ca^{2+}]_i$ and (*B*) $[Ca^{2+}]_{NSR}$ at each beat while the ventricular cardiac myocyte is stretched from 0 to 200 ms, -200 to 0 ms, -400 to -200 ms, -600 to -400 ms, and -800 to -600 ms from the time point of application of stimulus. The stretching protocol is shown in Supplemental Fig. S1. A maximal increase in peak Ca^{2+} transient amplitude is observed when the stretching immediately precedes electrical excitation (-200 to 0) ms. (*C*) Decline of the peak Ca^{2+} seen in (*A*) with the continuing heartbeat during stretching requires reduction of the SR Ca^{2+} content. The protocol for -200 to 0 ms (*cyan bars*) was used with $[Ca^{2+}]_{NSR}$ held constant. When $[Ca^{2+}]_{NSR}$ is constant, the corresponding peak $[Ca^{2+}]_i$ is also constant.

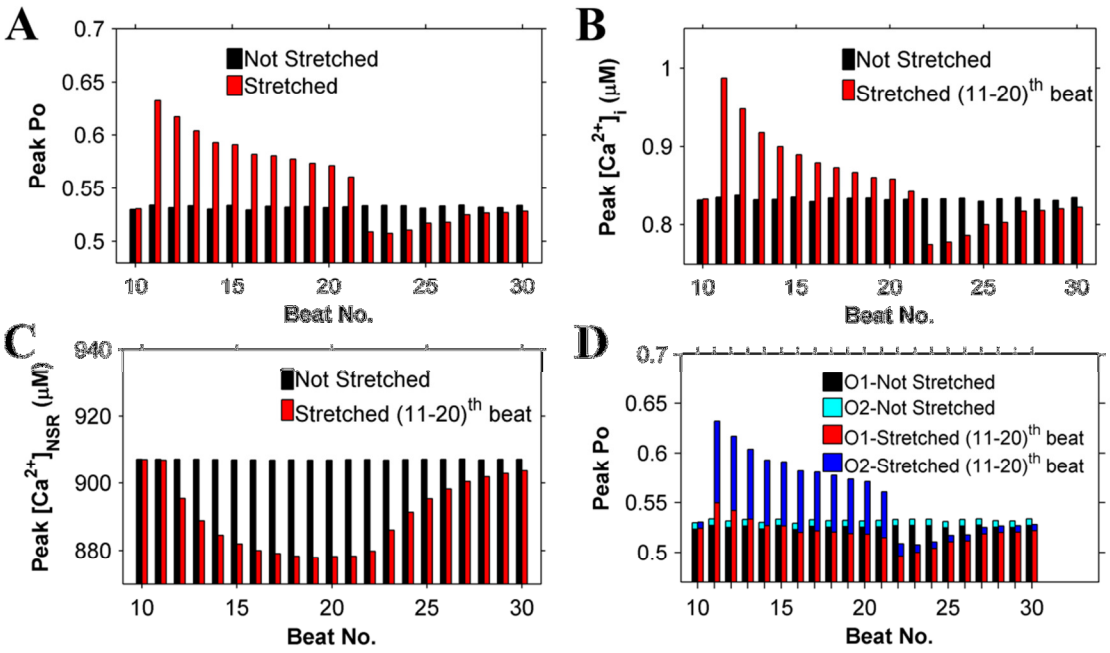

FIGURE 12: Continuous stretching of cells from 10 to 20 s displays a transient increase in peak $[Ca^{2+}]_i$ followed by a recovery toward control. This is caused by an increase in P_o followed by a decline in both P_o and SR Ca^{2+} load. The opposite is seen during release of stretch. (*A*-*C*) Peak P_o, (*A*), peak $[Ca^{2+}]_i$ (*B*), and peak $[Ca^{2+}]_{NSR}$ (*C*)at each beat while the ventricular cardiac myocyte is stretched (beats 11-20) (*red bars*) and not stretched (*black bars*). (*D*) Detailed breakdown of peak P_o in (*A*) into the fraction of channels in O1 and in O2.

To gain further insight into X-ROS signaling, the stimulation protocol used in Fig. 11 was repeated and a 10 s period of stretching was imposed from stimulation 11 through stimulation 20. The stretching occurred 200 ms before the 11th stimulation. The peak RyR2 P_o increased abruptly with the 11th stimulation and then declined gradually (Fig. 12 *A*). The peak $[Ca^{2+}]_i$ transient followed the same time course (Fig. 12 *B*). This demonstrates that with an abrupt increase of ROS production, EC coupling is affected as the RyR2 P_o increases and the $[Ca^{2+}]_i$ also transiently increases. The peak P_o of the Ca^{2+}

channels increases due to the increase of fraction of channels in mode 2, and this leads to an increase in the fraction of channels in the open state of mode 2 (O2) (Fig. 12 *D*).

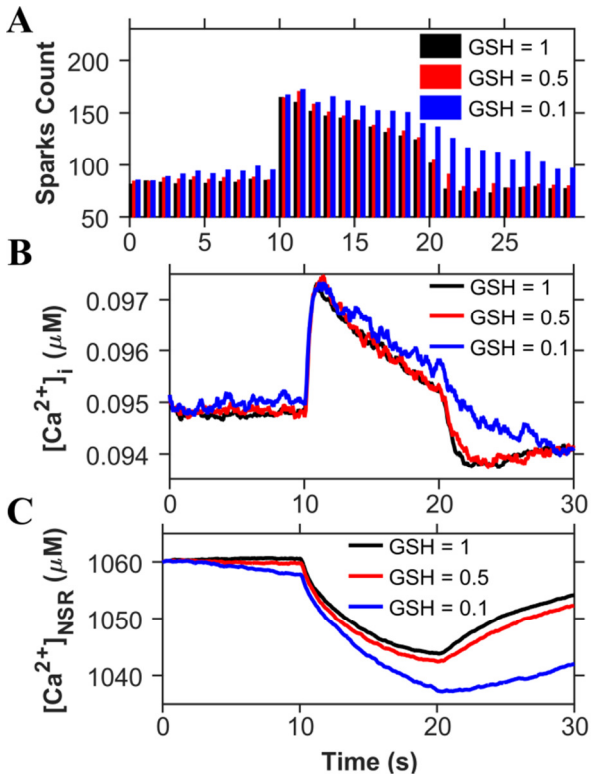

FIGURE 13: Decreasing the reducing capacity by lowering GSH leads to increased spark activity and Ca^{2+} mobilization during stretching from 10 to 20 s. Shown are traces for the $[GSH]/[GSH]_{control}$ ratio assuming values of 1 (*black*) (control), 0.5 (*red*), and 0.1 (*blue*). Comparison of (*A*) Ca^{2+}-spark count, (*B*) $[Ca^{2+}]_i$, and (*C*) $[Ca^{2+}]_{NSR}$.

Oxidative stress

OS is the condition where the concentration of ROS overwhelms the chemical reducing power of the myocyte. This can occur either through increased ROS production or through a decreased reducing capacity of the myocyte. To study the effect of sustained

OS in the myocyte, simulations were carried out with a decreased concentration of the primary cellular reducing biochemical, glutathione. Reduced glutathione (GSH) is estimated experimentally to be present in the rat ventricular myocytes at a concentration of 1-10 mM (21, 22). Given this variability, we chose to report the fraction of GSH. In the simulation, the GSH was reduced to 50% and 10% of the control level, as can occur in disease states (23, 24) (see Eqs. 6 and 7). Fig. 13 *A* shows that with decreases in GSH, there is an increase in the Ca^{2+} spark rate during both stretching and release of stretch. Furthermore, the recovery of Ca^{2+} spark rate after stretching is slowed when GSH decreases. This results in increased $[Ca^{2+}]_i$ both at rest and during stretching (Fig. 13 *B*) and decreased $[Ca^{2+}]_{NSR}$ (Fig. 13 *C*) as a result of the increased SR Ca^{2+} leak.

Furthermore, when the myocyte is acutely stretched 200 ms before each beat, the decrease in GSH results in a slight increase in RyR2 Po (Fig. 14 *A*) and peak $[Ca^{2+}]_i$ (Fig. 14 *B*) due to an increase in the fraction of channels in mode 2 (Fig. 14 *C*). However, the peak P_o and peak $[Ca^{2+}]_i$ decrease with heartbeat number (Fig. 14, *A* and *B*) due to the accompanying decrease in $[Ca^{2+}]_{NSR}$ (Fig. 14 *D*). This is attributable to an increased $[ROS]_{ds}$ and $[ROS]_i$ (Fig. 14, *E* and *F*). Thus, the model illustrates how a large decrease in the reducing capacity of the cell could dramatically elevate global ROS concentrations during X-ROS signaling, possibly to damaging levels, leading to the progression of pathological conditions.

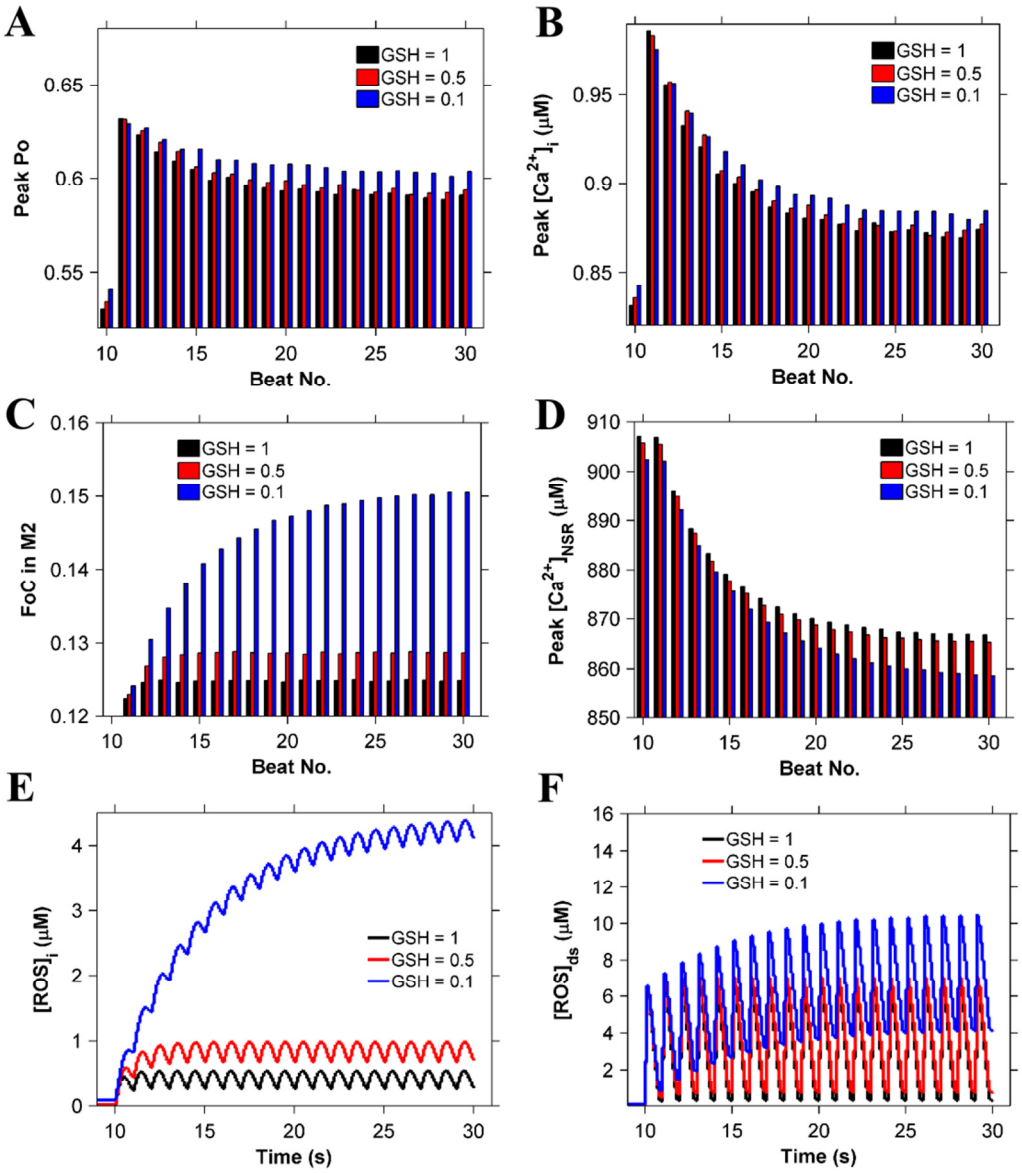

FIGURE 14: Lowering of the reducing capacity (GSH ratio) from Fig. 13 during 1 Hz pacing with myocyte stretched for 200 ms before each stimulus leads to increased [ROS] and increased Ca^{2+} release. (*A-D*) Comparison of (*A*) peak P_o, (*B*) peak $[Ca^{2+}]_i$, (*C*) the corresponding fraction of channels (FoC) in mode 2 (open, closed, and inactivated), and (*D*) peak $[Ca^{2+}]_{NSR}$ at each beat. (*E* and *F*) Presence of (*E*) $[ROS]_{ds}$ and (*F*) $[ROS]_i$ in the myocyte due to cyclic stretching and release of stretch.

DISCUSSION

The computational model presented here suggests the underlying mechanisms of regulation of EC coupling by ROS and predicts both physiological and pathophysiological roles of X-ROS signaling. Experiments indicate that stretching a cardiac myocyte triggers ROS production from Nox2, which is localized to the sarcolemmal and T-tubule membranes. The model suggests the following four predictions: 1) *X-ROS signaling is local:* [ROS] is produced locally near the RyR2 complex during X-ROS signaling and increases by an order of magnitude more than the global ROS signal during myocyte stretching; 2) *X-ROS enhances EC coupling:* X-ROS activation just before the AP, which could correspond to ventricular filling, optimally increases the magnitude of the Ca^{2+} transient; 3) *X-ROS signaling is attenuated during prolonged stretch:* during prolonged stretching, the X-ROS-induced increase in spark rate is attenuated so that sustained stretching alone no longer significantly increases SR Ca^{2+} leak; and 4) *OS affects X-ROS signaling during disease:* when the chemical reducing capacity of the cell is decreased, X-ROS signaling increases SR Ca^{2+} leak and global OS, thereby increasing the possibility of arrhythmia.

Local ROS signaling

The model suggests that this raises local ROS in the dyadic subspace significantly and hence affects the nearby RyR2s by increasing the opening rate of these channels. ROS currently cannot be imaged with the precision needed to identify local domains. We have performed simulations in which X-ROS signaling occurs either locally in the dyad

or globally. The simulations with local X-ROS signaling simulate experimental data effectively. However, simulations with global ROS production failed to simulate experimental data adequately. This suggests that X-ROS signaling occurs locally. The implications of highly localized signaling of X-ROS are that it enables the ROS-dependent modulation of RyR2s while maintaining myoplasmic [ROS] at relatively low levels. This has the advantage of limiting the targets activated by X-ROS signaling.

The RyR2 channel is assumed in the model to be the main target for X-ROS signaling. The effect of ROS on RyR2 was described by a mode switching mechanism where the ROS –dependent oxidation of RyR2 increases their open probability. The model suggests that this is a reversible process as simulations with irreversible oxidation of RyR2s fail to simulate the experimental data. A mechanistic model of the RyR2 and CRUs has thus been developed that is able to demonstrate the abrupt increase in Ca^{2+} sparks in the presence of stretch-induced ROS and the immediate fall in the Ca^{2+} spark rate when ROS concentration decreases to its control level after release of stretch. In our four-state model of RyR2, the RyR2 behaves differently in quiescent cells, where $[ROS]_{ds}$ is thought to be in the nanomolar range, compared to acutely stretched cells, where $[ROS]_{ds}$ is in the micromolar range. Upon stretching of a cardiomyocyte, those RyR2s that are in mode 1 in the presence of nanomolar concentration of ROS can switch to mode 2, which has higher open probability, due to the abrupt elevation of ROS to the micromolar level, leading to the increased Ca^{2+} spark rate. This increase in the Ca^{2+} spark rate causes a corresponding decrease in $[Ca^{2+}]_{NSR}$ and increase in $[Ca^{2+}]_i$. It should be noted that there are additional targets of ROS in the myocyte. For example, the L-type

calcium channel can display increased open probability when its thiol groups are oxidized, and calcium/calmodulin dependent kinase II (CaMKII) can also be activated by oxidation (4, 25, 26). The SR Ca^{2+} -ATPase (SERCA) can be inhibited when oxidized but the effect of oxidation by ROS on Na^{+}-Ca^{2+} exchanger (NCX) is controversial (4, 27). Study of the contribution of these other targets is left for future work.

The increase in intracellular [ROS] is consistent with levels observed experimentally. The levels of ROS in different cells can vary widely. At the low end of the spectrum, a study using Amplex red dye in neurons measured [H_2O_2] below the detection threshold of 7 nM at rest that increased to 66 nM after treatment with insulin (28). On the other hand, *Escherichia coli* display a somewhat higher [H_2O_2] of 200 nM (29). Muscle, however, seems to have higher ROS levels. We found two studies estimating ROS in the heart. In a computational study, the Cotassa model has [ROS] transients peaking above 100 μM during metabolic oscillations (30). Experimental studies in isolated cardiac myocytes have biochemically measured [H_2O_2] at 15 μM in control hearts, at 50 μM after 30 minutes of ischemia, and at 100 μM 2 minutes after reperfusion (31). Skeletal muscles, whose mitochondria produce ROS at 40% the rate of cardiac mitochondria, experience a 50- to100-fold increase in ROS going from rest to exercise (19). Cardiac myocytes seem to have the ability to survive high ROS levels. In experiments, cardiac myocytes have been exposed to ROS levels as high as 10 mM without cell death (32). In fact, exposing skeletal muscle to increasing doses of H_2O_2 (up to 1 mM) increases endurance (33).

X-ROS signaling enhances E-C coupling

During contraction of the heart, cardiac cells undergo cyclic periods of stretching and release of stretch. Comparing this cyclic process of elongation and shortening at 1 Hz, 2 Hz, and 4 Hz demonstrates that $[ROS]_{ds}$ and $[ROS]_i$ increase with increasing frequency of stretching and release of stretch. Accompanying the higher rate of $[ROS]_{ds}$ production is a higher Ca^{2+} spark count, and hence a higher $[Ca^{2+}]_i$ with the cycle of stretching and release of stretch at 2 Hz and 4 Hz compared to that at 1 Hz. This increase seems to plateau at 4 Hz. This suggests that X-ROS signaling may increase the gain of EC with increases in pacing rate.

Furthermore, during electrical pacing, the model predicts that X-ROS signaling leads to a modest increase in the amplitude of the $[Ca^{2+}]_i$ transient. This was accomplished by inducing a 200 ms period of stretching (and ROS production) at different times during the cardiac cycle. Interestingly, the biggest effect of the frequency of stretching seems to be the increase in myoplasmic ROS (Fig. S2 in the Supporting Material), with a small effect on $[Ca^{2+}]_i$ (this matches our unpublished experimental observations). This potentiation of the $[Ca^{2+}]_i$ transient is maximal when the 200 ms period of stretching immediately precedes the AP. The model shows that under these conditions, $[ROS]_{ds}$ is maximal when the AP begins and triggers the Ca^{2+} transient. Teleologically, this makes sense as the filling of the ventricles with blood stretches the myocytes immediately before contraction. Hence, the stretching of the ventricular wall combined with X-ROS signaling seems to optimize Ca^{2+} release during contraction. Of note, the experimentally measured increase in free $[Ca^{2+}]_i$ may fall short of that predicted

by the model due to the subsequent increase in myofilament Ca^{2+} buffering that occurs during stretching(34).

X-ROS signaling is attenuated during prolonged stretch

The model suggests that prolonged distension of the wall (10 s), and the accompanying stretching of the myocyte, enhances Ca^{2+} release modestly. However, with prolonged stretch, the X-ROS production is attenuated consistent with experiments. Furthermore, this small potentiation of Ca^{2+} release is attenuated by depletion of the NSR due to the increased RyR2 Ca^{2+} leak. This is similar to the results of Trafford and colleagues (35), which showed that increasing RyR2 open probability pharmacologically resulted in a transient increase in the Ca^{2+} transient, which then returned to the control amplitude after several beats (35). This recovery was due to changes in $[Ca^{2+}]_{NSR}$ (35, 36). The opposite effect was seen with washout, i.e. there was a transient decrease in Ca^{2+} transient amplitude that returned to control level after several beats.

Oxidative stress affects X-ROS signaling during disease

OS occurs when the cellular ROS levels rises. The model suggests that when the removal of ROS is impaired, the systolic and diastolic spark rates increase due to an increase in the level of cellular ROS. An example of a disease in which ROS removal is impaired due to reduction in the available glutathione pool is HF(37). Increased Ca^{2+} leak has been observed in HF and has been implicated in arrhythmia (38). Although increased X-ROS signaling might not be the primary cause of the increase leak, it could contribute

to it. Similarly, if the rate of ROS production increases, the cellular ROS levels will also rise. X-ROS signaling is enhanced in muscular dystrophy (*mdx*) by increased microtubule density transmitting stretching to the NADPH oxidase (13). In fact, muscle cells from *mdx* mice show an increased susceptibility to OS (39, 40). This increase in SR Ca^{2+} leak likely plays a role in arrhythmia. In fact, inhibition of NADHP oxidase reduces the propensity for arrhythmia in *mdx* heart (41). The model also predicts that a significant depletion of reducing compounds could result in a dramatic change in redox status of the myocyte, driving the cell towards pathology. Lowering the GSH concentration by factors observed in disease states elevated the $[ROS]_i$, which significantly increased the $[Ca^{2+}]_i$ and depleted the $[Ca^{2+}]_{NSR}$.

Other considerations

During sarcomere lengthening, there is an observed increase in force that is thought to be due to an increase in troponin affinity for Ca^{2+} independent of Ca^{2+} level. During a single stretch from rest, the spontaneous spark rate can double due to X-ROS signaling. Furthermore, the model suggests that during the initial twitch, the calcium transient amplitude increases by 20%. This increase in the Ca^{2+} transient amplitude may be partially obscured and offset by the increased myofilament Ca^{2+} sensitivity, i.e., increased Ca^{2+} buffering, a feature not included in th current model and left for future work. Therefore, it is possible that the stretch activation of Ca^{2+} release might be also involved in force-length effects. However, that is speculative, and further studies are planned to explore this topic more thoroughly.

The model suggests that during the AP, the myocyte spark count increases 15.6% when X-ROS signaling is added. This means additional sites are seeing elevated calcium in the form of Ca^{2+} sparks. Others might be seeing calcium elevations as nonspark openings (15). Low affinity cellular Ca^{2+} sensors (e.g. calmodulin, K_d 5 μM (42)), will only be activated during RyR2 opening. Hence, the increased spark activity, though only modestly affecting Ca^{2+} release, can activate molecules such as calmodulin, which can then act on downstream targets like CaMKII to alter cell function. In fact, there is evidence that CaMKII is activated during stress by Nox2-ROS production at the release sites and that CaMKII directly increases RyR2 open probability (43, 44). Dries and co-workers (43) observed that RyR2s that are in release sites with intact dyadic structure are regulated by Nox2-ROS and CaMKII during high-frequency stimulation. However, orphaned sites without adjacent T-tubules (and therefore presumably far from Nox2) did not show the same frequency-dependent regulation by ROS and CaMKII. Furthermore, Jian and co-workers (44) suggest that the increase of RyR2 open probability with mechanical stress can occur via the synergistic effects of Nox2-ROS production and CaMKII activation as well as nitric oxide synthase signaling (38). Finally, computational modeling by Saucerman and Bers has demonstrated that local Ca^{2+} signaling in the dyadic cleft affects targets of calmodulin such as calcineurin and CaMKII differently than in the bulk myoplasm, supporting the idea that the increase spark activity during stretching may play a further signaling role (45).

The simulations presented here explore only the effects of X-ROS signaling on RyR2s. However, it is likely that X-ROS acts on multiple targets, such as CaMKII,

mechano-sensitive channels (13) and nitric oxide synthase (46), and when these targets are affected in concert, the consequences may be more dramatic. Inclusion of these effects likely will be possible in the future, as we and others carry out new relevant experiments. The experiments used to constrain the modeling might have some of these effects present. If this is the case, the model will need to be reparametrized when new information is included. Hence, the effects of X-ROS signaling are likely greater than its effects on the size of the Ca^{2+} transient and will require further detailed study.

ROS has many targets in the cell and multiple sources. Here, we have considered ROS production by the NADPH-oxidase in response to stretch and how that might affect the RyR. Future work should explore other targets, such as SERCA pumps, L-type channels, the NCX, and the sarcolemmal Ca^{2+} ATPase (4). Other sources of ROS production, such as mitochondria and xanthine oxidase, should also be considered.

In summary, this model for X-ROS signaling has been validated using available data and simulates the stretch-induced increase in spark rate and ROS production. The model suggests that the signaling is local and affects RyR2s in the dyad. It also suggests that as a result, the increase in sparks leads to activation of local calcium-dependent signaling. The model has been used to understand the physiological implication of X-ROS signaling, suggesting that it augments EC coupling gain with increased pacing frequency. The model suggests that diastolic stretching of the ventricular wall due to blood filling the ventricle optimally increases Ca^{2+} release from the SR during systole to maximize contraction. Furthermore, during prolonged stretching, the stretching alone is

not likely to augment calcium release. During OS, however, there will be an increased level of ROS and increased RyR2 activity due to X-ROS signaling.

REFERENCES

1. Mieyal, J. J., and P. B. Chock. 2012. Posttranslational modification of cysteine in redox signaling and oxidative stress: Focus on s-glutathionylation. Antioxidants & redox signaling 16:471-475.

2. Sun, J., C. Xin, J. P. Eu, J. S. Stamler, and G. Meissner. 2001. Cysteine-3635 is responsible for skeletal muscle ryanodine receptor modulation by NO. Proceedings of the National Academy of Sciences of the United States of America 98:11158-11162.

3. Marengo, J. J., C. Hidalgo, and R. Bull. 1998. Sulfhydryl oxidation modifies the calcium dependence of ryanodine-sensitive calcium channels of excitable cells. Biophysical journal 74:1263-1277.

4. Zima, A. V., and L. A. Blatter. 2006. Redox regulation of cardiac calcium channels and transporters. Cardiovascular research 71:310-321.

5. Boraso, A., and A. J. Williams. 1994. Modification of the gating of the cardiac sarcoplasmic reticulum Ca(2+)-release channel by H2O2 and dithiothreitol. The American journal of physiology 267:H1010-1016.

6. Eu, J. P., J. Sun, L. Xu, J. S. Stamler, and G. Meissner. 2000. The skeletal muscle calcium release channel: coupled O2 sensor and NO signaling functions. Cell 102:499-509.

7. Xu, L., J. P. Eu, G. Meissner, and J. S. Stamler. 1998. Activation of the cardiac calcium release channel (ryanodine receptor) by poly-S-nitrosylation. Science 279:234-237.

8. Marks, A. R. 2000. Cardiac intracellular calcium release channels: role in heart failure. Circulation research 87:8-11.

9. Terentyev, D., I. Gyorke, A. E. Belevych, R. Terentyeva, A. Sridhar, Y. Nishijima, E. C. de Blanco, S. Khanna, C. K. Sen, A. J. Cardounel, C. A. Carnes, and S. Gyorke. 2008. Redox modification of ryanodine receptors contributes to sarcoplasmic reticulum Ca2+ leak in chronic heart failure. Circulation research 103:1466-1472.

10. Cheng, H., W. J. Lederer, and M. B. Cannell. 1993. Calcium sparks: elementary events underlying excitation-contraction coupling in heart muscle. Science 262:740-744.

11. Prosser, B. L., C. W. Ward, and W. J. Lederer. 2011. X-ROS signaling: rapid mechano-chemo transduction in heart. Science 333:1440-1445.

12. Prosser, B. L., C. W. Ward, and W. J. Lederer. 2013. X-ROS signalling is enhanced and graded by cyclic cardiomyocyte stretch. Cardiovascular research 98:307-314.

13. Khairallah, R. J., G. Shi, F. Sbrana, B. L. Prosser, C. Borroto, M. J. Mazaitis, E. P. Hoffman, A. Mahurkar, F. Sachs, Y. Sun, Y. W. Chen, R. Raiteri, W. J. Lederer, S. G. Dorsey, and C. W. Ward. 2012. Microtubules underlie dysfunction in duchenne muscular dystrophy. Science signaling 5:ra56.

14. Wagner, E., M. A. Lauterbach, T. Kohl, V. Westphal, G. S. Williams, J. H. Steinbrecher, J. H. Streich, B. Korff, H. T. Tuan, B. Hagen, S. Luther, G. Hasenfuss, U. Parlitz, M. S. Jafri, S. W. Hell, W. J. Lederer, and S. E. Lehnart. 2012. Stimulated emission depletion live-cell super-resolution imaging shows proliferative remodeling of T-tubule membrane structures after myocardial infarction. Circulation research 111:402-414.

15. Williams, G. S., A. C. Chikando, H. T. Tuan, E. A. Sobie, W. J. Lederer, and M. S. Jafri. 2011. Dynamics of calcium sparks and calcium leak in the heart. Biophysical journal 101:1287-1296.

16. D'Autreaux, B., and M. B. Toledano. 2007. ROS as signalling molecules: mechanisms that generate specificity in ROS homeostasis. Nature reviews. Molecular cell biology 8:813-824.

17. Jafri, M. S. H.-T., M.T. 2012. Method and System for Utilizing Markov Chain Monte Carlo Simulations. In Patent, U. S.

18. Chen, K., and J. F. Keaney, Jr. 2012. Evolving concepts of oxidative stress and reactive oxygen species in cardiovascular disease. Current atherosclerosis reports 14:476-483.

19. Barbieri, E., and P. Sestili. 2012. Reactive oxygen species in skeletal muscle signaling. Journal of signal transduction 2012:982794.

20. Handayaningsih, A. E., G. Iguchi, H. Fukuoka, H. Nishizawa, M. Takahashi, M. Yamamoto, E. H. Herningtyas, Y. Okimura, H. Kaji, K. Chihara, S. Seino, and Y. Takahashi. 2011. Reactive oxygen species play an essential role in IGF-I

signaling and IGF-I-induced myocyte hypertrophy in C2C12 myocytes. Endocrinology 152:912-921.

21. Wendell, P. L. 1970. Measurement of oxidized glutathione and total glutathione in the perfused rat heart. The Biochemical journal 117:661-665.

22. Friedman, H. S., O. M. Colvin, K. Aisaka, J. Popp, E. H. Bossen, K. A. Reimer, J. B. Powell, J. Hilton, S. S. Gross, R. Levi, and et al. 1990. Glutathione protects cardiac and skeletal muscle from cyclophosphamide-induced toxicity. Cancer research 50:2455-2462.

23. Shite, J., F. Qin, W. Mao, H. Kawai, S. Y. Stevens, and C. Liang. 2001. Antioxidant vitamins attenuate oxidative stress and cardiac dysfunction in tachycardia-induced cardiomyopathy. Journal of the American College of Cardiology 38:1734-1740.

24. Renjini, R., N. Gayathri, A. Nalini, and M. M. Srinivas Bharath. 2012. Oxidative damage in muscular dystrophy correlates with the severity of the pathology: role of glutathione metabolism. Neurochemical research 37:885-898.

25. Hool, L. C. 2008. Evidence for the regulation of L-type Ca2+ channels in the heart by reactive oxygen species: mechanism for mediating pathology. Clinical and experimental pharmacology & physiology 35:229-234.

26. Erickson, J. R., M. L. Joiner, X. Guan, W. Kutschke, J. Yang, C. V. Oddis, R. K. Bartlett, J. S. Lowe, S. E. O'Donnell, N. Aykin-Burns, M. C. Zimmerman, K. Zimmerman, A. J. Ham, R. M. Weiss, D. R. Spitz, M. A. Shea, R. J. Colbran, P. J. Mohler, and M. E. Anderson. 2008. A dynamic pathway for calcium-independent activation of CaMKII by methionine oxidation. Cell 133:462-474.

27. Galan, C., I. Jardin, N. Dionisio, G. Salido, and J. A. Rosado. 2010. Role of oxidant scavengers in the prevention of Ca(2)+ homeostasis disorders. Molecules 15:7167-7187.

28. Storozhevykh, T. P., Y. E. Senilova, N. A. Persiyantseva, V. G. Pinelis, and I. A. Pomytkin. 2007. Mitochondrial respiratory chain is involved in insulin-stimulated hydrogen peroxide production and plays an integral role in insulin receptor autophosphorylation in neurons. BMC neuroscience 8:84.

29. Gonzalez-Flecha, B., and B. Demple. 1997. Homeostatic regulation of intracellular hydrogen peroxide concentration in aerobically growing Escherichia coli. Journal of bacteriology 179:382-388.

30. Cortassa, S., M. A. Aon, R. L. Winslow, and B. O'Rourke. 2004. A mitochondrial oscillator dependent on reactive oxygen species. Biophysical journal 87:2060-2073.

31. Slezak, J., N. Tribulova, J. Pristacova, B. Uhrik, T. Thomas, N. Khaper, N. Kaul, and P. K. Singal. 1995. Hydrogen peroxide changes in ischemic and reperfused heart. Cytochemistry and biochemical and X-ray microanalysis. The American journal of pathology 147:772-781.

32. Hayashi, H., H. Miyata, H. Watanabe, A. Kobayashi, and N. Yamazaki. 1989. Effects of hydrogen peroxide on action potentials and intracellular Ca2+ concentration of guinea pig heart. Cardiovascular research 23:767-773.

33. Shortt, C. M., and K. D. O'Halloran. 2014. Hydrogen peroxide alters sternohyoid muscle function. Oral diseases 20:162-170.

34. Janssen, P. M., and P. P. de Tombe. 1997. Uncontrolled sarcomere shortening increases intracellular Ca2+ transient in rat cardiac trabeculae. The American journal of physiology 272:H1892-1897.

35. Trafford, A. W., M. E. Diaz, and D. A. Eisner. 1998. Stimulation of Ca-induced Ca release only transiently increases the systolic Ca transient: measurements of Ca fluxes and sarcoplasmic reticulum Ca. Cardiovascular research 37:710-717.

36. Jafri, M. S., J. J. Rice, and R. L. Winslow. 1998. Cardiac Ca2+ dynamics: the roles of ryanodine receptor adaptation and sarcoplasmic reticulum load. Biophysical journal 74:1149-1168.

37. Hill, M. F., V. P. Palace, K. Kaur, D. Kumar, N. Khaper, and P. K. Singal. 2005. Reduction in oxidative stress and modulation of heart failure subsequent to myocardial infarction in rats. Experimental and clinical cardiology 10:146-153.

38. Chelu, M. G., and X. H. Wehrens. 2007. Sarcoplasmic reticulum calcium leak and cardiac arrhythmias. Biochemical Society transactions 35:952-956.

39. Rando, T. A., M. H. Disatnik, Y. Yu, and A. Franco. 1998. Muscle cells from mdx mice have an increased susceptibility to oxidative stress. Neuromuscular disorders : NMD 8:14-21.

40. Spassov, A., T. Gredes, T. Gedrange, D. Pavlovic, A. Lupp, and C. Kunert-Keil. 2011. Increased oxidative stress in dystrophin deficient (mdx) mice masticatory muscles. Experimental and toxicologic pathology : official journal of the Gesellschaft fur Toxikologische Pathologie 63:549-552.

41. Gonzalez, D. R., A. V. Treuer, G. Lamirault, V. Mayo, Y. Cao, R. A. Dulce, and J. M. Hare. 2014. NADPH oxidase-2 inhibition restores contractility and intracellular calcium handling and reduces arrhythmogenicity in dystrophic cardiomyopathy. American journal of physiology. Heart and circulatory physiology 307:H710-721.

42. Chin, D., and A. R. Means. 2000. Calmodulin: a prototypical calcium sensor. Trends in cell biology 10:322-328.

43. Dries, E., V. Bito, I. Lenaerts, G. Antoons, K. R. Sipido, and N. Macquaide. 2013. Selective modulation of coupled ryanodine receptors during microdomain activation of calcium/calmodulin-dependent kinase II in the dyadic cleft. Circulation research 113:1242-1252.

44. Jian, Z., H. Han, T. Zhang, J. Puglisi, L. T. Izu, J. A. Shaw, E. Onofiok, J. R. Erickson, Y. J. Chen, B. Horvath, R. Shimkunas, W. Xiao, Y. Li, T. Pan, J. Chan, T. Banyasz, J. C. Tardiff, N. Chiamvimonvat, D. M. Bers, K. S. Lam, and Y. Chen-Izu. 2014. Mechanochemotransduction during cardiomyocyte contraction is mediated by localized nitric oxide signaling. Science signaling 7:ra27.

45. Saucerman, J. J., and D. M. Bers. 2008. Calmodulin mediates differential sensitivity of CaMKII and calcineurin to local Ca2+ in cardiac myocytes. Biophysical journal 95:4597-4612.

46. Prosser, B. L., and C. W. Ward. 2014. Mechano-chemo transduction tunes the heartstrings. Science signaling 7:pe7.

SUPPLEMENT

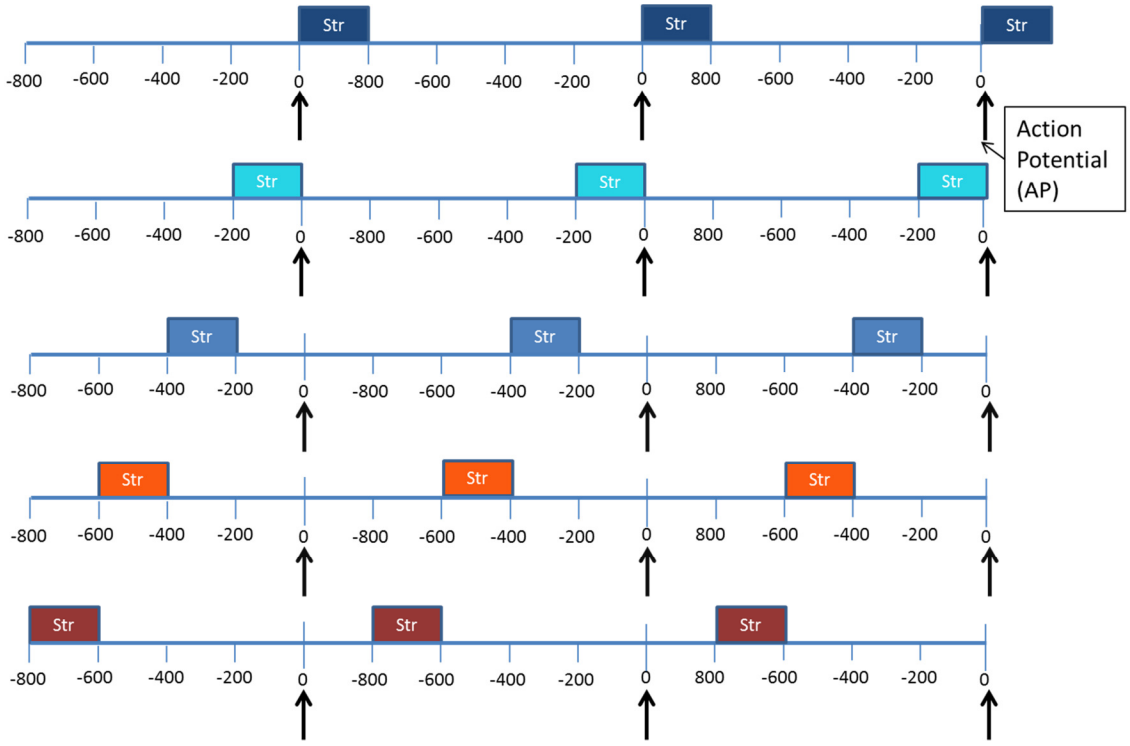

FIGURE S1: For the simulations shown in Fig. 7, the colored bars here indicate when stretching was applied in relation to the pacing electrical stimulus shown by the black arrow pointed upward. The colors here correspond to the colors in Fig. 7, *A* and *B*.

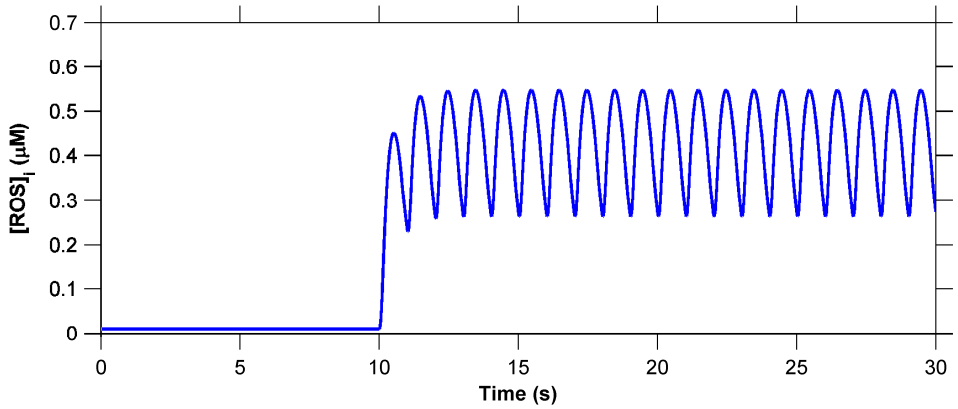

FIGURE S2: Myoplasmic ROS concentration $[ROS]_i$ for the simulations shown in Fig. 7 when the myocyte is stretched from 0 to 200 ms from the time point of application of stimulus.

CHAPTER 3: ROLE OF TROPONIN DYNAMICS ON X-ROS MEDIATED CALCIUM SIGNALING IN HEART

ABSTRACT

Regulation of Ca^{2+} signaling is critical for the excitation-contraction (EC) coupling in the cardiac myocytes. Various underlying mechanisms play crucial roles in imparting complex regulation on Ca^{2+} dynamics of the myocytes. Troponin C (TnC) is a regulatory subunit of troponin complex that binds Ca^{2+} and undergoes conformational change to reveal myosin binding site in actin to initiate myocyte contraction. Increasing sarcomere length of the cardiomyocytes increases the affinity of TnC for Ca^{2+}, increases the Ca^{2+} buffering by troponin and results in increased force of contraction. When a cardiomyocyte at rest is stretched, the stretch-induced Nox2 mediated ROS (X-ROS) is produced that elevates the intracellular Ca^{2+} concentration and on the contrary, the increase in affinity TnC for Ca^{2+} decreases this free cytosolic Ca^{2+} concentration. When stretched, the Ca^{2} binding affinity of troponin is increased by 20% in the model simulations and the affinity returns back to its original value after the release of stretch. In the control case, stretching the myocyte continuously for 10s while stimulus is applied at 0.5 Hz increases the average peak $[Ca^{2+}]_i$ and release of stretch resulted in the return of the average peak $[Ca^{2+}]_i$ to its level before the stretch. Experimental results showed that stretching the myocyte in the presence of blebbistatin, the myosin inhibitor that inhibits cross-bridge formation between actin and myosin, caused more increase in the average

peak $[Ca^{2+}]_i$ than the control case and the computational model that implemented no length-dependent change in affinity in the presence of blebbistatin reproduced the experimental results more closely when compared to the results obtained when the same length-dependent change in affinity is applied in the presence of blebbistatin (as with the control case). Stretching the myocyte in the presence of gp91ds, an NADPH Oxidase peptide inhibitor that inhibits X-ROS production, decreased the peak $[Ca^{2+}]_i$ even after stretching due to the increase in Ca^{2+} buffering by troponin. From these studies, we can conclude that physiologic stretching of cardiac myocyte is critical for complex regulation of Ca^{2+} signaling and the EC coupling, and the stretching contributes in maintaining the Ca^{2+} homeostasis by activating various key players.

INTRODUCTION

Our recent experimental studies have shown that mechanical stretch of cardiac myocytes stimulates production of reactive oxygen species (ROS) by the NADPH Oxidase 2 (Nox2) which results in an increase in RyR2 open probability as indicated by an increase in spontaneous spark rate.(1, 2). This phenomenon is known as X-ROS signaling. We have developed a computational model to dissect the mechanism of X-ROS signaling and predict the impact it has on normal and pathological physiology (3). One prediction of the model was that that stretch just prior to the action potential, such as that which might occur by the filling of the ventricles, optimally potentiates Ca^{2+} release.

In this manuscript, we pursue an integrative experimental and computational modeling approach to improve our understanding of X-ROS signaling and its effect on

excitation contraction coupling by considering length dependent changes in troponin Ca^{2+} sensitivity. During systole the sarcoplasmic reticulum (SR) releases Ca^{2+} ions which binds to the troponin C (TnC) present on actin (the thin filament). The binding of Ca^{2+} ions to TnC changes the conformation of TnC, exposes myosin binding sites on actin and thus initiates the myocyte contraction. Crossbridge formation between the actin and the myosin increases the Ca^{2+} binding affinity of TnC and contribute in increasing the force of contraction of the cardiac myocytes.

Troponin C (TnC) is the Ca^{2+} binding subunit of the troponin complex that also comprises of the inhibitory subunit, troponin I (TnI) and the tropomyosin binding subunit, troponin T (TnT). TnC has two COOH-terminal high-affinity Ca^{2+} binding sites (site III and IV) that can also bind Mg^{2+} (also called Ca^{2+}-Mg^{2+} sites) and two NH_2-terminal low-affinity Ca^{2+} binding sites (site I and II) that are Ca^{2+}-specific. Only the Ca^{2+}-specific sites in TnC can trigger muscle contraction (4, 5) and in case of cardiac TnC, only site II can initiate muscle contraction (6, 7) as the site I is inactivated due to the substitution of some Ca^{2+}-binding amino acids and has only one Ca^{2+}-specific low affinity binding site in the cardiac isoform of TnC (6, 8).

Reduction in force or sarcomere length reduces the Ca^{2+} sensitivity of cardiac troponin C (cTnC) (9). The changes in Ca^{2+} sensitivity has been attributed to length-dependent changes in the spacing between actin and myosin filaments (10). An increase in sarcomere length decreases the separation between the actin and myosin filament.

The combination of experiments and modeling suggest that stretching offers two antagonistic effects on Ca^{2+} signaling during excitation-contraction coupling. Stretching

increases the affinity of troponin for Ca^{2+} which increases the buffering of Ca^{2+} and increases force generation. On the other hand, X-ROS signaling provides an increase of Ca^{2+} mobilization during stretching which increases Ca^{2+} signaling and also contributes contraction and offsets buffering by troponin.

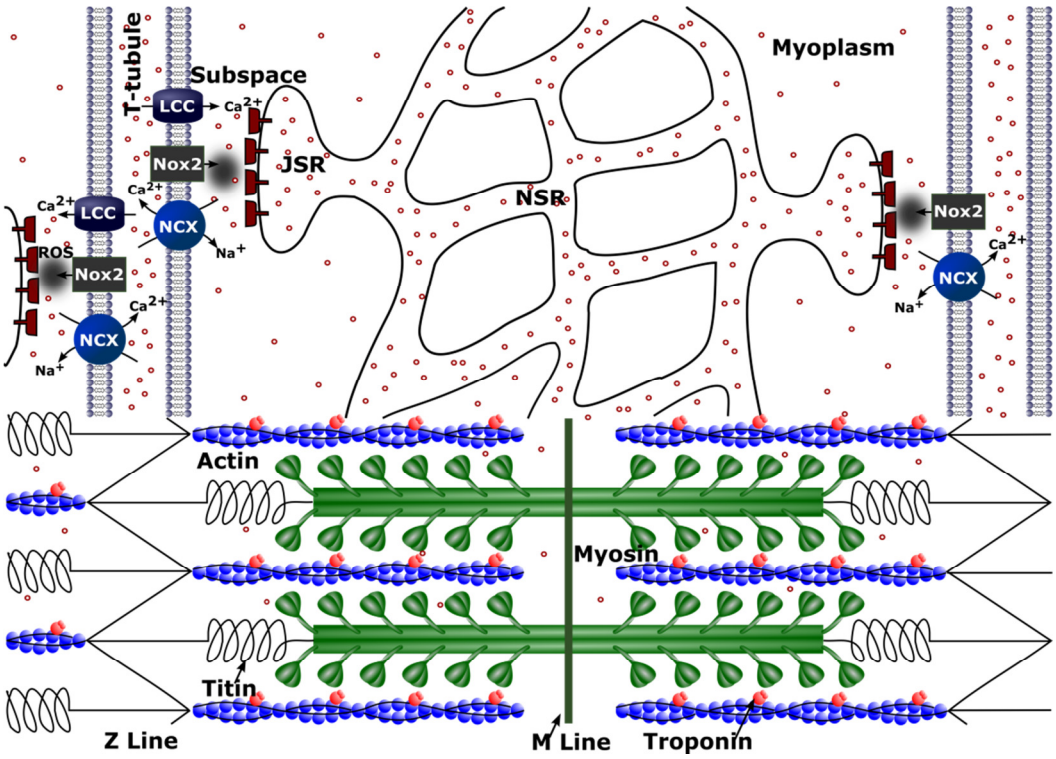

FIGURE 1: Schematic Figure for Calcium Handling Model of a sarcomere. ROS are produced by Nox2 at the Ca^{2+} release site as a result of stretching. Red circles indicate calcium ions (Ca^{2+}). Other abbreviations: NCX – Na^{+}-Ca^{2+} exchanger; LCC – L-type Ca^{2+} current; RYR2 – ryanodine receptor channel; ROS – reactive oxygen species; Nox2 – NADPH oxidase type 2, JSR – junctional sarcoplasmic reticulum; NSR – network sarcoplasmic reticulum;.

THE MODEL

We have developed a model previously for excitation-contraction coupling in the rat ventricular myocyte that included a novel 4-state formulation for the RyR that simulates the increase in open probability of an RyR channel due to its oxidation by stretch-induced ROS (Fig. 1) (3). To improve upon this model we now include the following: 1) addition of the low-affinity Ca^{2+} binding of sites on troponin and 2) stretch-dependent changes in Ca^{2+} affinity for both the low- and high-affinity Ca^{2+} binding sites on troponin.

Our previous work included only the high-affinity binding sites of the troponin buffer which are considered to be occupied by Mg^{2+} or Ca^{2+} most of the time. Therefore, a more realistic model for binding of Ca^{2+} to troponin buffer described by Jafri et al (11) that considers both the high-affinity and low-affinity binding sites is used. The equations describing troponin dynamics are:

$$J_{trpn-high} = k^{+}_{trpn-high}[Ca^{2+}]_i([trpnT]_{high} - [trpnCa]_{high}) - k^{-}_{trpn-high}[trpnCa]_{high}$$

$$J_{trpn-low} = k^{+}_{trpn-low}[Ca^{2+}]_i([trpnT]_{low} - [trpnCa]_{low}) - k^{-}_{trpn-low}[trpnCa]_{low}$$

where $k^{+}_{trpn-high}$ and $k^{+}_{trpn-low}$ are the rates of Ca^{2+} on, and $k^{-}_{trpn-high}$ and $k^{-}_{trpn-low}$ are the rates of Ca^{2+} off for high-affinity and low-affinity binding sites of troponin respectively. $[trpnT]_{high}$ and $[trpnT]_{low}$ are the total myoplasmic concentrations of high-affinity and low-affinity binding sites of troponin respectively, and $[trpnCa]_{high}$and $[trpnCa]_{low}$ are the concentrations of Ca^{2+} bound to high-affinity and

low-affinity troponin binding sites respectively. Added to this model is the increase in Ca^{2+} sensitivity of cTnC due to an increase in the sarcomere length. To represent this, we increased the opening rates (k^{+}_{trpn}) for both the high-affinity as well as low-affinity binding sites by 20% to simulate when the myocyte is stretched 10 %. The k^{+}_{trpn} rates goes back to its initial value once the myocyte is released from the stretch. The increase in the opening rates is constrained by recent experimental data (12).

RESULTS

To understand the consequence of stretch-dependent changes in Ca^{2+} affinity of troponin on excitation-contraction coupling and integrated series of laboratory and numerical experiments were performed. These studies were designed to isolate and dissect the mechanisms involved.

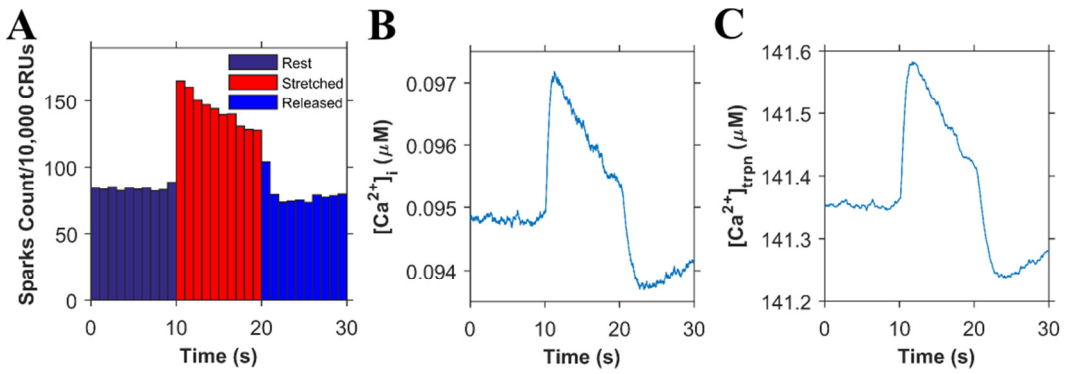

FIGURE 2: Simulation results (n = 20 simulations) when the troponin's affinity to Ca^{2+} does not increase during the stretching of cardiomyocytes (*A*) Ca^{2+} sparks histograms for 1 s bins. (*B*) Concentration of Ca^{2+} in the myoplasm ($[Ca^{2+}]_i$). (*C*) Concentration of Ca^{2+} bound to troponin ($[Ca^{2+}]_{trpn}$).

The first test of the model certified that the experimental results for stretching of the myocyte were still simulated with the addition of the low-affinity Ca^{2+} binding site on troponin. The improved model for X-ROS signaling that uses the model of troponin described by Jafri et al, (11, 13) doubles the Ca^{2+} spark frequency when the myocyte at rest is stretched (Fig. 2 *A*) as seen experimentally by Prosser et al. (14). The frequency returns back to its control level upon the release of the myocyte from the stretch. Stretching also results in the very small transient rise in the myoplasmic Ca^{2+} concentration ($[Ca^{2+}]_i$) (Fig. 2 *B*) as observed previously. Similar small transient rise of the total Ca^{2+} bound to the troponin was observed (Fig. 2 *C*). This is what one would expect as the $[Ca^{2+}]_i$ which is seen by troponin only fluctuates slightly. The simulations in Fig. 2 do not yet include the length-dependent changes in the affinity of troponin for Ca^{2+}.

The next set of simulations shown in Fig. 3 includes a 20% increase in the Ca^{2+} affinity of troponin with a 10% increase in length as observed experimentally (12). Simulations were carried out to investigate how this increase in the affinity of troponin to Ca^{2+} affects the concentration of myoplasmic Ca^{2+} ($[Ca^{2+}]_i$) and of Ca^{2+} bound to troponin ($[Ca^{2+}]_{trpn}$) when the stimulus is not applied (no AP). The Ca^{2+} spark frequency increases abruptly almost by 2-fold when the myocyte is stretched (Fig. 3 *A*). The abrupt increase in the sensitivity of troponin towards Ca^{2+} due to stretching results in a sudden decrease of the $[Ca^{2+}]_i$. But the simultaneous increase in the spark frequency and the subsequent increased extrusion of Ca^{2+} from the SR to the dyadic subspace and to the myoplasm immediately raises $[Ca^{2+}]_i$ level (Fig. 3 *B*). When the myocyte is released from

the stretch, the abrupt decrease in the sensitivity of troponin towards Ca^{2+} results in the transient elevation of the $[Ca^{2+}]_i$ which is compensated immediately by the decreased Ca^{2+} spark frequency. The increased affinity of Ca^{2+} binding by troponin when stretched persists throughout the stretch and hence, the $[Ca^{2+}]_{trpn}$ remains elevated throughout the stretched period (Fig. 3 *C*).

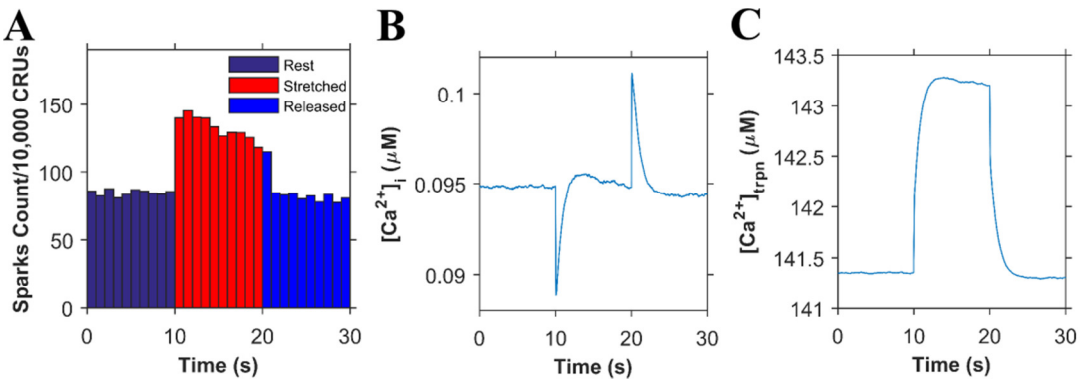

FIGURE 3: Simulation results (n = 20 simulations) when the troponin's affinity to Ca^{2+} increases during the stretching of cardiomyocytes (*A*) Ca^{2+} sparks histograms for 1 s bins, (*B*) concentration of Ca^{2+} in the myoplasm ($[Ca^{2+}]_i$) and (*C*) concentration of Ca^{2+} bound to troponin ($[Ca^{2+}]_{trpn}$).

Stretch dependent mechanisms underlying Ca^{2+} dynamics

Stretching a myocyte (control) activates two mechanisms, 1) X-ROS signaling and 2) increase in the Ca^{2+} binding affinity of the troponin. X-ROS signaling increases the Ca^{2+} released from the SR, i.e. the spark count (Fig. 2 *A*) as well as $[Ca^{2+}]_i$ (Fig. 2 *B*). The increase in the Ca^{2+} binding affinity of the troponin increases the Ca^{2+} buffering which decreases the actual rise in $[Ca^{2+}]_i$ caused by the X-ROS. To explore this further, experiments were performed that measure the relative values of peak Ca^{2+} concentration

($\Delta F/F_0$) with stimulus applied at 0.5 Hz to simulate physiologic stretching under various pharmacological conditions to dissect the relative contributions of the different mechanisms (Fig. 4). Fig. 4 *A* shows experimental results demonstrating a small rise in $[Ca^{2+}]_i$ during stretching. Releasing of the myocyte from the stretching caused the peak $[Ca^{2+}]_i$ to return to its unstretched level. Blebbistatin is a chemical that inhibits myosin and thus inhibits the crossbridge formation between actin and myosin by lowering the affinity of myosin binding to actin. In the presence of blebbistatin, the Ca^{2+} binding affinity of the troponin does not increase even when the myocyte is stretched. Therefore, X-ROS signaling results in an increased $[Ca^{2+}]_i$ transient compared to the control case during the stretch (Fig. 4 *B*). The chemical gp91ds is an NADPH oxidase (Nox2, the source of X-ROS) peptide inhibitor. When the myocyte is stretched in the presence of gp91ds, no X-ROS is produced to increase the flux of Ca^{2+} from SR but there are strong crossbridge formed which increases the Ca^{2+} binding affinity of troponin and hence, the Ca^{2+} buffering. This increase in Ca^{2+} buffering without the elevation of $[Ca^{2+}]_i$ results in decreased $[Ca^{2+}]_i$ during the stretch (Fig. 4 *C*). The peak $\Delta F/F_0$ remains consistent throughout 30 s when the cell is not stretched (Fig. 4 *D*). The peak $\Delta F/F_0$ within were averaged in 2 s bins for rest, stretched and released conditions and normalized (Fig. 4 *E*). This averaged result exhibits the overall consequences of every case experimented here. During the stretch, the peak $[Ca^{2+}]_i$ level in the presence of blebbistatin increases by almost double of its level of increase during the control case. The peak normalized $\Delta F/F0$ increases by 1% in the control case, by 3% when blebbistatin is used. The peak

normalized ΔF/F0 decreases by 3% when gp91ds is used and by 1.5% when colchicine is used. gp91ds and colchicine, both inhibits X-ROS production.

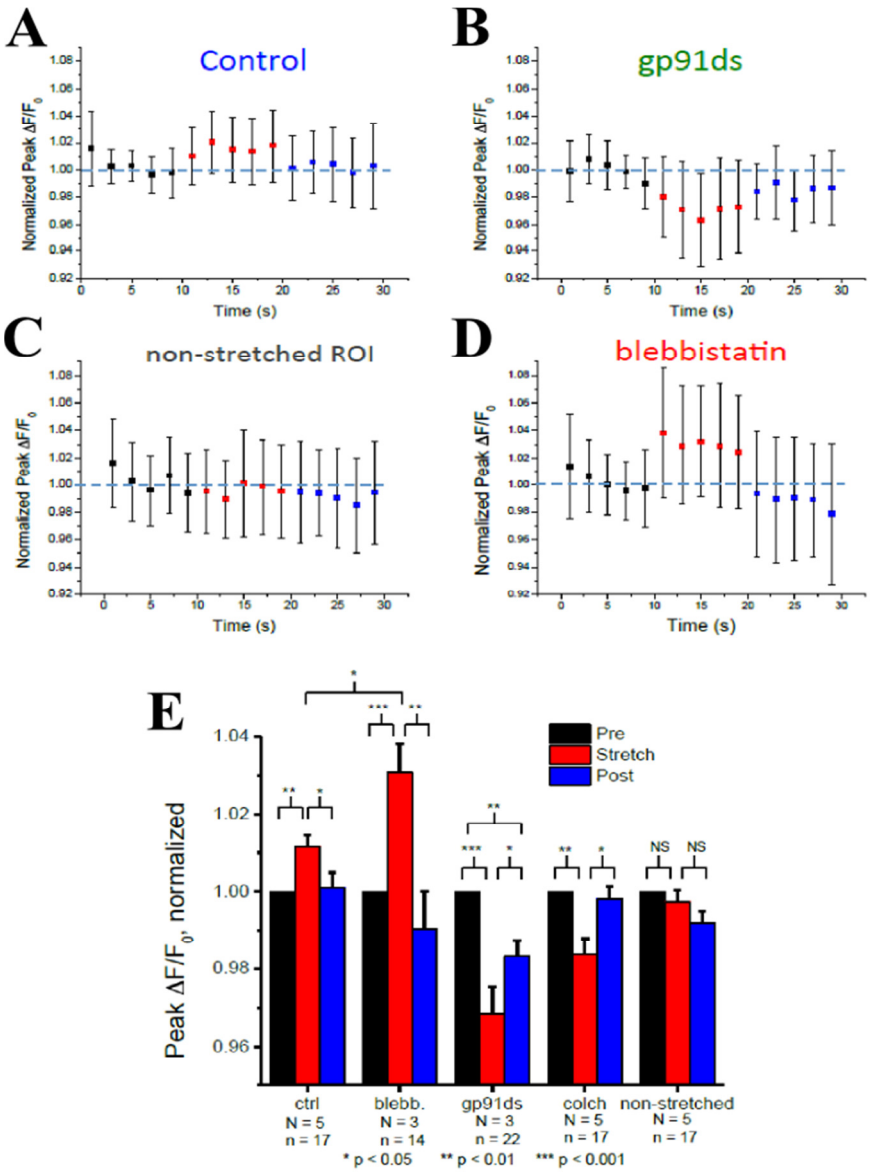

FIGURE 4: Experimental results for the normalized peak ΔF/F0 for the concentration of Ca^{2+} in the myoplasm ($[Ca^{2+}]_i$) with 0.5 Hz stimulus when the cardiomyocyte is at rest (*black*), stretched (*red*) and released after the stretch (*blue*) (*A*) under control condition, (*B*) when blebbistatin is used which inhibits the actin myosin bridge, (*C*) when gp91ds is used which inhibits NOX2 from producing stretch-dependent ROS, (*D*) when the myocyte is not stretched for the entire 30 s duration and (*E*) the calculated average of peak ($[Ca^{2+}]_i$) under each subgroup (*rest*, *stretched* and *released*) of each group (*ctrl*, *blebb*, *gp91ds*, *colch* and *non-stretched*).

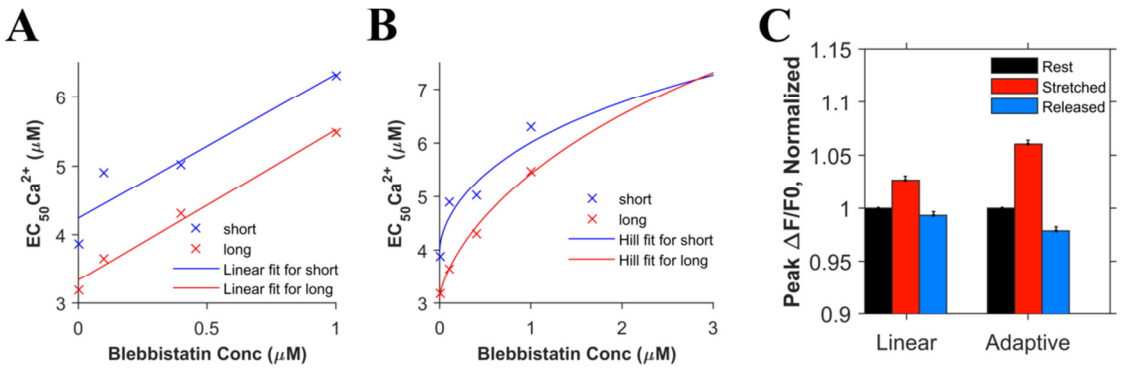

FIGURE 5: The effects of blebbistatin on the Ca^{2+} binding affinity of troponin**.** (*A*) A linear fit shows that the length dependent-difference in binding affinity remains constant at ~20%. The × symbols represent the experimental data from Farman et al .(12) and the lines the fit. (mean squared error = 0.085) (*B*) An adaptive fit using the Hill equations show that the length dependent difference in the binding affinity decreases and eventually disappears with increasing blebbistatin concentration. (mean squared error = 0.062) (*C*) Simulation results (n = 20 simulations) for the comparison between linear and adaptive cases.

Numerical simulations confirm this analysis of the experiments from Fig. 4. In order to model the effects of blebbistatin, experimental data quantifying the effects of blebbistatin on the Ca^{2+} affinity of troponin was considered. According to the observation by Farman et al. (12), there was a decrease in calcium sensitivity with an increase in the blebbistatin concentration, However, using the approximately linear fit suggested in the paper the length dependent differences remain constant in the calcium binding affinity of troponin as seen by the constant difference between the two lines in Fig 5A. On the other hand, fitting the EC_{50} data for calcium sensitivity to a hill equation gave a better least squared error compared to the linear fit in both the short and long sarcomere. The result was that length dependent differences disappear as the the blebbistan concentration increases blebbistatin (Fig 5B) which we will call 'adaptive'. To

assess which of these interpretations was more likely, we carried out two sets of simulations considering the data for the linear and adaptive cases.. For the first set of simulations, we considered that there was no length dependent change in the calcium binding affinity of troponin even in the presence of blebbistatin (Fig. 5C, Linear) and hence, when the myocyte is stretched, the $k^{+}_{trpn-high}$and $k^{+}_{trpn-low}$ increases by 20% in both the presence of blebbistatin and the absence of blebbistatin (Fig. 6 *D,* ctrl). For the second set of simulations, we considered that there was length dependent change in the calcium binding affinity of troponin in the presence of blebbistatin (Fig. 5C, Adaptive) and hence, when the myocyte is stretched, the $k^{+}_{trpn-high}$and $k^{+}_{trpn-low}$ remain unchanged. The results of the second set of simulations resembled the experimental data (Fig. 4 *E*, blebb) more closely than did the results of the first set of simulations.

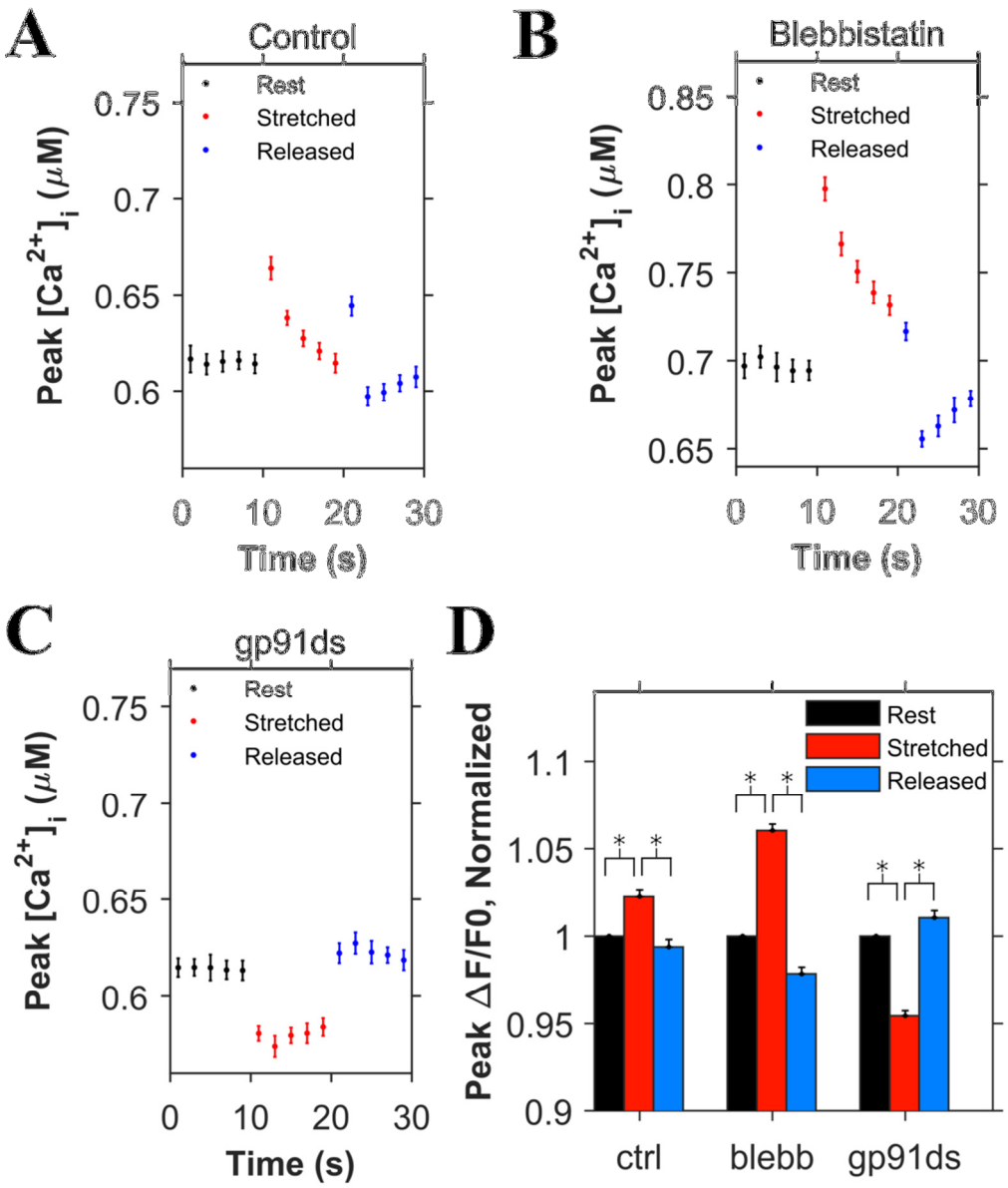

FIGURE 6: Simulation results (n = 20 simulations) for the peak concentration of Ca^{2+} in the myoplasm ($[Ca^{2+}]_i$) with 0.5 Hz stimulus when the cardiomyocyte is at rest (*black*), stretched (*red*) and released after the stretch (*blue*) (*A*) under control condition, (*B*) when blebbistatin is used which inhibits the actin myosin bridge, (*C*) when gp91ds is used which inhibits Nox2 from producing stretch-dependent ROS and (*D*) the peak ($[Ca^{2+}]_i$) under each subgroup (*rest*, *stretched* and *released*) of each group (*ctrl*, *blebb* and *gp91ds*) is averaged, its corresponding ΔF/F0 is calculated and normalized. *$p< 10^{-14}$.

Using the adaptive fit described above, the simulation data was used to simulate the experiments displayed in Fig 4. In the control simulations (Fig 6A), the k_{trpn}^{+} rates for both the high and low affinity binding sites were increased by 20% when the myocyte is stretched to simulate the effects of length-dependent change in Ca^{2+} affinity displayed by troponin. With this affinity increase, there is a small transient increase in $[Ca^{2+}]_i$ (Fig. 6A). Removal of this increase in affinity to simulate the presence of blebbistatin (adaptive case) resulted in the expected almost doubling of the increase $[Ca^{2+}]_i$ level during the stretching (Fig 6B) over control stretchin (Fig 6A) similar to experiment. Also, the block of X-ROS signaling to simulate the presence of gp91ds, show the buffering effect of troponin that increases during stretching (Fig 6C). The peak $[Ca^{2+}]_i$ within every 2 s were averaged for rest, stretched and released conditions, corresponding ΔF/F0 values were calculated, and normalized (Fig 6D). This data shows results similar to experiments (Fig 4E). When stretched, the peak normalized ΔF/F0 increased by 2.2% in control case whereas by 6% when there is no change in the Ca^{2+} binding affinity of troponin (blebb). When no X-ROS is produced (gp91ds), the peak normalized ΔF/F0 decreased by 4.6%. The agreement of the experiment and simulation indicate the relative contributions of X-ROS signaling and buffering by troponin to stretching-induced changes in calcium signaling.

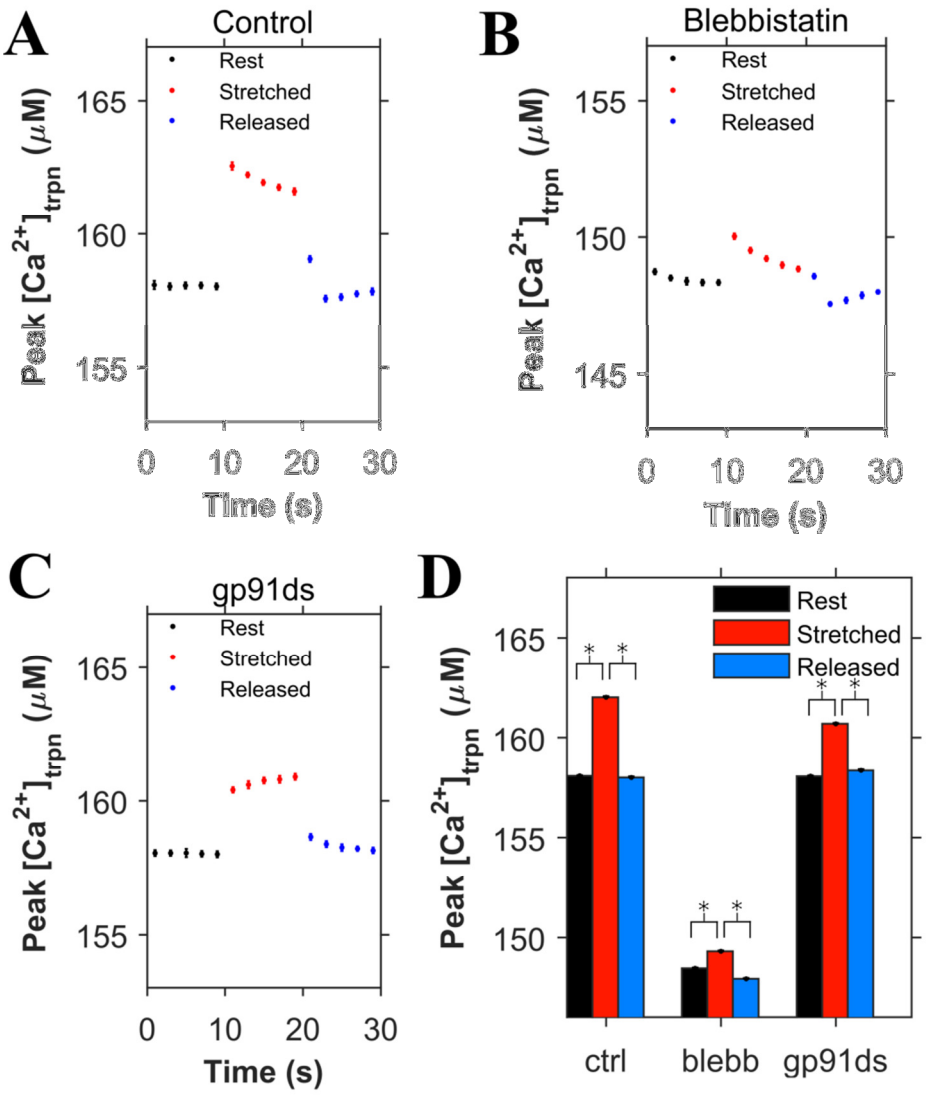

FIGURE 7: Simulation results (n = 20 simulations) for the peak value of Ca^{2+} bound to troponin ($[Ca^{2+}]_{trpn}$) with 0.5 Hz stimulus when the cardiomyocyte is at rest (*black*), stretched (*red*) and released after the stretch (*blue*) (*A*) under control condition, (*B*) when blebbistatin is used which inhibits the actin myosin bridge, (*C*) when gp91ds is used which inhibits NOX2 from producing stretch-dependent ROS and (*D*) the calculated corresponding average of peak ($[Ca^{2+}]_{trpn}$) under each subgroup (*rest*, *stretched* and *released*) in each group (*ctrl*, *blebb* and *gp91ds*). *p< 10^{-22}.

Ca^{2+} bound to troponin

The concentration of Ca^{2+} bound to troponin ($[Ca^{2+}]_{trpn}$) was determined in each of the cases (control, blebb, and gp91ds) simulated in Fig 6 (Fig 7). In control case, the peak $[Ca^{2+}]_{trpn}$ was 158 μM while the myocyte is at rest, increased when the myocyte was stretched and returned back to its initial resting level of concentration when the myocyte was released from the stretch (Fig 7A). When the use of blebbistatin was simulated, with no increase in the Ca^{2+} binding affinity of troponin with the stretch, smaller increase of the peak $[Ca^{2+}]_{trpn}$ was seen due to increase in the $[Ca^{2+}]_i$ as a result of X-ROS production and the peak $[Ca^{2+}]_{trpn}$ decreased to previous level at rest when the myocyte was released (Fig 7B). Similarly, when the use of gp91ds was simulated with no X-ROS produced even with the stretch, there was an increase in peak $[Ca^{2+}]_{trpn}$ due to the increase in the Ca^{2+} binding affinity of the troponin and the peak $[Ca^{2+}]_{trpn}$ returned to previous level at rest when the myocytes was released from the stretch (Fig 7C). The peak values of $[Ca^{2+}]_{trpn}$ in each subgroup of rest, stretched and released are averaged for control, blebbistatin and gp91ds (Fig 7D). Fig 7D clearly demonstrates the decrease in the concentration of Ca^{2+} bound to troponin during the stretch when no actin-myosin crossbridge is formed than any other cases.

DISCUSSION

In order to explore the interplay of X-ROS signaling and the length dependent changes in the Ca^{2+} binding affinity of troponin, an integrated series of simulations were performed. The initial model predictions suggested that the transient increase in

myoplasmic [Ca^{2+}] induced by X-ROS signaling during stretching would be reduced by the increased buffering by troponin due to the length-dependent increase in Ca^{2+} binding affinity. The model also suggested that there would be, in fact, a quick transient decrease in $[Ca^{2+}]_i$ due to troponin followed by the small transient rise due to X-ROS dependent activation of the RyR. Upon relaxation there is a predicted transient increase in myoplasmic [Ca^{2+}]. This is consistent with the observation by Backx and ter Keurs that saw a transient increase in myoplasmic Ca^{2+} at the end of a twitch that they attributed to troponin dynamics (15).

Experiments to dissect the relative contribution during stretch used blebbistatin to reduce the length dependent effects on Ca^{2+} binding by troponin. Recent results by Farman et al. suggested that there might be reductions in Ca^{2+} binding affinity with the addition of blebbistatin with no reduction in the length dependent changes in affinity when a linear fit to the data was considered. This however, was inconsistent with the experimental data presented in Fig 4. Instead, when the Farman data was described by an adaptive fit where the reductions in the Ca^{2+} binding affinity of troponin with increases in blebbistatin were accompanied by a reduction and eventual elimination of length dependent differences in binding affinity, the experimental data presented in Fig 4 could be reproduced in the simulations. In fact, the adaptive fit resulted in a better fit as measured by mean squared error than the linear fit (Fig 5). This suggests that blebbistatin plays these two roles i.e., a reduction and eventual elimination of length dependent differences in binding affinity, when applied.

The modeling also suggests that the reduction in the myoplasmic [Ca^{2+}] in the presences of of gp21ds is consistent with its putative role as a blocker of the NADPH oxidase and hence the block of X-ROS signaling. Furthermore, the reduction seen in the myoplasmic [Ca^{2+}] is due to the increased buffering of Ca^{2+} by troponin during stretching (Fig 7). Once again these results suggest that the increased buffering by troponin during stretch is offset by the increased Ca^{2+} release induced by X-ROS signaling.

These results demonstrate how the integration of experiment and modeling can be used to effectively dissect the mechanisms of Ca^{2+} dynamics in the cell with regards to the relative roles of X-ROS signaling and Ca^{2+} buffering by troponin. It adds to our previous work, suggesting physiologic roles of X-ROS signaling in cardiac myocytes (3). In the future, expanded models exploring the spatial aspects of X-ROS signaling are planned to further understand potential targets of X-ROS signaling and how X-ROS signaling may play a role in Ca^{2+} entrained arrhythmias.

REFERENCES

1. Prosser, B. L., C. W. Ward, and W. J. Lederer. 2011. X-ROS signaling: rapid mechano-chemo transduction in heart. Science 333:1440-1445.

2. Prosser, B. L., C. W. Ward, and W. J. Lederer. 2013. X-ROS signalling is enhanced and graded by cyclic cardiomyocyte stretch. Cardiovascular research 98:307-314.

3. Limbu, S., M. T. Hoang-Trong, T. M. Hoang-Trong, B. L. Prosser, W. J. Lederer, and M. S. Jafri. 2015. Modeling Local X-ROS and Calcium Signaling in Heart. Biophys. J. Biophys J http://dx.doi.org/10.1016/j.bpj.2015.09.031.

4. Potter, J. D., and J. Gergely. 1975. The calcium and magnesium binding sites on troponin and their role in the regulation of myofibrillar adenosine triphosphatase. The Journal of biological chemistry 250:4628-4633.

5. Sheng, Z., W. L. Strauss, J. M. Francois, and J. D. Potter. 1990. Evidence that both Ca(2+)-specific sites of skeletal muscle TnC are required for full activity. The Journal of biological chemistry 265:21554-21560.

6. Sweeney, H. L., R. M. Brito, P. R. Rosevear, and J. A. Putkey. 1990. The low-affinity Ca2(+)-binding sites in cardiac/slow skeletal muscle troponin C perform distinct functions: site I alone cannot trigger contraction. Proceedings of the National Academy of Sciences of the United States of America 87:9538-9542.

7. Putkey, J. A., H. L. Sweeney, and S. T. Campbell. 1989. Site-directed mutation of the trigger calcium-binding sites in cardiac troponin C. The Journal of biological chemistry 264:12370-12378.

8. van Eerd, J. P., and K. Takahashi. 1975. The amino acid sequence of bovine cardiac tamponin-C. Comparison with rabbit skeletal troponin-C. Biochemical and biophysical research communications 64:122-127.

9. Wang, Y. P., and F. Fuchs. 1994. Length, force, and Ca(2+)-troponin C affinity in cardiac and slow skeletal muscle. The American journal of physiology 266:C1077-1082.

10. Fuchs, F., and Y. P. Wang. 1996. Sarcomere length versus interfilament spacing as determinants of cardiac myofilament Ca2+ sensitivity and Ca2+ binding. Journal of molecular and cellular cardiology 28:1375-1383.

11. Jafri, M. S., J. J. Rice, and R. L. Winslow. 1998. Cardiac Ca2+ dynamics: the roles of ryanodine receptor adaptation and sarcoplasmic reticulum load. Biophysical journal 74:1149-1168.

12. Farman, G. P., E. J. Allen, K. Q. Schoenfelt, P. H. Backx, and P. P. de Tombe. 2010. The role of thin filament cooperativity in cardiac length-dependent calcium activation. Biophysical journal 99:2978-2986.

13. Luo, C. H., and Y. Rudy. 1994. A dynamic model of the cardiac ventricular action potential. I. Simulations of ionic currents and concentration changes. Circulation research 74:1071-1096.

14. Prosser, B. L., C. W. Ward, and W. J. Lederer. 2011. X-ROS signaling: rapid mechano-chemo transduction in heart. Science 333:1440-1445.

15. Backx, P. H., and H. E. Ter Keurs. 1993. Fluorescent properties of rat cardiac trabeculae microinjected with fura-2 salt. The American journal of physiology 264:H1098-1110.

CHAPTER 4: USING A SPATIOTEMPORAL MODEL OF X-ROS SIGNALING TO STUDY ITS ARRHYTHMOGENIC ROLE DURING PATHOLOGICAL CONDITIONS

ABSTRACT

Stretching a cardiac ventricular myocyte is physiologically similar to diastolic stretching of the heart cells during filling of the ventricles with blood and this stretching has been shown to produce NADPH oxidase 2 (Nox2)-activated reactive oxygen species (ROS) (X-ROS). ROS can regulate the Ca^{2+} signaling in the cardiac myocytes by targeting various Ca^{2+} signal handling channels and proteins. Experimentally, it is difficult to gather detailed spatial information on X-ROS signaling in cardiac myocytes as the low signal-to-noise ratio requires averaging across many spatial points. Therefore, spatial model of a cardiac ventricular myocyte with X-ROS signaling was developed to study how the stretch-induced ROS produced in the subspace would behave globally in the 3-D space in the myoplasm and how it can affect the cardiac Ca^{2+} signaling in excitation-contraction coupling. The ROS was shown to diffuse rapidly from the subspace where it is produced into the myoplasm of the sarcomere with its rise in concentration more elevated at the central region of the myocyte and a uniform depletion throughout the myocyte during sustained stretching of the whole myocyte. However, in the inactive regions where the X-ROS is not produced (no stretching or no dyadic subspaces), the ROS levels remain near baseline with a steep drop-off in the boundary

between the active and inactive regions. Finally, the role X-ROS signaling might play in the generation of cardiac arrhythmia is explored.

INTRODUCTION

Reactive oxygen species (ROS) are oxygen derived, highly reactive molecules involved in cellular signaling, defense and homeostasis. Stretching a cardiac ventricular myocyte in the resting condition produces Nox2-activated ROS mediated by microtubules (1). Nox2 produces ROS in the form of superoxide anions, which are highly unstable and are reduced to hydrogen peroxide by superoxide dismutase.

Ca^{2+} released from a group of calcium release units (CRUs) can trigger Ca^{2+} release from nearby CRUs via fire-diffuse-fire based on calcium induced calcium release (CICR) and can lead to propagation of the local elevation of intracellular Ca^{2+} throughout the myocyte in the form of wave. These local Ca^{2+} waves were previously noted as local sarcomeric contractions propagating in the cells by various groups (2, 3). Pathological conditions such as Ca^{2+} overload can cause spontaneous Ca^{2+} waves. The elevation in the intracellular Ca^{2+} can activate inward current via Na^{+}-Ca^{2+} exchanger (NCX) and other currents which could depolarize the cell to initiate a triggered contraction or arrhythmia (4).

Duchenne muscular dystrophy (dmd) is a muscular disorder disease with progressive ventricular wall motion abnormalities due to fibrosis, left ventricular dysfunction and arrhythmias leading to heart failure and sudden death (5). About 90% of the dmd patients show clinical cardiac involvement but causes death in about 20% of the

patients and is the second most common cause of death in dmd patients, the primary cause being the respiratory failure. Increase in the ROS concentration has been associated with abnormalities in the skeletal (6) and cardiac (7) myocytes of *mdx* mice. In the resting condition, ROS concentration is shown to increase by 1.19-fold and the NADPH oxidase activity increased by 1.4-fold in *mdx* cardiomyocytes when compared to wild type (7). The increased ROS concentration in *mdx* mice myocyte is further increased after stress is applied in the form of osmotic shock (8) . Stretching a cardiac ventricular myocyte in the resting condition produces Nox2-activated ROS mediated by microtubules and elevates the intracellular ROS concentration (1). The increase in stretch-induced ROS production was significantly increased in the *mdx* myocytes when compared to WT (1). The frequency of Ca^{2+} waves increased in the *mdx* mice which further increased upon stretching. The resting level of intracellular Ca^{2+} was elevated by ~1.5-fold in case of old *mdx* mice in comparison to old WT mice (9) whereas it increased by ~1.27 fold in case of 5-9 month old *mdx* mice (8). The SR calcium content of *mdx* old mice was highly elevated in comparison to old WT mice (9) and modestly elevated in case of 6-12 months *mdx* mice in comparison to their WT (10). In *mdx* mouse, the myofilament Ca^{2+} sensitivity decreased (7), the microtubule level increased by 1.4-fold (11), the RyR2 protein expression levels increased by 2-fold in case of young *mdx* mice compared to young WT, whereas it increased by 3-fold in case of old *mdx* mice compared to old WT (9). Diastolic stretch that causes abrupt increase in Ca^{2+} spark often in normal myocyte can generate Ca^{2+} waves in *mdx* myocytes due to increased RyR2 opening probability which helps in CICR based triggering of Ca^{2+} spark propagation. Oxidative stress has

been associated with diastolic leak causing Ca^{2+} leak and arrhythmia in *mdx* myocytes (7, 12).

Oxidative stress has been associated with SR Ca^{2+} leak in the HF (13) as well as with progression of hypertrophy to HF (14). ROS produced due to increased NADPH oxidase activity has been implicated in the HF myocytes (15, 16) as well as in myocytes progressing from hypertrophy to HF (17). Thus, it has been suggested that stretching HF myocytes also produces excessive ROS to cause oxidative stress, Ca^{2+} leak and abnormal Ca^{2+} handling (18).

Here, we have developed a spatial model of a rat ventricular myocyte with stretch-induced Nox2 activated ROS (X-ROS) signaling included in the model in order to investigate the impact X-ROS signaling may have on various cellular components and abnormalities associated with cardiomyopathy.

METHODS

The four-state RyR2 model with X-ROS signaling that we previously developed (19) was integrated into the 3D spatial myocyte model developed in our lab to develop a new spatial rat ventricular myocyte model with X-ROS signaling. The model considers the length, width and height of the myocyte as 120, 20.8 and 10 μm respectively with each grid element of 0.2 x 0.2 x 0.2 μm^3. The ROS is produced locally in each subspace of 20,000 CRUs upon stretch and the ROS may oxidize RyR2 or may diffuse out into its closest myoplasmic grid.

Molecular crowding within the cytosol can reduce the diffusion coefficients of Ca^{2+} by 18% to 60% in the case of highly crowded environment (20). Considering similar crowding effect on the diffusion coefficient of hydrogen peroxide as done by Vestergaard et al. (21), the value of 1,000 $\mu m^2 s^{-1}$ is used in comparison to its value of 1,700 $\mu m^2 s^{-1}$ in solution (22). The use of diffusion coefficient in the model resulted in a speedy diffusion of ROS from subspace to myoplasm and the myoplasmic ROS profile matching the ROS production flux profile of Fig. 4 *C* of Limbu et al. (19). Thus, the 4-state RyR2 model was used with a modification in the 4 time-dependent ROS production equations (Eqs 8.1 to 8.4) in order to adjust the myoplasmic ROS concentration so that it matches the experimental ROS profile as shown by Prosser et al. (1).

$$J^k_{ROSProduction} = ROS_{preStr} + \frac{(.00024 - ROS_{preStr})}{.12} t \qquad \text{for} \quad t < t_{Str}$$

$$J^k_{ROSProduction} = .0000072(t^2) - .0000508(t) + .000246 \qquad t_{Str} \leq t < 1.5s$$

$$J^k_{ROSProduction} = .0000015(t^2) - .0000324(t) + .000232 \qquad 1.5s \leq t < 4s$$

$$J^k_{ROSProduction} = .000216(exp^{-.133t}) \qquad t \geq 4s$$

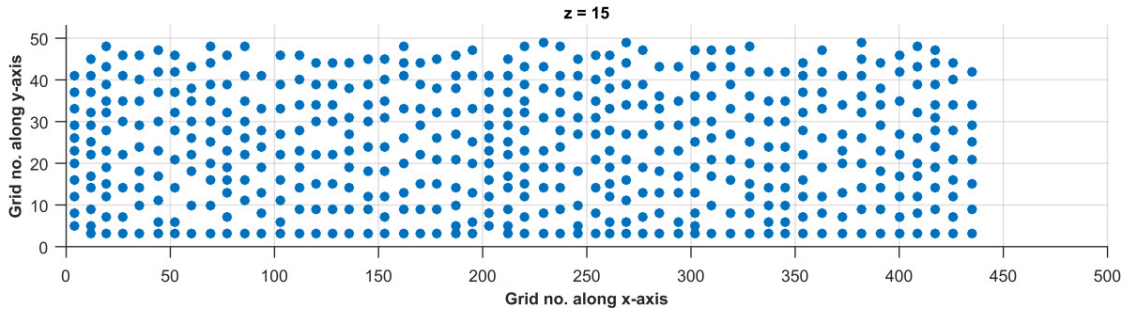

FIGURE 1: CRUs placement at grids along given x and y locations at a specific depth (at 15th grid along the z-axis).

The stretch-induced ROS is produced locally in each dyadic subspace at each CRU. The CRUs are distributed along the z-lines at a distance of the longitudinal length of a sarcomere i.e. approximately 2 μm along x-axis as shown in Fig. 1. Note in Fig. 1 that there are regions at the right and in the top and bottom left corners that lack release sites.

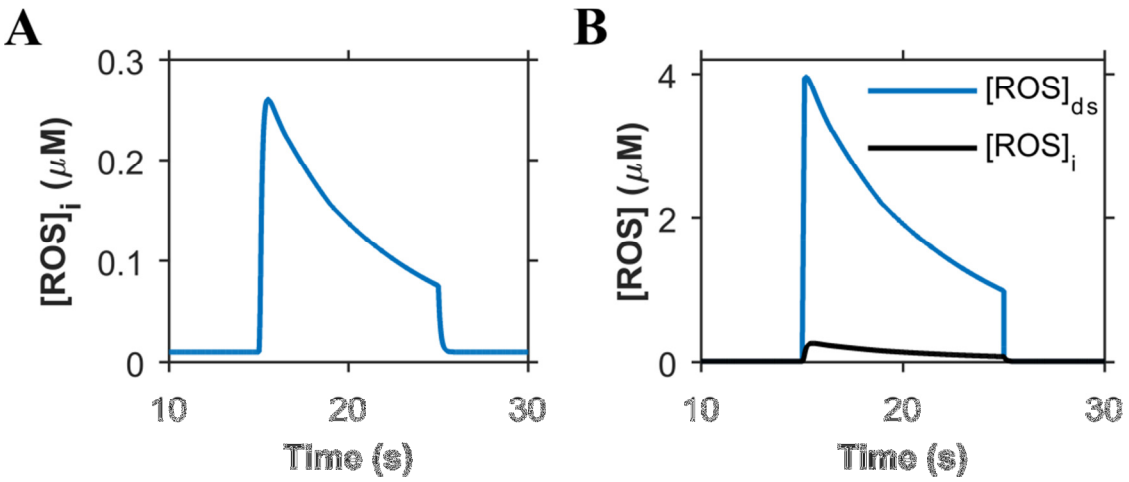

FIGURE 2: ROS dynamics during the stretching from 15 - 25 s (*A*) Concentration of ROS in the myoplasm ($[ROS]_i$). (*B*) Concentration of ROS in the dyadic subspace($[ROS]_{ds}$) compared to $[ROS]_i$.

The myoplasmic ROS concentration ($[ROS]_i$) thus produced by the model averaged for each grid element is as shown in Fig. 2 *A* and the corresponding subspace ROS concentration ($[ROS]_{ds}$) compared to $[ROS]_i$ is as shown in Fig. 2 *B*. The model is able to produce almost 2-fold increase in spark frequency when the myocyte is stretched as shown in Fig. 3 *A* as seen experimentally by Prosser et al and as our compartmental model of the rat ventricular myocyte was able to produce. The transient increase in the

myoplasmic Ca^{2+} concentration ($[Ca^{2+}]_i$) and the corresponding transient depletion of network SR Ca^{2+} concentration ($[Ca^{2+}]_{NSR}$) is as shown in Fig 3. *B* and *C* respectively.

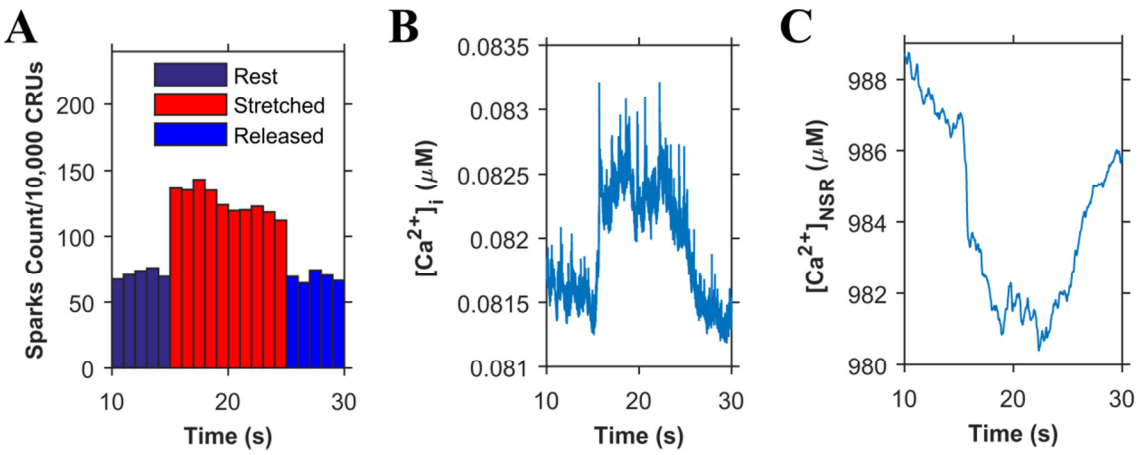

FIGURE 3: Simulation results using the 4-state ventricular cardiac myocyte model (*A*) Ca^{2+} sparks histograms for 1 s bins, (*B*) myoplasmic Ca^{2+} concentration ($[Ca^{2+}]_i$) and (*C*) network SR Ca^{2+} concentration ($[Ca^{2+}]_{NSR}$). The myocyte is stretched continuously from 15-25 s displaying a transient increase in Ca^{2+} spark rate.

RESULTS

The ROS in this temporal-spatial model with X-ROS signaling presented here diffuses out from the subspace to the myoplasm in a few milliseconds of time due to its very fast diffusion coefficients towards x, y, and z directions from each subspace. The 3-dimensional profile of myoplasmic ROS, due to its diffusion from the subspace where it is locally produced, measured at a specific depth at various times is as shown in Fig. 3 at the whole-cell level. The diffusion of ROS is very rapid and within 100 ms of stretching the myoplasmic ROS rises from basal level of 10 nM to 90 nM as seen in Fig 4. *A*. The ROS concentration peaks at around 250 ns with peak value of 160 nM around the centre

of the myocyte (Fig. 4 *B*). With sustained stretching the ROS concentration gradually depletes throughout the myocyte (Fig. 4 *C*). The myoplasmic ROS profiles shown in the Fig. 4 clearly demonstrates that ROS peaks to higher concentration level towards the centre of the myocyte compared to the periphery. At the corners on the left and on the right edge, the ROS concentration is considerably lower, i.e. close to the baseline. This is because ROS is not produced in these regions. This is important to note because it suggests that while ROS diffusion is rapid, its degradation is also rapid so it does not have a long diffusional distance.

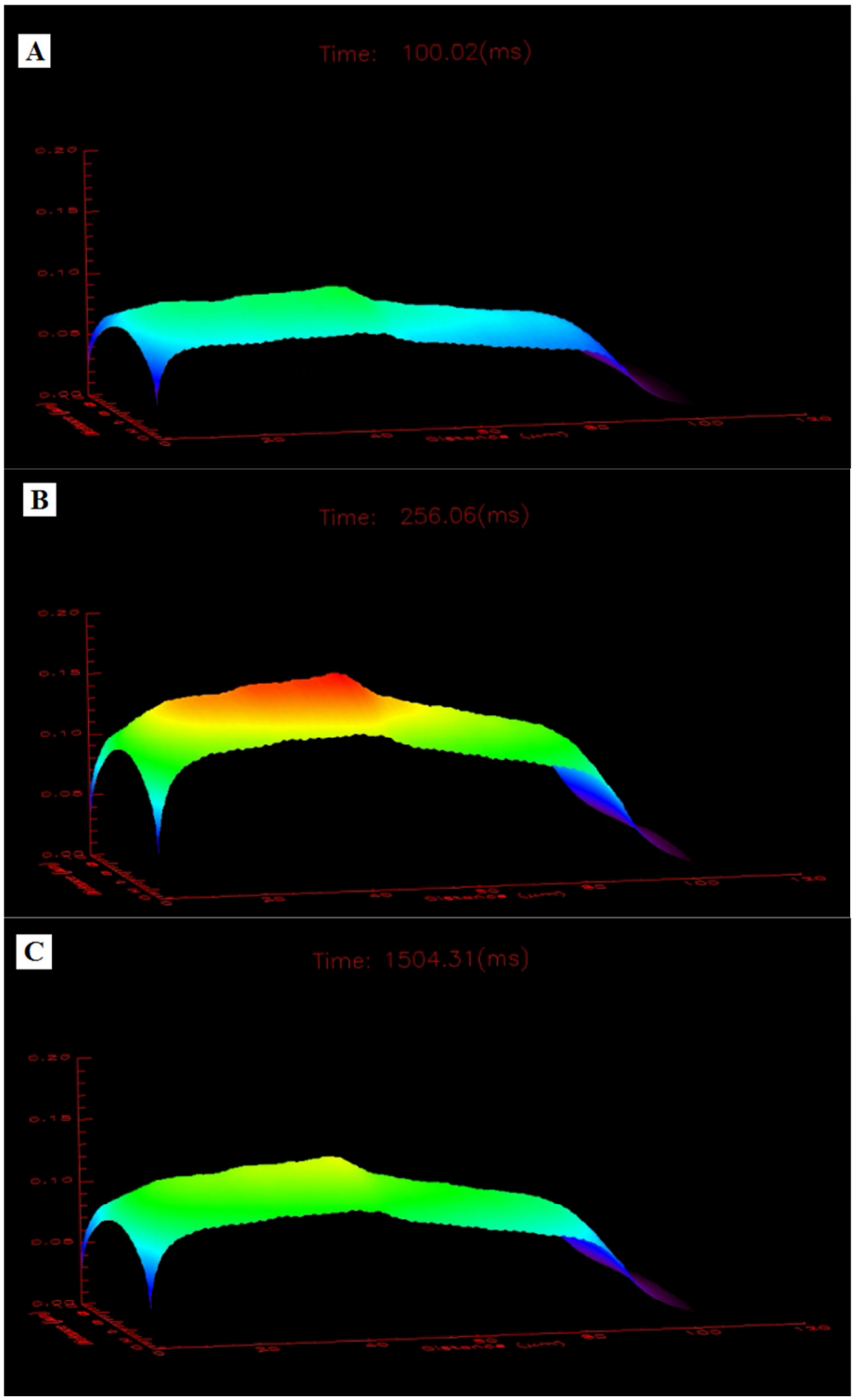

FIGURE 4: Myoplasmic ROS concentration $[ROS]_i$ after stretching the myocyte at (*A*) 100 ms, (*B*) 250 ms, and (*C*) 1.5 s after stretching.

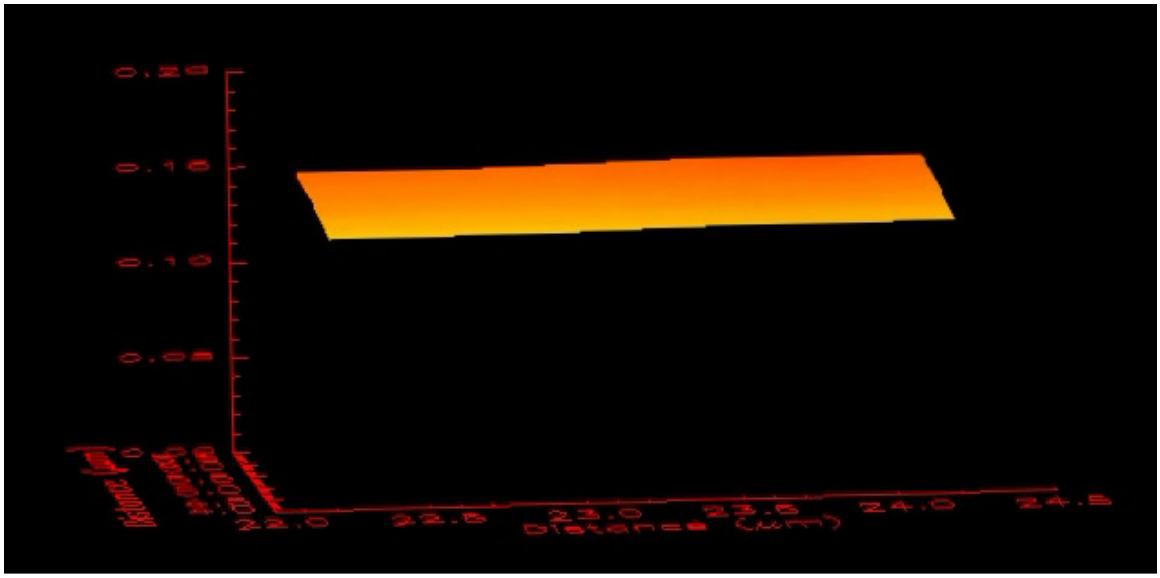

FIGURE 5: Myoplasmic ROS concentration $[ROS]_i$ in a sarcomere when the elevation in the concentration is at peak. 2 μm x2 μm size.

When the data is analyzed at a more microscopic level at the length of a sarcomere, it is evident from Fig. 5 that the ROS concentration appears to be increasing uniformly along the longitudinal axis of the myocyte.

A series of simulations were carried out with Ca^{2+} overload condition to closely simulate some of the conditions of muscular dystrophy with elevated SR Ca^{2+} $[Ca^{2+}]_{NSR}$ to 1700 μM and the resting intracellular $[Ca^{2+}]_i$ to 0.15 μM (9). This greatly increased the frequency of Ca^{2+} spark and the propensity for Ca^{2+} waves as Ca^{2+} tides were observed. With stretching, the speed of propagation of Ca^{2+} tide to reach the other end of the myocyte increased due to the production of stretch induced ROS which could be elevated due to the decrease in glutathione concentration. Here, the simulations were done at reduced [GSH] to 0.5 of its control level for dmd.

DISCUSSION

The temporal-spatial model of the ventricular myocyte with X-ROS signaling was used to dissect the temporal and spatial aspects of stretch-induced ROS signaling in the myocyte. Stretch-induced ROS which is produced locally in the subspace diffuses into the myoplasm rapidly and thus there is elevation in the myoplasmic ROS concentration which peaks at around 250 ms. This simulated finding agrees well with the unpublished experiments of Prosser and Lederer where when the cell is stretched in the middle 2/3 but not at the ends, due to the placement of the glass rods used for stretching, the signal averaged ROS concentration over each region shows elevated ROS in the stretched region and a level close to baseline in the unstretched region. Signal averaging was required because of the low signal-to-noise ratio. To better simulate the experimental finding, a simulation is planned where only the middle 2/3 of the cell will be stretched. These preliminary results suggest that the model will agree with the experiment. These simulations are important because it will help to constrain the diffusion and degradation related parameters against experimental findings.

The model shows a uniform ROS concentration across the sarcomere. This is unexpected as the ROS concentration in the subspace is 10 fold higher than the average myoplasmic value. It was expected that gradients would exist with concentration near the dyadic subspaces be elevated. Two things much be checked in the simulation results. First, it appears that not all spatial points are shown in the figure. The way the code was designed was that only a subset of the spatial points were saved to limit the large amount of data stored and then values were interpolated when the image was computed. While

this approach might work with calcium with a diffusion constant of 270 $\mu m^2/s$, ROS has a diffusion constant of 1000 $\mu m^2/s$ so that the gradients away from a source are expected to be much steeper for ROS. This needs to be explored further.

The predictions about the ROS concentration at different places in the cell is important as it would suggest the importance of stretching on other myocyte components, such as L-type Ca^{2+} channel (LCC) and SR Ca^{2+} -ATPase (SERCA) pump, involved in excitation-contraction coupling via X-ROS signaling. In the heart, the continuous stretching of the myocyte continues during the diastolic phase while the ventricle is filled with blood which could rapidly and continuously elevate the myoplasmic ROS concentration and target various channels and pumps by their oxidation. ROS is shown to inhibit SERCA pump by oxidation (23). During pathological conditions when ROS concentration is elevated at the basal level (7), stretching results in higher increase than in the control condition (1). This could highly activate RyR2s for Ca^{2+} release from SR whereas at the same time inhibit SERCA to hinder the Ca^{2+} uptake back to SR during diastolic stretching and have a serious pathological impact by depleting the SR Ca^{2+} concentration significantly during the diastole progressing the heart for a weaker systolic contraction.

The results presented in this chapter are preliminary. Additional work is needed in the following areas.

- Calcium profiles with and without stretching need to be shown and analyzed further. An averaging of several simulations is needed for Fig. 3 to better represent the experiment.

- The preliminary results indicated increased wave activity during Ca^{2+} overload. Additional simulations are needed to generate statistics to properly quantify the changes.
- The effect of increased X-ROS during dmd need to be explored further. A more detailed study of all the required changes in various simulation parameters needs to be done in order to study the disease dmd so that the disease can be investigated with more accuracy.
- Other studies are also possible. Many disease conditions are accompanied by cellular oxidative stress. For example, oxidative stress is present during heart failure. In late heart failure there is also distension of the wall of the heart that might cause stretching of the myocytes. The role of X-ROS signaling on heart function and the generation of arrhythmia for heart failure could be explored.

This spatial model presents a novel description of X-ROS signaling that provides additional insight over the compartmental models presented earlier. It is clear that many new topics can be explored yielding insight into X-ROS signaling roles in normal and pathophysiology.

REFERENCES

1. Prosser, B. L., C. W. Ward, and W. J. Lederer. 2011. X-ROS signaling: rapid mechano-chemo transduction in heart. Science 333:1440-1445.

2. Endo, M., M. Tanaka, and Y. Ogawa. 1970. Calcium induced release of calcium from the sarcoplasmic reticulum of skinned skeletal muscle fibres. Nature 228:34-36.

3. Fabiato, A., and F. Fabiato. 1972. Excitation-contraction coupling of isolated cardiac fibers with disrupted or closed sarcolemmas. Calcium-dependent cyclic and tonic contractions. Circulation research 31:293-307.

4. Schlotthauer, K., and D. M. Bers. 2000. Sarcoplasmic reticulum Ca(2+) release causes myocyte depolarization. Underlying mechanism and threshold for triggered action potentials. Circulation research 87:774-780.

5. Finsterer, J., and C. Stollberger. 2003. The heart in human dystrophinopathies. Cardiology 99:1-19.

6. Rando, T. A. 2002. Oxidative stress and the pathogenesis of muscular dystrophies. American journal of physical medicine & rehabilitation / Association of Academic Physiatrists 81:S175-186.

7. Williams, I. A., and D. G. Allen. 2007. The role of reactive oxygen species in the hearts of dystrophin-deficient mdx mice. American journal of physiology. Heart and circulatory physiology 293:H1969-1977.

8. Jung, C., A. S. Martins, E. Niggli, and N. Shirokova. 2008. Dystrophic cardiomyopathy: amplification of cellular damage by Ca2+ signalling and reactive oxygen species-generating pathways. Cardiovascular research 77:766-773.

9. Williams, I. A., and D. G. Allen. 2007. Intracellular calcium handling in ventricular myocytes from mdx mice. American journal of physiology. Heart and circulatory physiology 292:H846-855.

10. Ullrich, N. D., M. Fanchaouy, K. Gusev, N. Shirokova, and E. Niggli. 2009. Hypersensitivity of excitation-contraction coupling in dystrophic cardiomyocytes. American journal of physiology. Heart and circulatory physiology 297:H1992-2003.

11. Wilding, J. R., J. E. Schneider, A. E. Sang, K. E. Davies, S. Neubauer, and K. Clarke. 2005. Dystrophin- and MLP-deficient mouse hearts: marked differences in morphology and function, but similar accumulation of cytoskeletal proteins. FASEB journal : official publication of the Federation of American Societies for Experimental Biology 19:79-81.

12. Fauconnier, J., J. Thireau, S. Reiken, C. Cassan, S. Richard, S. Matecki, A. R. Marks, and A. Lacampagne. 2010. Leaky RyR2 trigger ventricular arrhythmias in Duchenne muscular dystrophy. Proceedings of the National Academy of Sciences of the United States of America 107:1559-1564.

13. Terentyev, D., I. Gyorke, A. E. Belevych, R. Terentyeva, A. Sridhar, Y. Nishijima, E. C. de Blanco, S. Khanna, C. K. Sen, A. J. Cardounel, C. A. Carnes, and S. Gyorke. 2008. Redox modification of ryanodine receptors contributes to sarcoplasmic reticulum Ca2+ leak in chronic heart failure. Circulation research 103:1466-1472.

14. Dhalla, A. K., M. F. Hill, and P. K. Singal. 1996. Role of oxidative stress in transition of hypertrophy to heart failure. Journal of the American College of Cardiology 28:506-514.

15. Heymes, C., J. K. Bendall, P. Ratajczak, A. C. Cave, J. L. Samuel, G. Hasenfuss, and A. M. Shah. 2003. Increased myocardial NADPH oxidase activity in human heart failure. Journal of the American College of Cardiology 41:2164-2171.

16. Xu, Q., A. Dalic, L. Fang, H. Kiriazis, R. H. Ritchie, K. Sim, X. M. Gao, G. Drummond, M. Sarwar, Y. Y. Zhang, A. M. Dart, and X. J. Du. 2011. Myocardial oxidative stress contributes to transgenic beta(2)-adrenoceptor activation-induced cardiomyopathy and heart failure. British journal of pharmacology 162:1012-1028.

17. Li, J. M., N. P. Gall, D. J. Grieve, M. Chen, and A. M. Shah. 2002. Activation of NADPH oxidase during progression of cardiac hypertrophy to failure. Hypertension 40:477-484.

18. Prosser, B. L., R. J. Khairallah, A. P. Ziman, C. W. Ward, and W. J. Lederer. 2013. X-ROS signaling in the heart and skeletal muscle: stretch-dependent local ROS regulates [Ca(2)(+)]i. Journal of molecular and cellular cardiology 58:172-181.

19. Limbu, S., T. M. Hoang-Trong, B. L. Prosser, W. J. Lederer, and M. S. Jafri. 2015. Modeling Local X-ROS and Calcium Signaling in the Heart. Biophysical journal 109:2037-2050.

20. Straube, R., and D. Ridgway. 2009. Investigating the effects of molecular crowding on Ca2+ diffusion using a particle-based simulation model. Chaos 19:037110.

21. Vestergaard, C. L., H. Flyvbjerg, and I. M. Moller. 2012. Intracellular signaling by diffusion: can waves of hydrogen peroxide transmit intracellular information in plant cells? Frontiers in plant science 3:295.

22. Pena, R. C., J. C. M. Gamboa, M. Bertotti, and R. L. C. Paixao. 2011. Studies on the electrocatalytic reduction of hydrogen peroxide on a glassy carbon electrode modified with a ruthenium oxide hexacyanoferrate film. International Journal of Electrochemical Science 6:394-403.

23. Morris, T. E., and P. V. Sulakhe. 1997. Sarcoplasmic reticulum Ca(2+)-pump dysfunction in rat cardiomyocytes briefly exposed to hydroxyl radicals. Free radical biology & medicine 22:37-47.

CHAPTER 5: CONCLUSIONS AND FUTURE DIRECTIONS

CONCLUSIONS

Reactive oxygen species (ROS) have been shown to play both a physiological and pathological role in cellular signaling pathways. This work described the development of a novel model for cardiac ventricular myocyte model that incorporates stretch-activated ROS (X-ROS) production by Nox-2 to understand it's physiological and pathological roles. X-ROS signaling oxidizes RyR2s to increase their opening probability. The RyR2s release Ca^{2+} from the sarcoplasmic reticulum (SR) and thus, increase the myoplasmic Ca^{2+} concentration of the myocyte. The model was used in studying various effects X-ROS could have on excitation-contraction (EC) coupling. The simulation results showed that the increase in frequency of stretching and release of stretch of the myocyte from 1 Hz to 2 Hz and 4 Hz results in elevation of the ROS concentration both in the subspace and in the myoplasm and as a result, the spark frequency and the myoplasmic Ca^{2+} increases suggesting that increasing pacing rate could increase the EC gain via X-ROS signaling. The increase seems to plateau at 4 Hz. The model also suggested that the X-ROS enhances EC coupling. Stretching the myocyte just prior to the application of stimulus emulates the filling of the cardiac ventricles with blood just before the blood is pumped. The simulation results demonstrated that the X-ROS produced by stretching the myocytes just before the action potential optimally potentiates the magnitude of the Ca^{2+}

transient for enhancing the contractility. Stretching of a myocyte causes an abrupt increase in the peak myoplasmic Ca^{2+} but as the stretch is prolonged, the peak myoplasmic Ca^{2+} also attenuates due to decrease in the X-ROS production as well as due to the depletion in the SR Ca^{2+} load. Lowering the concentration of the reducing agent glutathione (GSH) elevated the ROS concentration significantly resulting in higher peak myoplasmic Ca^{2+} and in depleted peak SR Ca^{2+} while studying how oxidative stress affects the X-ROS signaling during diseased condition such as heart failure.

Stretching of a myocyte not only elevates the myoplasmic Ca^{2+} concentration via X-ROS signaling, it also reduces the free myoplasmic Ca^{2+} concentration elevated by X-ROS by increasing the Ca^{2+} binding affinity of troponin C in the actin and thus increasing the Ca^{2+} buffering. Both the experimental studies as well as simulations were carried out to investigate these opposing effects of mechanical stretching of a myocyte. The cardiac ventricular model was improved by integrating low-affinity Ca^{2+} binding site on troponin. In the new model, the myocyte produces X-ROS as well as increases the Ca^{2+} buffering when stretched. The simulations predict that the increase in Ca^{2+} buffering by the troponin due to stretching is offset by the increase in Ca^{2+} mobilization caused by X-ROS signaling. Our simulations results were in agreement with the experimental results obtained by our collaborators. When the myocyte is stretched in the presence of blebbistatin which inhibits crossbridge formation between actin and myosin, the increase in the peak myoplasmic Ca^{2+} with respect to the unstretched condition is higher than the increase without blebbistatin. Stretching a myocyte in the presence of gp91ds, a Nox2 inhibitor, the peak myoplasmic Ca^{2+} with respect to the unstretched condition decreases

as there is no ROS production to increase the Ca^{2+} release and the increase in Ca^{2+} buffering also reduces the peak value of Ca^{2+}. Stretching thus imparts complex regulation on excitation-contraction coupling (ECC) by activating more than one signaling mechanism.

A spatial model of the rat ventricular myocyte with X-ROS signaling was developed to study the spatial profile of various elements of ECC including ROS and investigate the impact stretch-induced ROS could have upon various components of the myocyte during physiological as well as pathological condition. The model suggests that due to the rapid diffusion of ROS during the stretching of the myocytes, ROS quickly spreads from the z-lines across the sarcomere. The ensuing increase in open probability increases the spontaneous spark rate in the myocyte. Furthemore, under Ca^{2+} overload conditions, stretching increases the propensity for spontaneous Ca^{2+} waves through X-ROS signaling. This has implications in disease such as Duchenne muscular dystrophy where there is increased X-ROS signaling due to increased microtubule density or dilated cardiac myopathy and heart failure where the myocytes are stretched and oxidative stress is increased.

FUTURE DIRECTIONS

Reactive oxygen species comprises of highly active radical and less active non radical molecules with many potential targets such as L-type Ca^{2+} channels, NCX and SERCA pump besides RyRs. Our current ventricular myocyte model considers RyR2 as the only target of stretch-activated ROS and this model could be extended in the future to

incorporate the posttranslational modification of the other protein targets in various signaling pathways. Such extension of the model would refine the model and make the investigation of the physiological as well as the pathological conditions of cardiomyocytes more precise. A more detailed study to investigate the underlying mechanisms of a particular disease would provide us with an in-depth answer to the questions related to many biological processes which could direct us towards a particular direction of pharmacological intervention. Elevation in the ROS production has been associated with various neurodegenerative diseases (1) and this increase in ROS concentration also could cause cellular DNA mutations which could initiate the progression of carcinogenic diseases (2). This model would also give an insight and inspiration on studying these ROS mediated non-cardiac diseases.

REFERENCES

1. Kirkinezos, I. G., and C. T. Moraes. 2001. Reactive oxygen species and mitochondrial diseases. Seminars in cell & developmental biology 12:449-457.

2. Waris, G., and H. Ahsan. 2006. Reactive oxygen species: role in the development of cancer and various chronic conditions. Journal of carcinogenesis 5:14.

BIOGRAPHY

Sarita Limbu grew up in Kathmandu, Nepal. She received her Bachelor of Engineering in Computer Engineering in 2004 from Kathmandu Engineering College, Tribhuvan University, Kathmandu. She completed Master of Science in Computer Science from the University of Akron, Akron, Ohio in Dec 2009. She is a PhD student in the Bioinformatics and Computational Biology program, School of Systems Biology, George Mason University since Fall 2010.